THE ROLE OF THE RESPIRATORY SYNCYTIAL VIRUS FUSION PROTEIN IN VIRAL FILAMENTOUS ASSEMBLY

By

Fyza Yusuf Shaikh

Dissertation submitted to the

Faculty of the Graduate School of Vanderbilt University

in partial fulfillment of the requirements for the degree of

DOCTOR OF PHILOSOPHY

in

Microbiology and Immunology

August 2012

Nashville, Tennessee

Approved:

Terence Dermody

Christopher Aiken

Andrew Link

Todd Graham

Anne Kenworthy

James Crowe

To my father, Yusuf Suleman Shaikh, who always wanted a doctor in the family and taught me never to settle for anything less than excellence

and

To my mother, Razia Yusuf Shaikh, who will always be my model for strength, compassion, and kindness in this world

ACKNOWLEDGEMENTS

I am truly grateful to the many people that have contributed to this work. This project would not have been possible without my mentor, James Crowe, and the members of the Crowe laboratory. The encouragement and assistance I received from my mentor and co-workers, both past and present, has been invaluable throughout the course of my graduate studies. I would like to thank my collaborators Aaron Lifland and Phillip Santangelo at the Georgia Institute of Technology, Anne Hotard and Martin Moore at Emory University, and Reagan Cox and John Williams at Vanderbilt University Medical Center. I would also like to thank the students who have worked with me, particularly Ryan Craven and Meredith Rogers, who contributed to the data presented in this thesis.

This work is a result of many excellent suggestions and guidance from my thesis committee: Terence Dermody, Christopher Aiken, Andrew Link, Anne Kenworthy, and Todd Graham. I would also like the thank the Vanderbilt Medical Scientist Training Program, the former Department of Microbiology and Immunology, and the current Department of Pathology, Microbiology, and Immunology for support during my graduate studies. This work has been supported by the Burroughs Wellcome fund, the March of Dimes Foundation, and the NIH.

Finally, I would like to thank my family and friends for the countless hours of support during the last five years. Without the support of my parents, I would never have had this opportunity. They are the reason I am here today. I must also thank my brothers and my friends for their endless support, that never wavered throughout the good and bad times. I am truly lucky to have such wonderful people in my life.

TABLE OF CONTENTS

Appendix

LIST OF TABLES

LIST OF FIGURES

LIST OF ABBREVIATIONS

ATCC	American type culture connection
CT	cytoplasmic tail
ER	endoplasmic reticulum
ESCRT	endosomal sorting complex required for transport
F	fusion protein
FBS	fetal bovine serum
FHL2	Four and a half LIM domains 2
FI	formalin inactivated
FLNA	filamin A
G	glycoprotein
GLUL	glutamate-ammonia ligase
GNAL	guanine nucleotide-binding protein
HMPV	human metapneumovirus
h.p.i.	hours post inoculation
L	large polymerase protein
LRT	lower respiratory tract
M	matrix protein
MDCK	Madin Darby canine kidney
MOI	multiplicity of infection
N	nucleoprotein
NS	non-structural

OPTN	optineurin
P	phosphoprotein
pfu	plaque forming unit
PICALM	phosphatidylinositol binding clathrin assembly protein
RSV	respiratory syncytial virus
SDS-PAGE	sodium dodecyl sulfate polyacrylamide gel electrophoresis
SH	short hydrophobic protein
SRP9	signal recognition particle 9kDa
STX18	syntaxin 18
TBC1D15	TBC1 domain family, member 15
TEM	transmission electron microscopy
TM	transmembrane
VLP	virus-like particle
wt	wildtype
Y2H	yeast two-hybrid

Chapter I

INTRODUCTION

Respiratory syncytial virus

Respiratory syncytial virus (RSV) is a leading cause of serious viral lower respiratory tract (LRT) illness in infants (41) and the elderly worldwide (25). RSV infects 4-5 million children each year, and with more than 125,000 admitted to the hospital in the US, RSV is the leading cause of hospitalization in children less than one year old (40). Although mortality is only 1% among admitted infants, infants with chronic lung disease, congenital heart disease, or marked prematurity are at higher risk of increased length of hospitalization and increased mortality (53). Globally, RSV causes more than 30 million LRT infections annually, resulting in more than 3 million hospitalizations (40). RSV is also an important cause of LRT infections in adults with cardiopulmonary disease, severe combined immunodeficiency, or following transplantation (21, 24, 40).

RSV illness presents primarily as bronchiolitis or pneumonia with peak incidence between the ages of 2-8 months. Most children have been infected by the age of 3 years, and reinfection is common but is often limited to the upper respiratory tract (53). Therapy for RSV infection is limited to supportive care, including supplemental oxygen, mechanical ventilation, and fluid replacement. Ribavirin, a purine RNA analog, may be used in severe cases of RSV infection. In high-risk infants, passively administered antibody (Synagis ®, palivizumab) is effective for prophylaxis but not therapy (53).

Due to the high morbidity and mortality associated with RSV infection and the lack of available therapies, an RSV vaccine is of high priority. However, RSV presents a unique challenge for vaccine development, including age of first infection, immune evasion, and the legacy of a failed clinical trial using a formalin-inactivated (FI) whole virus vaccine. Immunization of children with the FI-RSV actually resulted in exacerbated disease, with increased rates of hospitalization and mortality (20, 51). Current vaccine efforts for pediatric populations are largely focused on live-attenuated strains, produced by either serial passage in the cold or generated using recombinant virus systems (21). Live-attenuated vaccines, however, are often too restricted for replication in older populations that have previously been exposed to RSV (37). Vaccine strategies in these populations include subunit vaccines, virus-like particle (VLP) vaccines, and both replication-competent and defective gene-base vectors (21, 40). While many strategies are being explored, further insights into the biology of the virus and its interaction with the host may contribute to vaccine development or targeted therapeutics.

RSV proteins and the life cycle

RSV was isolated from chimpanzees with upper respiratory tract infections in 1956. The virus is a member of the *Paramyxoviridae* family, subfamily *Pneumovirinae,* with a single-stranded, negative-sense RNA genome encoding 11 proteins. Figure 1-1 shows a schematic of a filamentous RSV virion consisting of a lipid membrane that is derived from the host cell and three glycoproteins: fusion (F) protein, attachment (G) protein, and small hydrophobic (SH) protein. The F protein mediates viral fusion with the cellular membrane. The G protein plays a role in viral attachment, and SH protein is

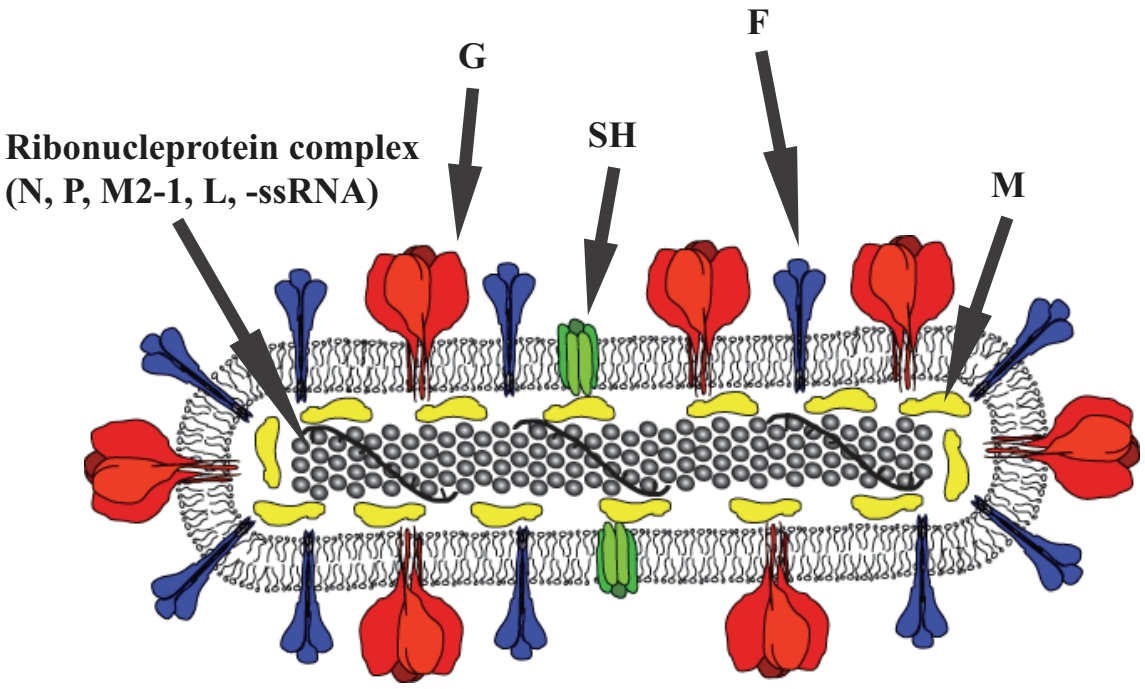

Figure 1-1. Schematic of RSV filamentous virion. RSV F (blue), G (red), SH (green) are depicted on the surface of the virion as transmembrane proteins, while M (yellow) and the viral RNP complex (black) are shown on the interior of the viral particle. Figure provided by Thomas Utley.

thought to inhibit apoptosis (31). RSV also contains six internal structural proteins: matrix (M) protein, nucleoprotein (N), phosphoprotein (P), large (L) polymerase protein, and two isoforms of matrix protein 2 (M2-1 and M2-1). The M protein provides the structural framework for the virus particle. RSV N, P, and L form the ribonucleoprotein (RNP) complex, which encapsidates the RSV genome, and functions as the RNA-dependent RNA polymerase. M2-1 and M2-2 are accessory proteins that control transcription and translation (103). RSV also encodes two non-structural proteins, NS1 and NS2, which inhibit interferon induction, interferon signaling, and apoptosis (21). Figure 1-2 shows a transmission electron micrograph of an assembling virion at the cell surface and provides a summary of the function of each viral protein (21).

RSV infects the apical surface of polarized lung epithelial cells (Figure 1-3). Infection begins with attachment of the virion to the cell membrane, a process that is mediated by the F and G proteins. Low-affinity interaction with cellular glycosaminoglycans, particularly heparin sulfate (26, 54), are thought to stabilize the virion on the cell surface so that F can specifically interact with nucleolin (89). Although nucleolin is sufficient for infection of non-permissive cells, the trigger for virus-cell fusion is unknown. The F protein is sufficient for fusion *in vitro*, but other cellular proteins may play a role (5, 60, 94). After fusion, the viral genome and viral RNA-dependent RNA polymerase, consisting of N, P, L, and M2-1, are released into the cytoplasm. The viral polymerase begins making viral transcripts for each viral protein in the cytoplasm, which is followed by translation using the host ribosomal machinery (103). The viral glycoproteins are thought to traffic through the secretory pathway to the apical surface of polarized epithelial cells, while the internal proteins are translated in the cytoplasm (10).

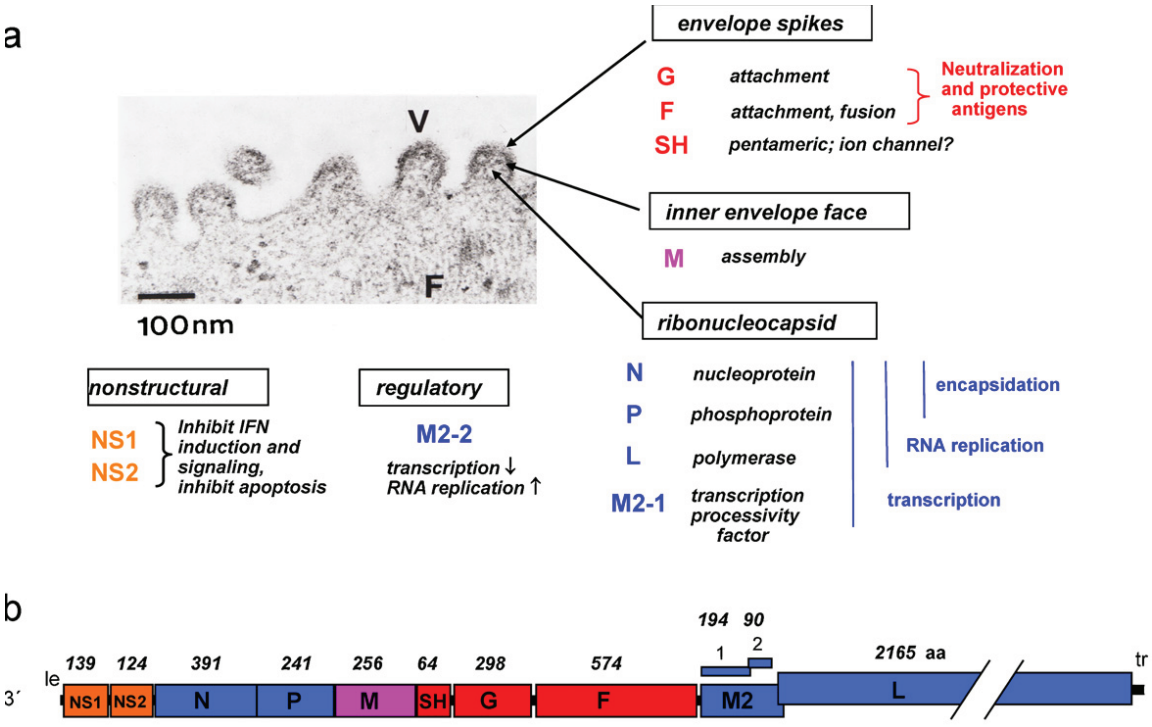

Figure 1-2. RSV proteins and their role in viral replication. Panel A shows a negatively stained transmission electron micrograph of RSV virions assembling and budding from the cell membrane. Individual proteins and their functions are indicated. Panel B shows a schematic of the viral genome is shown. The amino acid length of each protein is indicated above each gene. Figure was originally published by Collins and Melero, 2001 (21).

Upon accumulation of viral proteins, the viral polymerase switches from transcription to viral replication, a process thought to be controlled by M2-2. Viral proteins accumulate in the cytoplasm in discrete aggregates, termed inclusion bodies. These viral inclusion bodies contain RSV M, N, P, L, M2-1 and -2 proteins and the vRNA (55, 57). It is suspected that the ribonucleoprotein (RNP) complexes form in the inclusions and then traffic to the apical membrane, where they meet with the surface glycoproteins F, G, and SH arriving from the Golgi apparatus through the secretory pathway (9). RSV proteins and viral RNA assemble into virus filaments at the apical cell surface (77). These filaments are thought to contribute to cell-cell spread of the virus and morphologically resemble the filamentous form of virions seen in EM studies of virus produced in polarized cells (97). Live imaging has shown these structures to be dynamic, with rotation and directional movement (3, 80). Membrane scission is thought to occur in a Vps4-independent manner (97), resulting in pleomorphic particles ranging from 150-250 nm in diameter for spherical forms and up to 10 μm long in filamentous forms (4).

RSV assembly and budding

To produce progeny virions, RSV must coordinate assembly between proteins translated in the cytoplasm, glycoproteins that have trafficked to the cell surface through the secretory pathway, and the newly synthesized genomic RNA. RNP assembly is thought to occur within the viral inclusion bodies since the viral polymerase proteins and genomic RNA are found to co-localize at these structures (57). However, it is unknown how the RNP complex traffics to the cell surface to meet with the other viral proteins at the cell surface. When the M protein is not present, N and P accumulate in viral inclusion

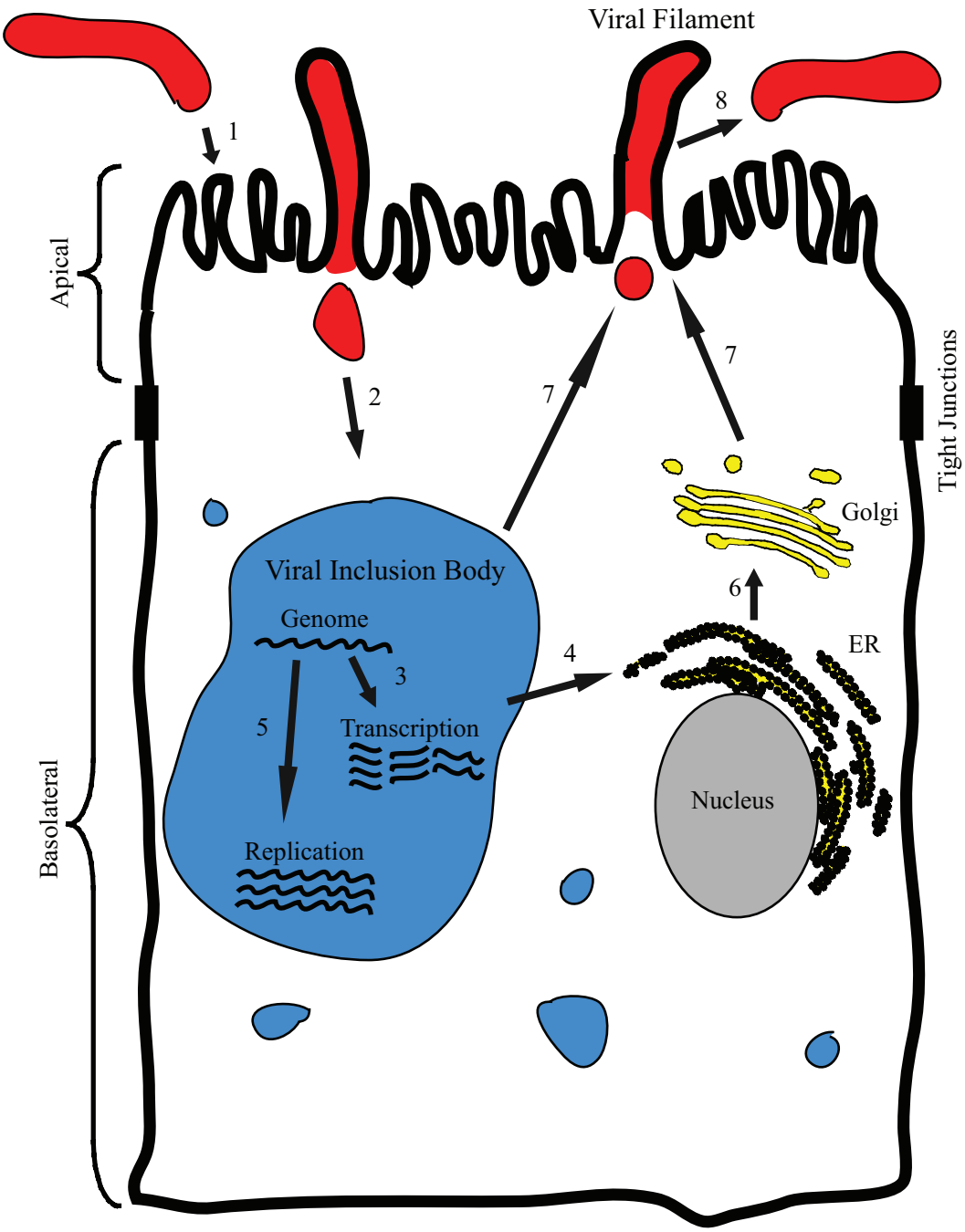

Figure 1-3 Diagram of the RSV life cycle. (1) The RSV virion attaches to the epithelial cell. (2) The viral ribonucleoprotein complex is delivered to the cytoplasm. (3) The genome is transcribed into viral mRNAs, which are then translated on host ribosomes (4) either at the endoplasmic reticulum for the glycoproteins or free cytoplasmic ribosomes. (5) A switch occurs from transcription to replication of the viral genome. (6) Glycoproteins are trafficked from the endoplasmic reticulum to the Golgi apparatus where they are modified. (7) All the virion components must be trafficked to the apical membrane. (8) Assembled virions bud from the infected cell. Figure provided by Thomas Utley

bodies and viral filaments do not form, suggesting that M might be responsible for trafficking the RNP complex to the cell surface (64). This hypothesis is consistent with the observation of M colocalization with N in inclusion bodies and co-precipitation with RNP complexes (33, 95). RSV M has been shown to associate with the plasma membrane (61) and specifically sorts into detergent-resistant membranes when F is present (44). M has two distinct domains that have a large positively charged surface, allowing it to interact with phospholipids (43, 66). In contrast, specific residues in the cytoplasmic domain of G affect M colocalization with G. However, G is not essential for the generation of progeny virus, and M can localize with F in the absence of G. Thus, M may associate with both F and G independently (34). Furthermore, F and G form a complex at the cell surface that is detectable by immunoprecipitation (59). These data suggest a model for RSV assembly in which viral polymerase proteins produce nascent genomic RNA in inclusion bodies in the cytoplasm and form the RNP complex. The RNP complex can then associate with M, which is capable of associating with the plasma membrane, F, and G at the cell surface, carrying along the RNP complex to that site.

Localization of viral proteins to the cell surface, however, is not sufficient for viral assembly into filaments. In order for filaments to form, viral proteins must deform the host cell membrane outward to initiate bud formation and then elongate the bud through the incorporation of additional membrane to create long filaments. To form a free particle, a membrane scission event must occur to release the viral particle from the cell membrane. All of these processes are energy intensive and require complex coordination of surface proteins and nucleocapsids containing RNA and viral proteins (18). Several models have been proposed for membrane bending by viral proteins. Figure 1-4 shows

how the membrane can be either pulled outward by packing of surface proteins to promote positive or negative membrane curvature. The membrane could also be pushed outward by internal virion proteins or interactions between viral surface and internal proteins, allowing coordination of multiple forces to drive membrane deformation (99). Previous work in the field has shown F, M, N, and P to be the minimum requirements for passage of a minigenome construct, indicating that these four proteins are the minimum requirements for packing vRNA into cell free particles (91). Many other paramyxoviruses also require both internal and membrane proteins for budding. For example, parainfluenza virus (PIV) 5 and mumps both require M, NP, and a glycoprotein. However, other paramyxoviruses require only the M protein for efficient VLP formation, *e.g.* PIV1, Sendai virus, and measles virus (43). Since both internal and surface proteins are required, RSV assembly into filaments likely involves a combination of surface and internal protein driven forces.

The final step in viral assembly and budding involves a membrane scission event to sever the assembled viral particle from the host cell membrane. Many viruses accomplish this task by usurping host machinery for multivesicular body formation (46). Endosomal sorting complex required for transport (ESCRT) proteins utilize a final common ATPase Vps4 to perform membrane scission (46). Using dominant-negative inhibitors of Vps4, the pathway can be disrupted, resulting in membranous vesicles still tethered to the original membrane (82). The use of ESCRT proteins in viral budding has been well characterized for many viruses, including HIV and other paramyxoviruses (18). However, RSV budding is unaffected by inhibition of Vps4, suggesting that it uses a novel mechanism to accomplish membrane scission (97). Furthermore, there is evidence

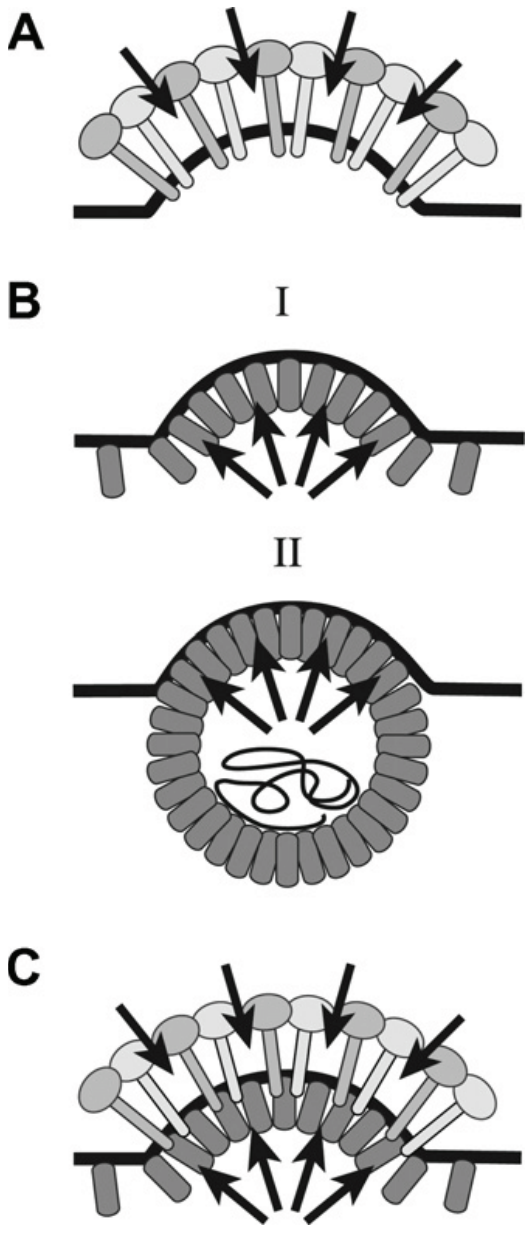

Figure 1-4. Models of virus budding driven by viral proteins. Panel A shows a model of viral budding driven by glycoproteins pulling on the host membrane. Panel B shows a model of virus budding driven by internal virion proteins pushing outward on the host membrane as internal protein oligomerize (I) or by pre-assembled proteins (II). Panel C shows both pulling and pushing forces acting in concert to drive viral bud formation. Figure was originally published by Welsch *et al*, 2007. (99).

that budding for a number of viruses is ESCRT independent (102). Although the mechanism for ESCRT independence is unknown for many viruses, influenza appears to use a viral protein mediated mechanism to accomplish membrane scission through use of an amphipathic helix in the cytoplasmic tail of the M2 protein (78). While it is likely that host proteins play some role in viral budding, viral proteins may be sufficient to perform membrane scission to produce free virions.

RSV F protein

The RSV F protein is a trimeric type I integral membrane protein that traffics though the cellular secretory pathway. It is responsible for viral fusion with the host cell membrane as well as the characteristic syncytia produced in RSV-infected cultures. The F protein has an endoplasmic reticulum (ER) signal sequence, a large ectodomain that mediates fusion, a 23-amino-acid transmembrane domain (TM), and 24-amino-acid cytoplasmic tail (CT). The non-fusogenic single-chain F_0 precursor is cleaved by furin-like proteases at two sites to produce F_1 and F_2 which remain connected by disulfide bridges (84). Unlike other paramyxovirus F proteins, RSV F does not require other viral proteins to fuse membranes (21). Fusion is accomplished through the use of two heptad repeats (HR1 and HR2) and a hydrophobic fusion peptide. In the pre-fusion form of the protein, the fusion peptide is thought to be sequestered, and HR1 and HR2 are not associated. Following an unknown trigger, the fusion peptide is thought to insert in the target membrane. The F protein goes through a conformation change in which HR1 interacts with HR2 to form a six helix bundle in the F trimer. The formation of the six-helix bundle brings the viral and target membranes together so fusion can occur (23, 84).

Although the fusion function of the F protein has been well characterized, the F protein also plays a role in viral assembly. The F protein traffics to the apical surface in the absence of other viral proteins or viral RNA. The CT is completely dispensable for apical trafficking (10). Deletion of the CT leads to a 100- to 1,000-fold decrease in viral titer in a multi-cycle growth assay and results in a virus that is incapable of assembling into filaments. Deletion of the CT, however, dos not affect the capacity of the F protein to mediate cell-cell fusion, suggesting that the CT plays a role in assembly rather than entry (8, 69).

Coordination of RSV assembly by protein F's CT is consistent with many other studies citing paramyxovirus glycoprotein cytoplasmic tails as crucial to both assembly and budding (reviewed in 43). For RSV and HMPV, both members of the *Pneumovirus* subfamily, the G protein is dispensable for viral replication *in vitro* (6, 92). Although the F CT may be sufficient for generation of progeny virions, optimal incorporation of viral proteins and RNA might require both F and G since residues in the RSV G protein CT are thought to be important for interactions with M (35). However, for the *Paramyxoviridae* subfamily, the requirement of glycoprotein CTs varies with each virus. For measles virus and Sendai virus assembly, the F protein CT is required. Newcastle disease virus F and HN glycoproteins interact with different internal viral proteins, M and N respectively. In contrast, the F and HN CTs of parainfluenza virus 5 serve somewhat redundant functions (43). The lack of a common theme for role of CT domains in paramyxoviruses may simply indicate that many questions about the specific mechanisms of viral assembly remain unanswered, and further investigation into the RSV F CT may contribute to general knowledge regarding glycoprotein CT-mediated viral assembly.

RSV interactions with the host membrane

The formation of RSV particles at the cell surface also requires viral interactions with the host cell lipid membrane. The plasma membrane contains regions where lipid and protein composition differ from the rest of the plasma membrane. These microdomains can serve as platforms for cell signaling, protein trafficking, and other cellular functions. Lipid rafts, a type of lipid microdomain, are cholesterol- and sphingolipid-enriched regions that often function to concentrate proteins within defined regions for a functional purpose (11). Lipid rafts can function as assembly and budding platforms for viruses, including HIV-1, Ebola virus, and influenza virus (79).

Many membrane microdomain studies focus on cholesterol dependence and detergent insolubility, such as with Triton X-100, that results in detergent-resistant membranes (DRMs). Cholesterol-depletion studies indicate that cholesterol is required for viral filament formation but is dispensable for inclusion bodies (101). Inhibiting the synthesis of raft-associated phosphatidylinositol 3,4,5-triphosphate [PIP(3)] impairs the formation of progeny virus (101). Furthermore, RSV assembles into filaments at lipid microdomains that are rich in the lipid-raft ganglioside GM1 (13), and ultrastructural analysis indicates that GM1 incorporates into viral filaments (48). RSV proteins localize with lipid microdomain-specific dyes and raft-associated proteins, such as caveolin-1, CD44, and RhoA (62). Specifically, the RSV F protein associates with DRMs in the absence of other viral proteins though an unidentified domain in the extracellular portion of the protein (28) and localize with raft-associated clusters of differentiation (CD) 55 and 59 (13). Disruption of RhoA signaling using a *Clostridium botulinum* exotoxin C3 results in relocalization of F from DRMs to non-lipid raft structures (62).

Internal virion proteins also localize to lipid microdomains. RSV M associates with membranes by itself; however, this interaction is thought to be stabilized by viral glycoproteins and interaction with the host cytoskeleton (44). In the presence of the F protein, M is able to sort into DRMs using triton X-100 insolubility assays (44) and flotation gradients (61). Finally, the viral polymerase complex associates with lipid raft proteins, with M2-1 showing a greater degree of partitioning into these lipid structures (63). These studies indicate that viral proteins localize to specific lipid microdomains that facilitate viral assembly. However, the specific mechanisms by which lipid interactions aid viral assembly have not been well defined.

RSV and the host cytoskeleton

Manipulation of the plasma membrane also likely involves a variety of host proteins that function at the cell surface. Many cellular structures extending outward from the cell surface depend on actin polymerization (*e.g.,* microvilli, filapodia, lamellipodia, and membrane ruffles). Lipid microdomains have also been linked to the cortical actin network (56). In fact, is involved in multiple aspects of the RSV life cycle, but the specific role of actin in RSV assembly is not well understood. Gross disruption of the cytoskeleton using inhibitors of polymerization and depolymerization reduces viral replication (50). Both actin and profilin, an actin modulatory protein, are required for optimal RSV replication without the need for actin polymerization (14, 15, 42, 45). Consistent with these results, β-actin and other actin-related proteins colocalize with RSV F at the cell surface and have been found in a variety of sucrose gradient-purified RSV preparations by immunoblot analysis and mass spectrometry (14, 27, 75, 95). A caveat of

these studies, however, is that while many quality-control measures were used to ensure purification, the pleomorphic nature of RSV virions makes them difficult to purify from other membrane-bound vesicles of similar size that may contain actin (86). Therefore, while the role of actin has been well characterized for RSV transcription, the function of actin in RSV assembly and budding remains unclear.

In contrast to β-actin incorporation into viral particles, filamentous actin (F-actin) is found at the base of viral filaments, consistent with its role as the cortical actin network, but is absent from the filaments themselves (47). Additionally, inclusion bodies are often localized near the plasma membrane, near viral filaments. Actin is associated with both inclusion bodies and the base of filaments (47). These data support the hypothesis that F-actin may serve a structural role in viral filament formation, but it does not form the structure of the filament itself. Other cytoskeletal proteins are also excluded from viral filaments, such at ezrin and tubulin (97). The exclusion of F-actin and ezrin from viral filaments can be used to distinguish viral filaments from cellular structures protruding from the membrane. Other actin-associated proteins, however, colocalize with viral filaments. Filamin A and caveolin-1 associate with viral filaments by immunofluorescence and in budded particles by mass spectrometry (12, 75). Actin interacts with caveolin-1, a lipid raft protein, and filament A interacts with caveolin-1, suggesting another link between actin-associated proteins, lipid rafts, and RSV assembly. Exclusion and inclusion of certain cellular proteins from viral filaments also suggests some type of specific sorting of viral and host proteins into filaments (97), a process that likely is highly regulated and probably involves interactions among viral proteins, host proteins, and lipid microdomains.

Finally, disruption of actin-related proteins or actin-associated signaling pathways affects protein trafficking or filament formation, respectively. RSV infection results in activation of RhoA, a kinase involved in actin cytoskeletal rearrangement (38). Inhibition of RhoA results in a reduced number of blunted filaments and a shift to more spherical particle morphology, although the total number of progeny was unaffected (39). Treatment of RSV-infected cells with a phosphatidyl-3-kinase (PI3K) inhibitor or Rac GTPase, a downstream effector of PI3K, prevents formation of viral filaments but does not affect virus protein expression or trafficking of viral glycoproteins to the cell surface (47). These data suggest a role for actin signaling in viral assembly.

Host proteins associated with viral filaments

The apical recycling endosome (ARE) is implicated in RSV assembly and budding. The ARE is part of a network of endosomes present in polarized epithelium that is responsible for maintaining the composition of membranes at apical and basolateral membranes (68). The endosomal network is regulated by a series of Ras-related small GTPase proteins called Rabs (73). Rab11 and Rab25 are associated specifically with the ARE, which is responsible for the slow recycling of cargo to the apical membrane and is also involved in transcytosis (36, 67, 96). Rab proteins depend on motor proteins for trafficking and adapters to confer cargo specificity. Myosin Vb is an actin motor protein that binds Rab11, and Rab11-family interaction proteins (FIPs) confer cargo specificity for Rab11 endosomes. Dominant-negative inhibitors of myosin Vb or Rab11-FIP1 disrupts viral filament formation and results in diminished infectious viral progeny (9). In contrast, disruption of Rab11-FIP2 causes an increase in cell-associated virus and longer

viral filaments on the surface of infected cells, suggesting a defect in membrane scission to produce free virions (97). Although these studies show that ARE proteins are involved in RSV assembly and budding, a direct interaction between ARE and viral proteins has not been shown. Thus, the mechanism by which the ARE functions in RSV assembly and budding remains undetermined.

A number of heat shock proteins are also associated with viral structures. HSP90 is associated with viral filaments and inclusion bodies, as shown by immunofluorescence. Inhibition of HSP90 leads to loss of viral filament formation and reduced viral spread *in vitro*. Furthermore, HSP70 and HSC70 colocalize with RSV inclusion bodies and mass spectrometry studies suggest they are physically associated with budded particles. However, the mechanisms by which these proteins affect viral assembly are currently unknown.

Thesis overview

The experiments described in this thesis were designed to identify the host and viral determinants of RSV assembly and budding. In chapter II, I show that viral filaments are the likely sites of viral assembly at the cell surface. Interestingly, these data also show that viral filaments are formed by selective sorting of viral proteins into filaments and the exclusion of host cytosolic and membrane proteins. In chapter III, I identify viral determinants of filamentous assembly by showing that a specific Phe amino acid in the F CT is necessary for incorporation of internal virion proteins into virus-like filaments and virus-like particles (VLPs). Finally, in chapter IV, I discuss the viral interactions with the host cell as explored by yeast two-hybrid (Y2H) screens. The data

show that a number of host proteins localize to viral structures, but none are essential for viral replication. Collectively, these studies suggest that viral proteins are the driving factors behind viral assembly and budding. Chapter V summarizes the data and offers directions for future studies.

Chapter II

CHARACTERIZATION OF RSV FILAMENTS AT THE CELL SURFACE

Introduction

Although many aspects of the RSV life cycle have been studied, the mechanisms by which RSV assembles and buds are not well defined. For viral assembly, the viral structural proteins and the viral RNA must traffic to the cell surface and coordinate with viral glycoproteins to assemble into filaments and form free virions. RSV matures at the apical surface of infected polarized cells (77). RSV F protein can traffic to the apical surface independent of other viral proteins as directed by the transmembrane domain (10). Mutations in the cytoplasmic domain of F affect viral assembly into filaments (83). RSV N localizes underneath the apical surface independent of viral glycoproteins (2). The M protein may be responsible for targeting the viral RNP complex to the cell surface from inclusion bodies, which likely are the sites of RNA replication (64).

In addition to viral determinants, many host proteins have been implicated in the process of virus assembly and budding. The apical recycling system, lipid microdomains, actin-associated proteins, and actin-related signaling have been implicated in RSV assembly and budding. In this chapter, I sought to characterize the structural features of viral filaments, investigating both viral and host cell components. Viral assembly into filaments and budding of VLPs required F, M, N, and P. Additionally, viral filaments excluded host cytoskeleton proteins, actin-associated proteins, and lipid raft and non-raft proteins, and in fact, were shown to form independently of cytoskeletal rearrangement.

The results suggest that although some cytoskeletal elements are peripherally associated with the assembly mechanism, RSV assembles into filaments using a mechanism that is independent of the host cytoskeleton and most actin-associated proteins. These data suggest that viral proteins are the principal mechanical factors driving the formation of viral particles at the cell surface. This finding is remarkable considering the length and structural complexity of the viral filaments.

Materials and methods

Cell culture and *wt* RSV virus preparations. HEp-2 cells (ATCC CCL-23) were maintained in OPTI-MEM I medium (Invitrogen) containing 2% (v/v) fetal bovine serum (FBS), 1% (v/v) L-glutamine, 2.5 μg/mL amphotericin B, and 1% (v/v) penicillin-streptomycin. HEK 293T cells were maintained in DMEM/F12 containing 10% (v/v) FBS, 1% (v/v) L-glutamine, 2.5 μg/mL amphotericin B, and 1% (v/v) penicillin-streptomycin. MDCK cells were maintained in DMEM containing 10% (v/v) FBS, 1% (v/v) L-glutamine, and 1% (v/v) penicillin-streptomycin. All transfections were performed using Effectene Transfection Reagent (Qiagen) for HEp-2 cells according to package instructions, except as noted for filament formation and VLP assay. YFP-GL-GPI and YFP-GT46 were a kind gift from Anne Kenworthy. The RSV *wt* strain A2 was expanded in HEp-2 cells. For filament visualization, HEp-2 cell monolayers on 12 mm micro cover glasses (VWR, No. 2) were inoculated at an MOI=1.0 and incubated for 24 hours.

Filament formation by transfection. Plasmids encoding the RSV F protein along with pcDNA3.1 plasmids containing inserts encoding the RSV A2 strain matrix (M), nucleoprotein (N), and phosphoprotein (P) gene (synthesized by GeneArt, Regensburg, Germany) were transfected into HEp-2 cell culture monolayers using 0.2 μg of each plasmid DNA, and cells were incubated for 72 hours. Cells were fixed, immunostained, and imaged as described below.

Fixation and immunostaining. Cells were fixed with 3.7% (w/v) paraformaldehyde in phosphate buffered saline (PBS) for 10 min. Cells were permeabilized with 0.3% (w/v) Triton X-100 and 3.7% paraformaldehyde in PBS for 10 min at RT. After fixation, cells were blocked in 3% (w/v) BSA in PBS for 60 min followed by addition of primary antibody (ab) in the blocking solution for 60 min. Cells then were washed three times in PBS, and species-specific IgG Alexa Fluor (Invitrogen) was added at a dilution of 1:1,000 in block solution for 60 min to detect primary abs. Cells were washed three times in PBS and fixed on glass slides using Prolong Antifade kit (Invitrogen). All steps were performed at room temperature (RT). Images were obtained on a Zeiss inverted LSM510 confocal microscope using a 40x / 1.30 Plan-Neofluar or 63x/1.40 Plan-Apochromat oil lens. Anti-RSV M (clone B135), anti-RSV P protein (clone 3_5), and anti-RSV N protein (clone B130) monoclonal abs were a kind gift of Earling Norrby and Ewa Bjorling. An anti-RSV F protein humanized mouse monoclonal ab (palivizumab; MedImmune) was obtained from the Vanderbilt Pharmacy. F-actin was visualized using rhodamine phalloidin, and TO-PRO-3 iodide was used to visualize the nucleus (Invitrogen). Tubulin was visualized using an antibody to the alpha-tubulin (Abcam).

Imaging with RSV-specific RNA probe and live cell delivery. Single-copy sensitive RNA probes designed to target the RSV genomic gene-start regions were delivered into RSV *wt*- or mock-infected HEp-2 cells using streptolysin O reversible permeabilization 24 hours after inoculation, as previously described (81). After probe delivery, cells were immunostained for RSV proteins as described above. Images were processed in Volocity imaging software (version 5.1; Improvision). Shadow and highlight input sliders were adjusted to the beginning and end of the histogram curve to optimize tonal levels for the entire image; middle tones were not adjusted.

VLP assay with ^{35}S methionine and ^{35}S cysteine metabolic labeling. For each sample, 3 million HEK 293T cells were transfected using program Q-001 on an Amaxa electroporator with Nucleofector solution V and 5 μg of total DNA. After electroporation, cells were plated in 6 well plates that were pre-coated with poly-L-lysine in normal growth media. For the RSV infection, HEK 293T cells were inoculated with *wt* RSV stain A2 at an MOI=0.1. After a 5 hour recovery period, cell were transferred to 10% (v/v) dialyzed FBS containing DMEM that lacked the amino acids cysteine and methionine. ^{35}S-cysteine and ^{35}S-mehionine were added to the labeling media at 50 μCi/mL. After 72 hours, cell lysates were harvested using a single detergent lysis buffer (50 mM Tris-HCl, 150 mM NaCl, 1% Triton X-100, pH 8.0) containing 1:200 dilution of mammalian protease inhibitor cocktail (Sigma). Cell supernatant was clarified using low speed centrifugation and pelleted through a 20% sucrose cushion using a Sorvall AH-650 rotor at 28,000 rpm for 3 hours. Pellets were resuspended in 60% iodixanol and layered on top with 40% and 10% iodixanol. Gradients were centrifuged at 50,000 rpm for 18

hours at 4° C and collected in 1 mL fractions. Each fraction was immunoprecipitated for RSV F using a mixture of three mouse monoclonal antibodies to F (1 μg/mL) and protein G agarose beads. Cell lysates and immunoprecipitations were separated on 4-12% NuPAGE Bis-Tris gels and transferred to Invitrolon PVDF membrane (Invitrogen). Membranes were dried, and exposed to Kodak BioMax MS-1 autoradiography film using a Kodak Biomax TransScreen LE and incubated at -80° C for 2-7 days before film was developed.

Cytoskeletal inhibitors. HEp-2 cells were treated with actin or tubulin inhibitors, as previously described (50). Briefly, cytochalasin D (Sigma) was prepared at 2 mg/ml in ethanol; latrunculin A (Enzo Life Sciences) at 1 mg/ml in ethanol; nocodazole (Sigma) at 10 mg/ml in DMSO; and paclitaxel (Sigma) at 25 mg/ml in ethanol. Inhibitor concentrations were optimized previously for maximum effect by cell morphology with the least amount of toxicity. For immunostaining, HEp-2 cell monolayers on 12 mm micro cover glasses (VWR, No. 2) were inoculated at an MOI=1.0 and incubated with medium containing either vehicle or the indicated inhibitor for 24 hr.

RSV infections and viral titration. For quantification of viral yield in the presence of inhibitors, HEp-2 cell monolayers were inoculated at an MOI=0.05. Cells were then washed and medium was added containing either vehicle or indicated inhibitor. At 3 days post infection, cell supernatant was harvested and normalized for volume. The samples were then clarified of cellular debris by centrifugation in a microcentrifuge at 13,000 rpm for 10 min. The resulting supernatant was designated as supernatant virus. The cell

monolayer was resuspended in an equal volume of medium, scraped, and freeze/thawed 3x using a dry ice/ethanol bath and a 37 °C water bath. The samples then were clarified of cellular debris by centrifugation in a microcentrifuge at 13,000 rpm for 10 min. The resulting solution was designated cell-associated virus.

Flow cytometric assay for quantitative surface expression of RSV F. HEp-2 cells were inoculated with RSV for 1 hour at 37 °C at an MOI=3.0. The inoculum then was removed and each inhibitor was added, as described above. After 24 hours, cells were treated with 20 mM EDTA in PBS to form a single cell suspension. Cells were washed two times in wash buffer (2% FBS in PBS) and then incubated with palivizumab at 1 μg/mL for 30 min at RT. An Alexa Fluor goat anti-mouse 488 secondary antibody suspension was used at a final concentration of 2 μg/mL. Cells were analyzed on a five-laser custom LSR II flow cytometer (Becton Dickinson) in the Vanderbilt Medical Center Flow Cytometry Shared Resource. Data analysis was performed using FlowJo (version 7.6.1). Weighted mean fluorescent intensity (MFI) was calculated by multiplying the raw mean fluorescent intensity by the frequency of positive cells. Statistical analysis was performed using a Student *T*-test of three independent experiments. P values less than 0.05 were considered significant.

Live imaging of viral filaments. MDCK cells were grown on Mattek glass bottom dishes and infected with RSV at an MOI=1.0 for 18-24 hours. RSV genomic probes were delivered as described above, and live cells were imaged using a Zeiss Axiovert 200M microscope with an 63x, NA 1⁄4 1.4 Plan-Apochromat objective, using Chroma 49004

ET-Cy3 and 49006 ET-Cy5 filter sets, with 350-ms exposures. An EXFO excite 120 light source with a ND (neutral density) 1⁄4 0.4 (40% transmission) was used for fluorescence excitation, and a Hamamatsu ORCA-ER AG for taking digital images. Videos were deconvolved using Volocity iterative deconvolution algorithm (81).

Results

RSV infection induced virus filaments that contain viral structural proteins and viral genomic RNA. I first tested whether the cell-surface filaments induced by RSV infection of epithelial cells contained all of the expected RSV structural proteins. HEp-2 cell monolayer cultures were inoculated with *wt* RSV strain A2 and incubated in complete growth medium for 24 hours. The cell monolayers were fixed and immunostained for RSV F, M, N, or P protein. In addition, we also stained cells for the presence of RSV genomic RNA using a fluorescently-conjugated probe designed to hybridize to RSV gene start sequences (81). Figure 2-1 shows RSV filaments protruding from the cell membrane (A-P). Morphologically, these filaments often were clustered and kinked, and they stained brightly with antibodies to RSV F protein. The filamentous structures contained RSV F, M, N, P, and viral RNA, indicating that both structural and genomic components are present. Thus, these filaments likely are virions assembling at the plasma membrane prior to budding.[1]

[1] This figure has been previously published as part of an original manuscript. Shaikh et al. 2012. A critical phenylalanine residue in the respiratory syncytial virus fusion protein cytoplasmic tail mediates assembly of internal viral proteins into viral filaments and particles. mBio. 2012 Feb 7;3(1). pii: e00270-11. doi: 10.1128/mBio.00270-11. Print 2012

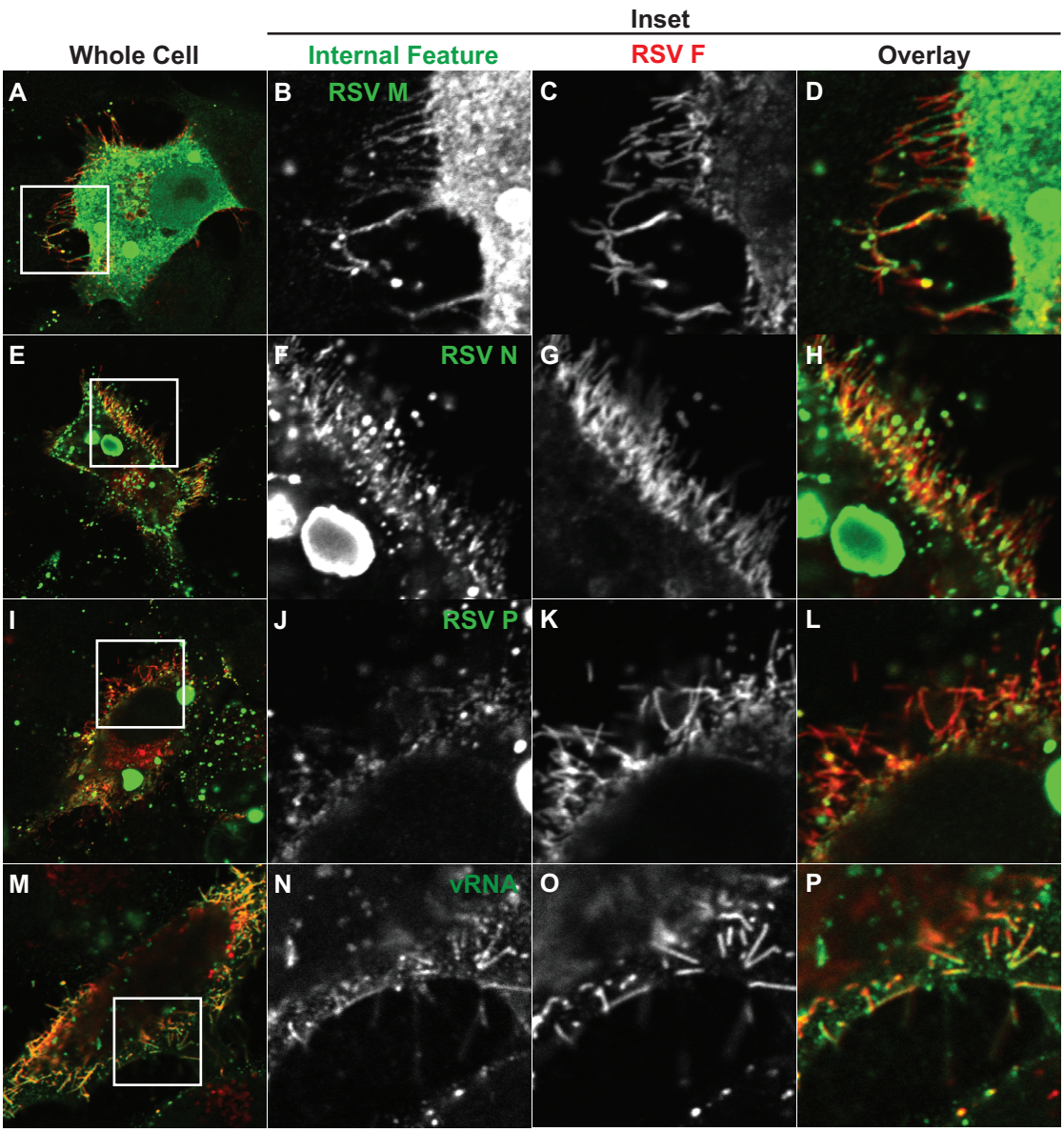

Figure 2-1. RSV F, M, N, P, and viral RNA localize to viral filaments during infection. HEp-2 cells were inoculated with RSV strain A2 at a MOI=1.0 and incubated for 24 hours. RSV F, M, N, and P were detected by indirect immunofluorescence; vRNA was detected using an RNA probe specific to the RSV genomic gene start sequences; actin was detected using phalloidin. Column 1 (panels A, E, I, and M) shows the entire cell. Panels B-D, F-H, J-L, and N-P show an enlargement of the inset shown in column 1. Column 2 (panels B, F, J, and N) shows RSV M, N, P, vRNA, or phalloidin staining only; column 3 (panels C, G, K, and O) shows RSV F only; and column 4 (panels D, H, L and P) shows the overlay with RSV F in red and RSV M, N, P, vRNA, or actin in green.

RSV virus-like filaments can be generated independent of viral infection. I next sought to determine the minimal requirements for RSV filament formation by transfecting combinations of plasmids encoding RSV proteins. Transfection of cDNAs encoding RSV F, M, N, and P genes into HEp-2 cells induced formation of virus-like filaments that resembled viral filamentous structures formed during infection. Figure 2-2 A-D shows a representative image of filaments formed when these four RSV structural proteins were expressed in HEp-2 cells. Consistent with RSV filaments formed during infection, virus-like filaments contained RSV proteins and were often kinked, clustered, and stained brightly for the F protein (Fig. 2-2A). RSV M was also present in these transfection based filaments (Fig. 2-2B), as were RSV N and P. RSV F was necessary for virus-like filament formation (Fig. 2-2 E-H), and in fact, exclusion of any single gene of the four during transfection eliminated filament formation (Fig. 2-2 I-T). Thus, the filaments formed using the transfection-based assay were similar to filaments formed during viral infection in both morphology and composition. [2]

Expression of RSV viral filament proteins also results in budded particles that contain F, M, N, and P. To determine whether expression of these four proteins could lead to production of budded particles, we developed a VLP assay using HEK 293T cells and radiolabeling, which was necessary due to the inefficiency of RSV VLP formation and subsequent inability to detect viral proteins by immunoblot. Figure 2-3A shows an overall schematic of the assay. Cells were transfected with empty vector, F only, or with

[2] Investigations into the minimum requirements for virus-like filament formation were based on the similar studies performed other members of the Crowe laboratory: Thomas Utley, Sunny Mok, and Mike Lindquist.

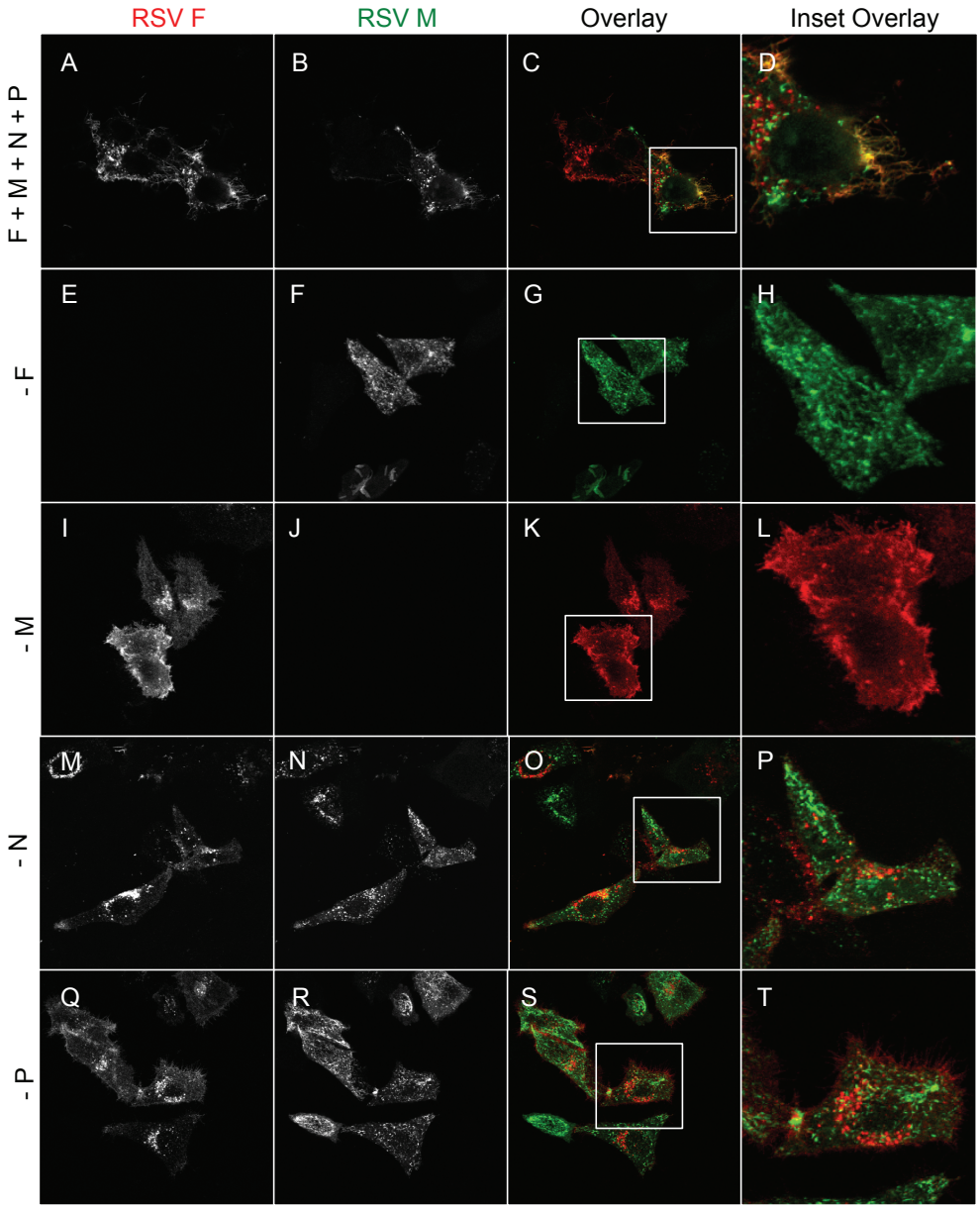

Figure 2-2: RSV F, M, N, and P are necessary and sufficient for generation of filaments independent of viral infection. HEp-2 cells were transfected with plasmids encoding cDNAs for all four proteins (F, M, N, and P) or with three proteins, with the missing protein indicated for the row. Column 2 (panels A, E, I, M, and Q) shows RSV F staining. Column 2 (panels B, F, J, N, and R) shows RSV M staining. Column 3 (panels C, G, K, O, and S) shows the overlay of columns 1 and 2 with RSV F in red and RSV M in green. Column 4 (panels D, H, L, P, and T) shows an enlargement of the inset indicated in column 3.

all four proteins. Cells were metabolically labeled with ^{35}S-methionine and ^{35}S-cysteine for 72 hours. Cell lysates were harvested, and expression of each protein was confirmed by immunoprecipitation with an antibody directed against each individual protein. Figure 2-3B shows the result of cell lysate immunoprecipitations. When transfected with plasmids encoding cDNAs for all four proteins, each was able to be detected using immunoprecipitation by their respective antibodies. RSV P, however, could not be detected due to the lack of available purified antibody. Supernatant from hybridoma clone 3_5 was used for immunoprecipitation, but insufficient antibody was present to detect the viral protein.

To detect budded particles, cell supernatants were clarified to remove cell debris, pelleted through a 20% sucrose cushion to remove free protein, and subjected to an iodixanol flotation gradient. Fractions from the flotation gradient were immunoprecipitated using a mixture of monoclonal antibodies to the F protein, separated using SDS-PAGE, and visualized by exposure to film using a ^{35}S intensifying screen. Figure 2-3C shows that in contrast to empty vector and F only controls, protein bands that correspond to the appropriate size of all four proteins were detected in the same flotation gradient fraction by immunoprecipitation using F-specific antibodies. These data suggest that all four proteins are present in particles that contain the F protein. In contrast to the cell lysates, a band corresponding to the P protein is detectable, since P is likely in the same particle as F. Additionally, cells were infected with RSV, and viral particles were harvested and processed in a similar manner as transfected samples. Figure 2-3D shows

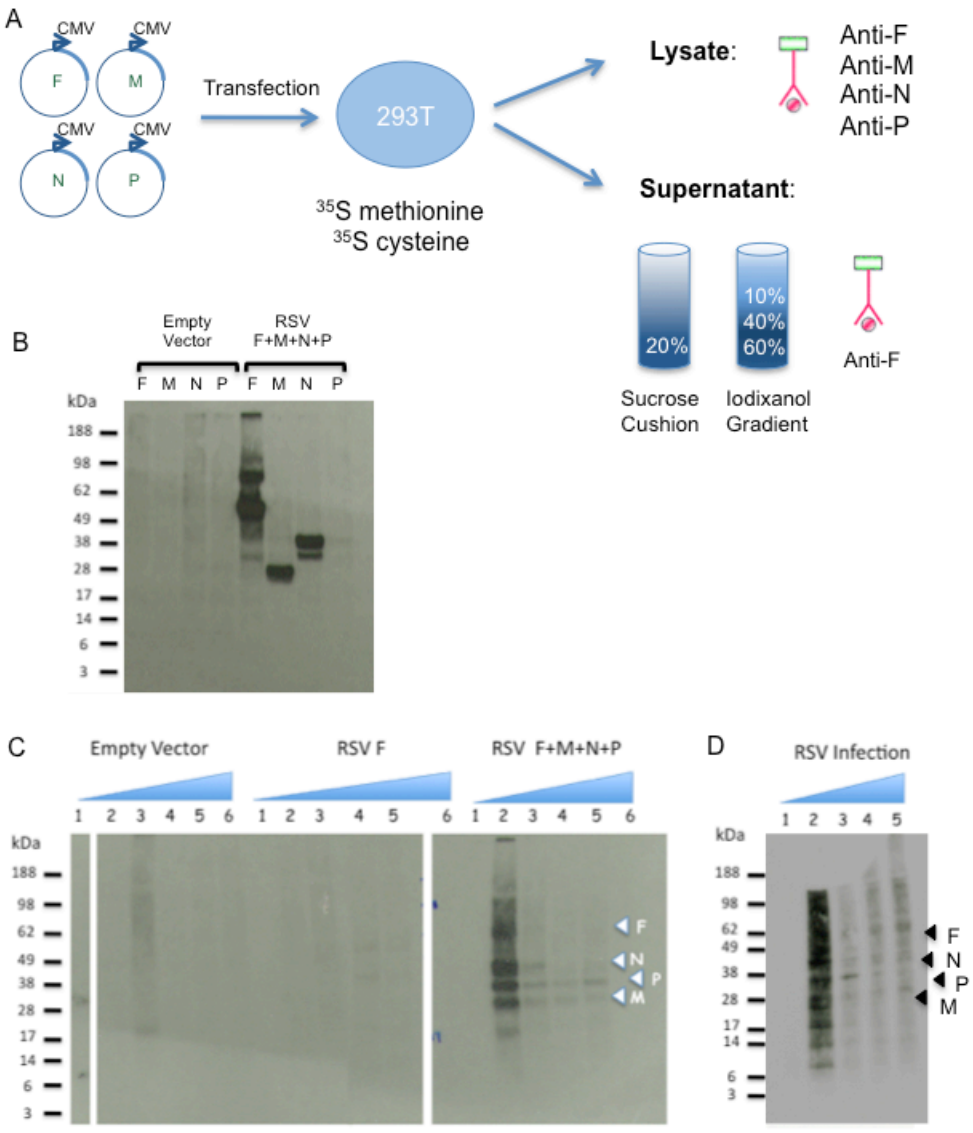

Figure 2-3: Expression of RSV F, M, N, and P results in budded particles containing all four proteins that are detectable using a ^{35}S-VLP assay. Panel A shows a schematic of the VLP assay. Panel B: total cell lysate was collected from transfected cells and bands were detected by immunoprecipitations with the corresponding antibody or hybridoma supernatant. Panel C: cell supernatant from transfected or infected cells was clarified, pelleted through a sucrose cushion, and floated on an iodixanol gradient. Bands were detected after immunoprecipitation with an antibody to F.

that virions are present the same density as VLPs, indicating that VLPs recapitulate viral budding. [3]

Viral filaments are distinct from cytoskeleton-based host protrusions at the cell surface. To adhere to the extracellular matrix, a host cell must use both cellular junctions and cytoskeleton-based protrusions (*e.g.,* microvilli, filapodia, lamellipodia, and membrane ruffles). Since RSV filaments resemble host cell protrusions that contain cytoskeletal proteins, we next sought to determine whether viral filaments are distinct from cell projections. Therefore, I visualized F-actin using phalloidin and tubulin using an antibody to alpha-tubulin. Figure 2-4 panels A-E show that viral filaments, marked by the presence of RSV F protein, did not contain F-actin, and panels F-J show that tubulin is also not present in filaments. Although the viral and host filamentous structures often occurred in the same regions of the plasma membrane, viral filaments were distinct from the cell projections that contained cytoskeletal proteins. These data are consistent with previously published data showing that F-actin is not found in viral filaments (47).

Viral filaments are formed by selective sorting of viral proteins into filaments and exclusion of both cytosolic and membrane proteins. Although F-actin is excluded from viral filaments, other studies have shown that β-actin can localize to viral filaments and budded virions (75, 95) and that actin-associated signaling pathways are important for RSV filamentous assembly (39). Previously, others in the Crowe laboratory found that

[3] Radiolabeling VLP studies were performed in collaboration with Sunny Mok, a former post-doctoral fellow in the laboratory of James Crowe.

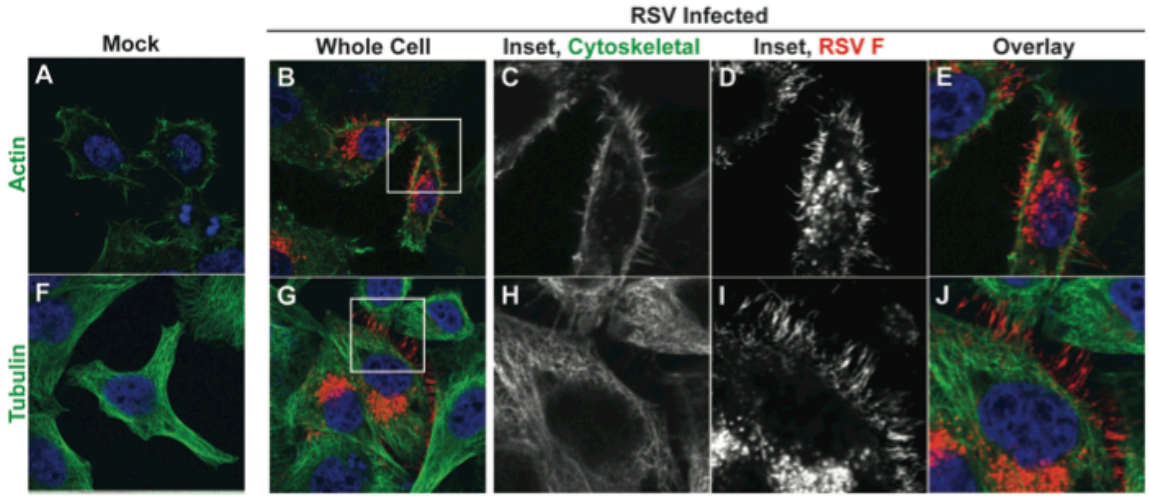

Figure 2-4: Viral filaments are distinct from host structures that contain actin or tubulin. Mock or RSV-infected HEp-2 cells were stained for F and actin or tubulin. Panels A and F show mock infected cells. Panels B and G show RSV infected cells. Panels C-E and H-J show an enlargement of the inset shown in panels B and G. Panels C and H show actin and tubulin staining only, respectively; panels D and I show F staining only; and panels E and J show the overlay with F in red and actin or tubulin in green.

disruption of the function of the apical recycling endosome (ARE) reduced RSV assembly and budding but did not interrupt trafficking of viral proteins to the cell surface (9). Additionally, many actin-associated proteins are found in myosin Vb-marked endosomes when the function of the protein was disrupted during RSV infection (Thomas Utley, unpublished data)[4]. I sought to replicate some of these data in HEp-2 cells by determining whether these actin-associated proteins localized to viral filaments. HEp-2 cell culture monolayers were either mock-infected or infected with *wt* RSV and incubated for 24 hours in complete growth medium. Figure 2-5 shows the localization of these proteins in mock- and RSV-infected cells. I first examined members of the ezrin, radixin, and moesin (ERM) family of proteins. Ezrin localized diffusely throughout the cytoplasm and to membrane protrusions at the cell surface (Fig. 2-5A). These protrusions, however, were distinct from viral filaments that form at the cell surface in RSV-infected cells (Fig. 2-5B). Moesin and radixin localized largely underneath the plasma membrane and also to membrane protrusions (Fig. 2-5C and 2-5E, respectively). Like ezrin, neither of these proteins co-localized with RSV F in viral filaments but remained in distinct host structures (Fig. 2-5D and 2-5F, respectively).

Next, we examined a number of other actin-associated proteins that either crosslink actin or connect the cortical actin network to the plasma membrane. Eplin, an actin crosslinker, did not localize to viral filaments (Figure 2-5G and 2-5H). EBP50, a scaffold protein that connects membrane proteins to ERM proteins, localized diffusely throughout the cytoplasm (Fig. 2-5I and 2-5J), but was excluded from viral filaments

[4] This work has been described previously as part of Thomas J. Utley's thesis entitled, "Investigations into the assembly and budding of respiratory syncytial virus."

(Fig. 2F). Annexin A2 is another protein that has been reported to link membrane glycoproteins to the actin cytoskeleton. Although this protein localized diffusely throughout the cell (Fig. 2-5K), it did not localize to viral filaments (Fig. 2-5L). Finally, we examined two α-actinin proteins that are members of the large and diverse spectrin family of proteins. The α-actinin 1 and 4 proteins, which are expressed in non-muscle cells, are actin-binding proteins that are involved in actin crosslinking and also may mediate attachment of the plasma membrane to the actin cytoskeleton (47). While α-actinin 1 was excluded from viral filaments completely (Fig. 2-5M and 2-5N), α-actinin 4 showed some minor co-localization with viral filaments, with variation from cell to cell (Fig. 2-5O and 2-5P). These data suggest that most actin-associated proteins are excluded from viral assembly structures, again providing evidence for specific sorting of proteins into viral filaments and exclusion of host proteins including cytoskeletal elements.

Next, I sought to determine whether membrane proteins were sorted selectively or excluded from viral filaments. I used two membrane-protein constructs, YFP-GL-GPI and YFP-GT46 to mark raft or non-raft membrane microdomains, respectively. These constructs were a gift from Anne Kenworthy at Vanderbilt University and have been described previously (52). YFP-GL-GPI is a GPI anchored membrane protein that associates with lipid rafts, while the YFP-GT46 membrane protein does not localize to lipid rafts (52). Figure 2-6 shows that while both membrane proteins localized to the plasma membrane (panels A and F), neither YFP-GL-GPI (panels B-E) nor YFP-GT46 (panels G-J) were present in viral filaments marked by RSV F. These data indicate that viral glycoproteins are selectively sorted into viral filaments.

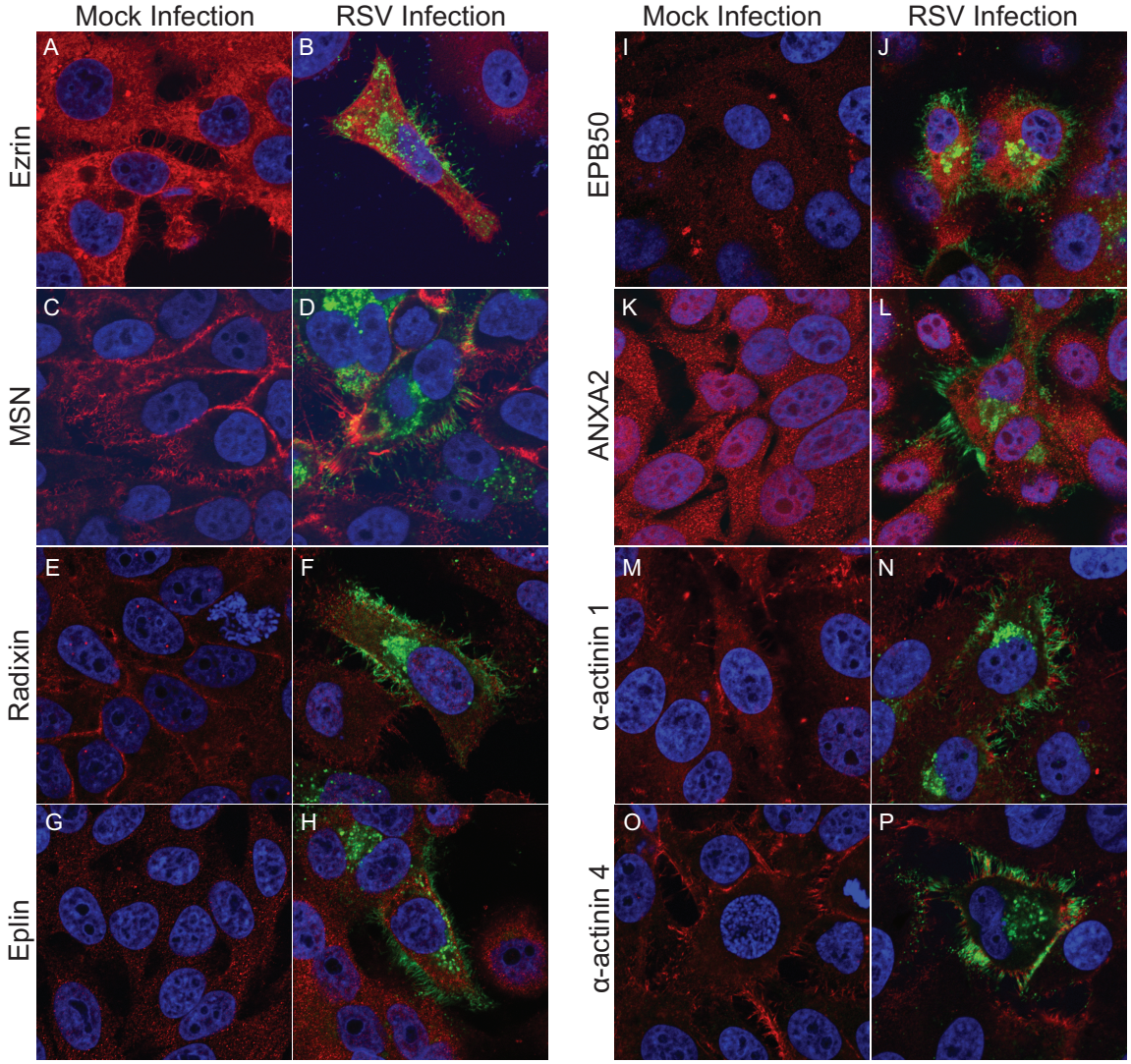

Figure 2-5: Actin associated cytoskeletal proteins are excluded from viral filaments. HEp-2 cells were inoculated with RSV stain A2 at an MOI=1.0 and incubated for 24 hours. RSV F and the indicated cellular proteins were detected by indirect immunofluorescence. Columns 1 and 3 (panels A, C, E, G, I, K, M and O) show mock infected cells, while columns 2 and 4 (panels B, D, F, H, J, L, N, and P) show RSV infected cells. RSV F is shown in green and the indicated cellular protein is shown in red.

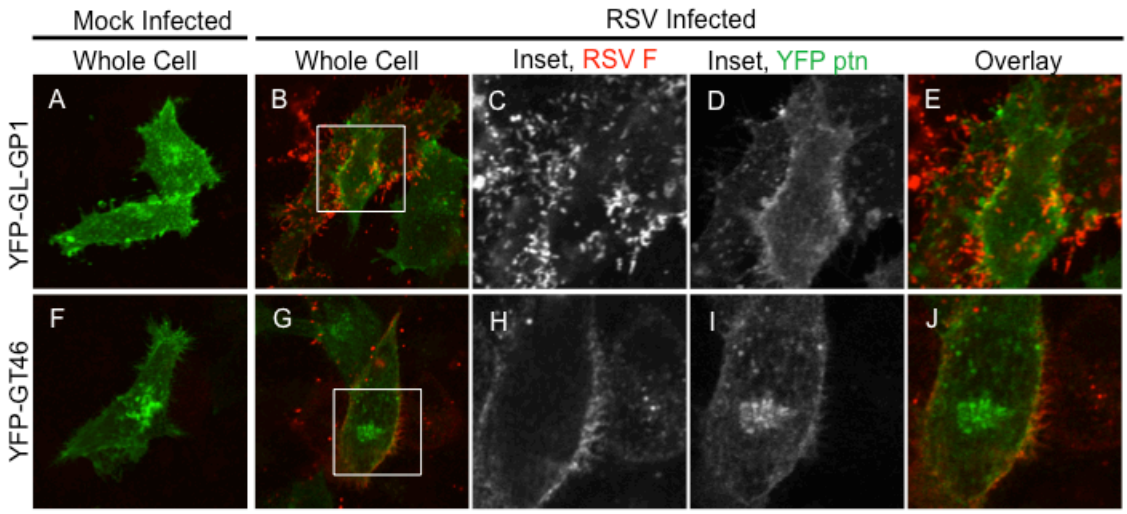

Figure 2-6: Raft and non-raft membrane protein constructs are excluded from viral filaments. HEp-2 cells were transfected with plasmids encoding YFP-GL-GP1 or YFP-GT46 and inoculated with RSV. Panels A and F show mock-infected HEp-2 cells with the indicated YFP construct. Panels B-E and G-J show RSV-infected cells with the indicated YFP construct. Panels B and G show the whole cell with F in red and the YFP protein in green. Panels C-E and H-J show an enlargement of the inset in panels B and G, respectively. Panels C and H show F staining only; panels D and I show the YFP protein staining only; and panels E and J show the overlay with F in red and the YPF protein in green.

Cytoskeletal rearrangement is not necessary for viral assembly into filaments. Since actin-associated proteins are mostly excluded from viral filaments and may not affect viral replication, I and a rotation student in the Crowe laboratory, Ryan Craven, next sought to determine whether cytoskeletal polymerization is necessary for viral assembly into filaments. Nicole Kallewaard, a former graduate student in the Crowe laboratory, had determined previously the inhibitor concentrations that resulted in maximum affect on the cytoskeleton with the least cellular toxicity (50). The effect of inhibitor concentrations on virus replication was determined to be similar to the previously reported results, showing 0.95 to 2.4 $\log_{10}$ pfu/mL reduction in supernatant-associated virus and 0.6 to 1.6 $\log_{10}$ pfu/mL reduction in cell-associated virus (Figure 2-7Q).

Using the same conditions, I tested whether gross cytoskeletal disruptions affected viral assembly into filaments. HEp-2 cell culture monolayers were inoculated with *wt* RSV strain A2 and incubated in growth medium containing the indicated inhibitor or vehicle for 24 hours. Cells were immunostained for RSV F protein to mark viral filaments and for actin or tubulin, depending on which cytoskeletal function was disrupted. Remarkably, viral assembly into filaments at the cell surface was not inhibited when actin or tubulin polymerization was disrupted (Fig. 2-7A-P). Cells treated with cytochalasin D (Fig. 2-7B and 2-7D) or latrunculin A (Fig. 2-7F and 2-7H) showed a lack of cortical actin structure underneath the plasma membrane. However, this disruption did not affect the formation of viral filaments (Fig. 2-7D and 2-7H). Viral filaments, however, often appeared to originate from depolymerized actin aggregates (highlighted by the insets in Fig. 2-7D and 2-7H). These images suggest that although actin polymerization is not necessary for viral filament formation, actin or actin-related

proteins in these aggregates may play in anchoring filaments. Inhibition of tubulin polymerization using nocodazole (Fig. 2-7I-L) or depolymerization of tubulin using paclitaxel (Fig. 2-7M-P) also did not affect viral assembly into filaments. Finally, we determined whether F protein surface expression was altered by disruption of the cytoskeleton, using flow cytometry (Fig. 2-7R). F protein surface expression was not altered in the presence of inhibitors, suggesting that cytoskeletal rearrangements are not necessary for F protein expression or trafficking to the cell surface. Collectively, these data indicate that viral filaments can initiate membrane deformation and elongate by a virus-mediated mechanism distinct from that used by actin- or tubulin-based cellular protrusions.

Since viral assembly into filaments was unaffected at 24 hours post inoculation (h.p.i.)., I next asked whether filaments form at earlier timepoints during infection. Figure 2-8 shows HEp-2 cells that were treated with vehicle, latrunculin A, or paclitaxel. Viral filaments were visualized at 12, 18, or 24 h.p.i. Actin was visualized for vehicle- and latrunculin A-treated cells, and tubulin was visualized for paclitaxel-treated cells. At 12 h.p.i., vehicle-treated cells show many viral filaments. However, the number and length of viral filaments were noticeably reduced in latrunculin A- or paclitaxel-treated cells. Similar results were obtained at 18 h.p.i., though the number of filaments in inhibitor-treated cells did increase compared to cells at 12 h.p.i.. As seen in Figure 2-7, many viral filaments were present at 24 h.p.i.. These data indicate that while viral filamentous assembly occurs when actin or tubulin polymerization is disrupted, cytoskeletal

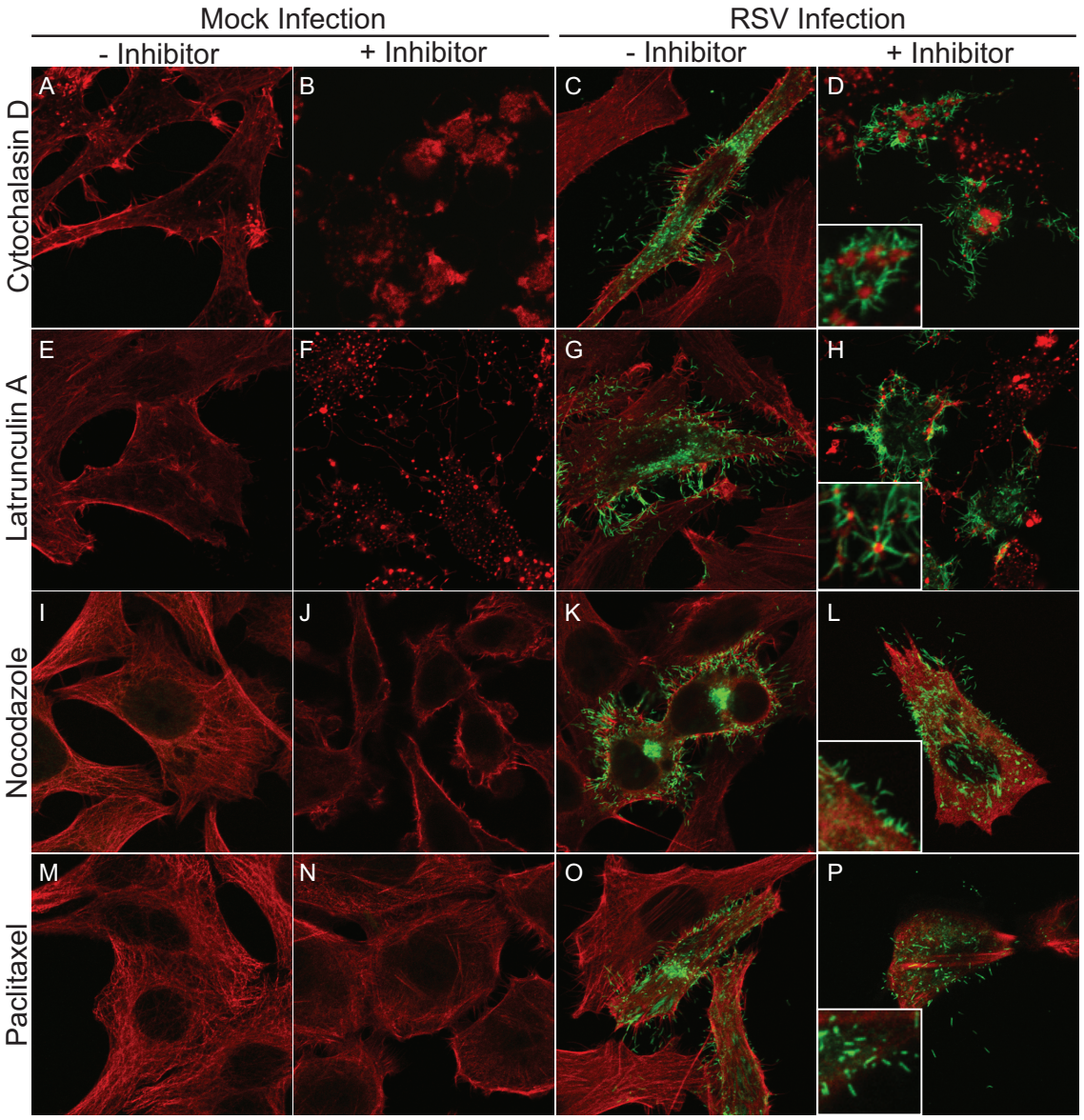

Q

Viral titers with indicated inhibitor (log_{10} pfu/mL)					
Virus Fraction	Vehicle	CytoD	LatA	Noco	Pac
Supernatant	6.0, 5.8	4.3, 4.1	4.5, 4.1	4.9, 5.0	3.7, 3.3
Cell-associated	4.8, 4.9	4.1, 4.0	4.0, 4.1	4.3, 4.2	3.3, 3.2

R

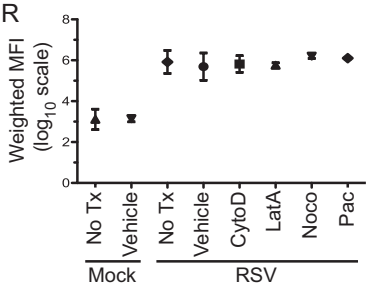

Figure 2-7: Viral assembly into filaments is not dependent on the cytoskeletal polymerization. HEp-2 cells were inoculated with RSV *wt* strain A2 at an MOI=1.0 and incubated for 24 hours with medium containing either vehicle of the indicated inhibitor. At 24 hours cells were fixed, and RSV F, actin, and tubulin were detected by indirect immunofluorescence. Column 1 (panels A, E, I, and M) shows mock-infected cells in the presence of vehicle. Column 2 (panels B, F, J, and N) shows mock-infected cells in the presence of the indicated inhibitor. Column 3 (panels C, G, K, and O) shows RSV-infected cells in the presence of vehicle. Column 4 (panels D, H, L, and P) shows RSV-infected cells in the presence of the indicated inhibitor. Panel Q: HEp-2 cells were infected with RSV at an MOI=0.1 for 72 hours. Supernatant and cell-associated fractions were collected in duplicate and quantified using a viral plaque assay. Viral yields are presented in $\log_{10}$ pfu/mL. Panel R: total surface expression of RSV F was determined by flow cytometric analysis in mock-infected or RSV-infected cells (MOI=3.0) treated with vehicle or the indicated inhibitor for 24 hours. Data are plotted as mean, and error bars represent standard deviation. Weighted mean fluorescence intensity (MFI) is MFI multiplied by the frequency of positive cells.

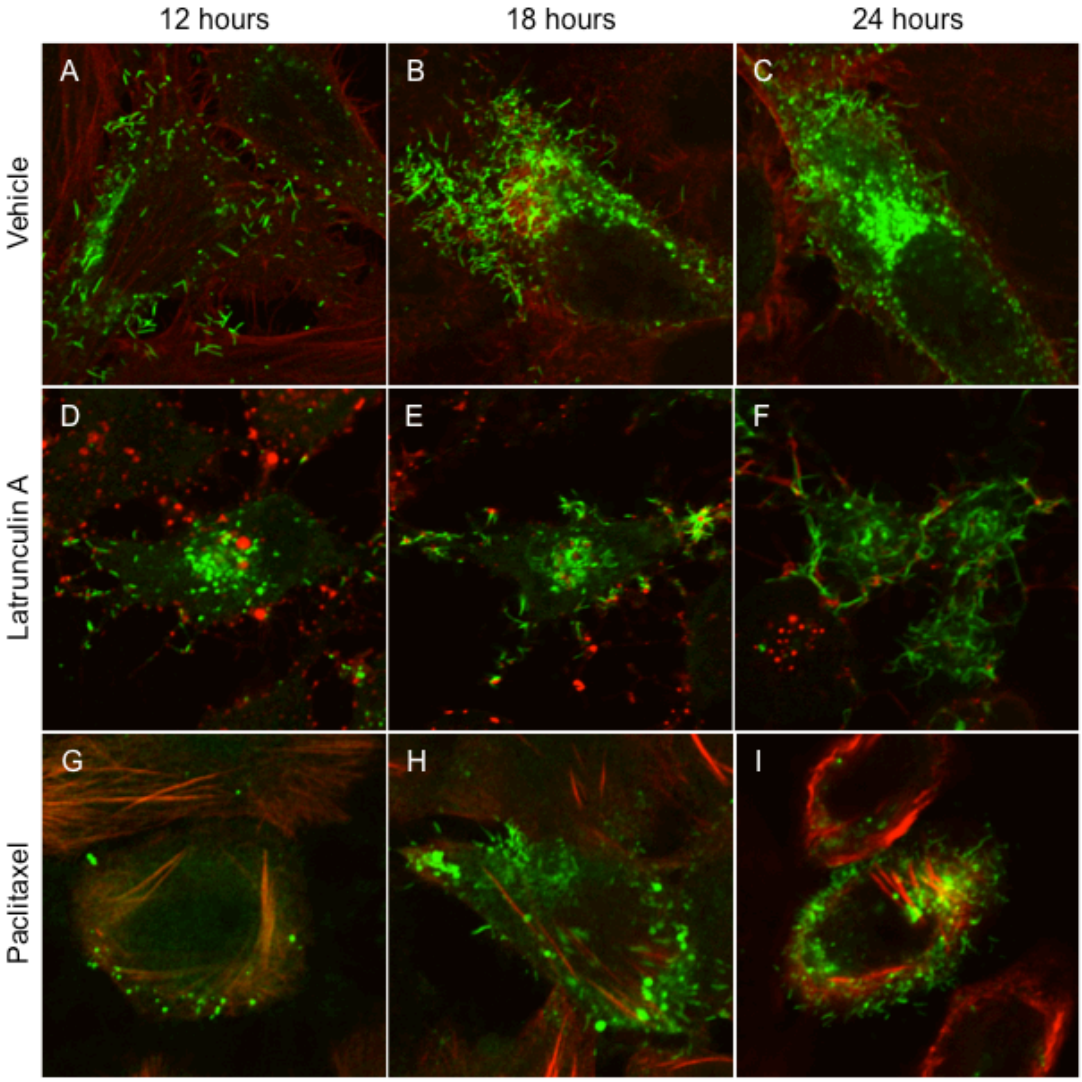

Figure 2-8: Disruption of the cytoskeleton affects the number and length of viral filaments early in infection. HEp-2 cells were inoculated with RSV *wt* strain A2 at an MOI=1.0 and incubated for 12, 18, or 24 hours with medium containing either vehicle of the indicated inhibitor. Cells were fixed, and RSV F, actin, and tubulin were detected by indirect immunofluorescence. Vehicle and latrunculin A treated cells were stained for F and actin. Paclitaxel treated cells were stained for F and tubulin. Column 1 (panels A, D and G) shows cells at 12 h.p.i.; column 2 (panels B, E, and H) shows cells at 18 h.p.i.; and column 3 show cells 24 h.p.i. RSV F is shown in green and actin or tubulin is shown in red.

polymerization may be required for other steps during viral replication or trafficking of host proteins required for viral assembly.[5]

Viral filaments are dynamic structures that may directly bud to form free virions. Although viral filaments contain all of the viral structural and genomic components, no direct evidence exists that viral filaments eventually pinch off from the host membrane to become free virions. To directly visualize viral filaments, I performed live-cell microscopy of RSV-infected cells and labeled the vRNA using the oligonucleotide probe described in Figure 2-1. The cells were imaged, and the resulting videos were deconvoluted using Volocity software to remove out-of-focus light. Figure 2-9 shows a timecourse of images obtained from a single video. The results indicate that viral filaments are not stationary structures on the cell surface. The directional and rotational movement has been described previously, indicating that it is not simply Brownian motion (80). However the source of this motion is unknown. In frame 2-9B, a viral filament (indicated by the white arrow) that was not in focus previously (frame 2-9A) appears in the focal plain. In frames 2-9C through 2-9E, a single viral filament appears to separate from the cell surface and can be seen moving away from the cell surface in frames 2-9F through 2-9I. Due the focal plane of the live-cell imaging and the tendency of RSV to remain cell-associated, the membrane scission event was not visualized.

[5] Cytoskeletal inhibitor studies was performed with assistance from Ryan Craven during a laboratory rotation in the Interdisciplinary Graduate Program in the Biomedical and Biological sciences

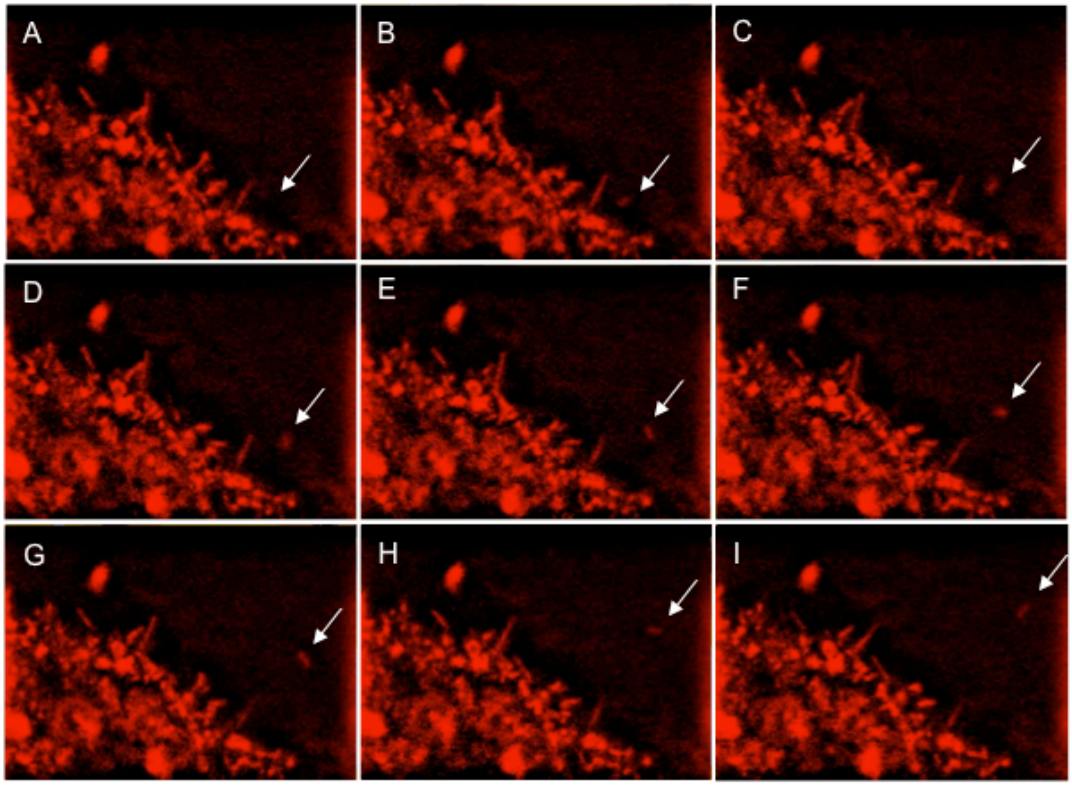

Figure 2-9: Viral filaments may directly become free virions. MDCK cells were infected with RSV and treated with a fluorescent vRNA probe (red). Collected video was deconvoluted using Volocity software. Frames A-I were captured as part of a timecourse using QuickTime player to best illustrate the path of viral filament that may have separated from the cell surface (indicated by the white arrow).

Therefore, further investigation of viral budding using live-cell imaging will be required to determine whether viral filaments eventually become free virions. [6]

Discussion

The mechanism of RSV assembly and budding is of interest since it appears to use an unconventional pathway that is independent of host proteins of the multi-vesicular body apparatus (97). A number of viruses coopt the host cytoskeleton and related proteins to accomplish viral assembly and budding, such as vaccinia virus, PIV3, and many herpesviruses (88). I sought to determine if RSV achieves its unique program using apical cytoskeleton or related proteins for assembly and budding. Although I and others have reported that actin-associated proteins localize in or near viral assembly structures (75), it is remarkable that viral assembly into long, complex filamentous structures that require the manipulation of the plasma membrane can occur without the need for actin polymerization. The data suggest that viral constituents achieve complex tasks at the membrane, including specific sorting of viral proteins into the filaments while excluding most host proteins, extrusion of long membranous structures from the cell without a cytoskeletal infrastructure, incorporation of nucleocapsids, and scission of the membrane to release infectious particles. Viral elements, or recruited host proteins, provide the dynamic mechanical force to initiate and extend viral filaments, not polymerization of the cytoskeleton.

The findings that inhibition of actin polymerization is not required for assembly and budding does not completely exclude the possibility that the cortical actin network or

[6] Live imaging of viral filaments was performed with assistance from Aaron Lifland and Phillip Santangelo at the Department of Biomedical Engineering, Georgia Institute of Technology and Emory University, Atlanta, Georgia, USA

associated proteins still function in an accessory structural role for viral replication. Actin polymerization is necessary for optimal viral replication (15, 47, 50), and our observation of multiple viral filaments radiating from actin aggregates under depolymerizing conditions also supports the hypothesis that actin plays an accessory structural role in replication. In fact, other groups have described actin at the base of viral filaments (47), and β-actin interacts with RSV N (95). Some investigators have reported β-actin in viral particles (75, 95). Furthermore, actin-associated pathways are important for viral filamentous assembly (7, 39). Finally, actin enhances viral transcription, although its role as a transcription enhancing factor does not rely on the ability to polymerize (42).

Since actin does not provide the physical infrastructure for a viral filament, the structure for a complex, kinked viral filament may be determined by the viral proteins themselves. I show here that the four major RSV structural proteins are required for filament formation independent of viral infection and budding of VLPs and that these viral filaments are distinct from actin-based cellular structures. Similarly, a study examining viral filaments by scanning electron microscopy showed that in the absence of the M protein, short filament-like structures with F and G were observed on the cell surface (64). These data suggest that while the viral glycoproteins are sufficient for the initial outward bud formation, the structure of the filament is driven by the M protein. The matrix proteins of other viruses, such as Ebola virus, have been shown to oligomerize into higher order structures (32); it is possible that oligomerization of the RSV M protein is responsible for elongation of the structure of viral filaments. Nevertheless, the remarkable finding of this study is that complex, structured RSV

filaments form apparently normally even when actin or microtubule function is completely inhibited.

Chapter summary

In this chapter, I present data that characterizes RSV assembly into filaments at the cell surface. I show that the minimum requirements for viral filament assembly and budding of VLPs are four structural proteins: F, M, N, and P. Second, I show sorting of viral protein constituents for viral assembly into filaments is a process that is highly regulated, involving viral proteins while excluding the host cytoskeleton, actin-associated proteins, and host lipid-raft and non-raft membrane proteins. Third, I show that the physical structure of viral filaments does not depend on rearrangement of the actin or tubulin cytoskeleton, although inhibition of cytoskeletal rearrangement does affect optimal viral replication. Finally, I show that viral filaments may directly become free virions. These data indicate that viral assembly into filaments is largely driven by viral proteins.

Chapter III

A CRITICAL PHENYLALANINE RESIDUE IS REQUIRED FOR VIRAL FILAMENTOUS ASSEMBLY AT THE CELL SURFACE[7]

Introduction

Previously, others in the Crowe laboratory showed that the F protein traffics to the apical surface in the absence of any other viral protein or viral RNA and that the F-protein cytoplasmic tail (F CT) was dispensable for apical trafficking (10). It is unlikely, however, that a paramyxovirus would retain such a domain if it did not play some role in replication or pathogenesis, and indeed other investigators showed that a virus lacking the F CT had a 100- to 1,000-fold decrease in viral titers in a multicycle growth curve. This mutant virus did not form filaments at the cell surface but was capable of mediating cell-cell fusion (8, 69). Furthermore, the cytoplasmic tail (CT) of many paramyxovirus glycoproteins is important for assembly and budding (43).

Since the F CT is required for efficient replication but not for fusion or trafficking, I hypothesized that the F CT coordinates the assembly of viral proteins into filaments at the cell surface. In this chapter, I demonstrate that a key phenylalanine (Phe) residue at position 22 in the F CT is critical for RSV assembly into filaments at the cell surface. Moreover, when this Phe was mutated, RSV F could not recruit RSV M, N, and P efficiently into VLPs. These findings indicate that the F CT, and specifically Phe22 of

[7] Data in this chapter were published in Shaikh *et al.* 2012. A critical phenylalanine residue in the respiratory syncytial virus fusion protein cytoplasmic tail mediates assembly of internal viral proteins into viral filaments and particles. mBio. 2012 Feb 7;3(1). pii: e00270-11. doi: 10.1128/mBio.00270-11. Print 2012

the F CT, is responsible for recruitment of internal viral proteins into filamentous structures at the cell surface for efficient assembly and subsequent budding.

Materials and methods

Cell culture and *wt* RSV virus preparations. HEp-2 cells (ATCC CCL-23) were maintained in Opti-MEM I medium (Invitrogen) containing 2% (vol/vol) fetal bovine serum (FBS), 1% (vol/vol) l-glutamine, 2.5 μg/ml amphotericin B, and 1% (vol/vol) penicillin-streptomycin. Suspension 293-F cells were maintained as recommended by the manufacturer (Freestyle 293 Expression System; Invitrogen). Transfections were performed using the Effectene transfection reagent (Qiagen) for HEp-2 cells and the Polyfect transfection reagent (Qiagen) for 293-F cells. The RSV *wt* strain A2 was expanded in HEp-2 cells.

RSV infections. For filament visualization, HEp-2 cell monolayers on 12-mm micro-cover glasses (no. 2; VWR) were inoculated at a multiplicity of infection (MOI) of 1.0 and incubated for 24 h. For flow cytometric analysis, HEp-2 cells in tissue culture flasks were inoculated at an MOI of 3.0 and incubated for 24 h. For the virus-like particle (VLP) assay, 293-F cells were infected at an MOI of 0.05 for 72 h.

Generation of RSV F protein mutant constructs. All DNAs encoding the RSV fusion (F) protein constructs in this study were made from a sequence-optimized cDNA encoding the RSV *wt* strain A2 F protein in the pcDNA3.1 plasmid vector (Invitrogen) (5). DNAs encoding RSV F proteins with truncations or other alterations of the cytoplasmic tail at

the C terminus of the protein were cloned using PCR primers to amplify the desired length of the tail and subcloned into pcDNA3.1. Targeted mutations, insertions, or deletions were introduced using the Lightning site-directed mutagenesis kit (Stratagene) and confirmed by sequencing.

Filament formation. Plasmids encoding the *wt* or a mutant RSV F protein along with pcDNA3.1 plasmids containing inserts encoding the RSV A2 strain matrix (M), nucleoprotein (N), and phosphoprotein (P) gene (synthesized by GeneArt, Regensburg, Germany) were transfected into HEp-2 cell culture monolayers using 0.2 μg of each plasmid DNA, and cells were incubated for 72 h. Cells were fixed, immunostained, and imaged as described below. All images for virus-like filament formation were collected in a single experiment using identical microscopy parameters.

Fixation and immunostaining. Cells were fixed with 3.7% (*wt*/vol) paraformaldehyde in phosphate-buffered saline (PBS) for 10 min. Cells were permeabilized with 0.3% (*wt*/vol) Triton X-100 and 3.7% paraformaldehyde in PBS for 10 min at room temperature (RT). After fixation, cells were blocked in 3% (*wt*/vol) bovine serum albumin (BSA) in PBS for 60 min, followed by addition of primary antibody (Ab) in the blocking solution for 60 min. Cells were then washed three times in PBS, and species-specific IgG Alexa Fluor (Invitrogen) was added at a dilution of 1:1,000 in block solution for 60 min to detect primary Abs. Cells were washed three times in PBS and fixed on glass slides using the Prolong Antifade kit (Invitrogen). All steps were performed at RT. Images were obtained on a Zeiss inverted LSM510 confocal microscope using a 63×/1.40 Plan-Apochromat oil

lens. Anti-RSV M (clone B135), anti-RSV P protein (clone 3_5), and anti-RSV N protein (clone B130) monoclonal Abs were a kind gift of Earling Norrby and Ewa Bjorling. An anti-RSV F protein humanized mouse monoclonal Ab (palivizumab; MedImmune) was obtained from the Vanderbilt Pharmacy. F-actin was visualized using rhodamine phalloidin, and TO-PRO-3 iodide was used to visualize the nucleus (Invitrogen).

Quantitative analysis of images. To determine filament length, images from 12 high-powered fields were obtained on a Zeiss inverted LSM510 confocal microscope using a 40×/1.30 Plan-Neofluar oil lens. Images were analyzed using laser scanning microscopy (LSM) image acquisition software (Rel 4.2; Zeiss). The length of virus-like filaments was determined using the ruler tool in the LSM software to trace individual filaments in the images. The four longest filaments measured per cell were used in calculation of overall filament length for each construct. For quantitation of the percentage of RSV F-transfected cells showing filaments, images from 20 high-powered fields were collected on a Zeiss inverted LSM510 confocal microscope using a 20×/0.75 Plan-Apochromat lens. The percentage of RSV F-transfected cells with filaments was calculated by counting the total number of RSV F-transfected cells with filaments and dividing that number by the total number of RSV F-transfected cells.

Quantitative analysis of total cell lysate. HEp-2 cells in 6-well plates were transfected with 0.4 μg of plasmid DNA encoding the indicated F-protein cytoplasmic tail (CT) construct using the Qiagen Effectene transfection reagent. Cells were harvested at 48 h after transfection using a single detergent lysis buffer (50 mM Tris-HCl, 150 mM NaCl,

1% Triton X-100, pH 8.0) containing a 1:200 dilution of mammalian protease inhibitor cocktail (Sigma). Lysates were separated on 4 to 12% NuPAGE Bis-Tris gels and transferred to polyvinylidene difluoride (PVDF) membranes using an iBlot dry blotting system (Invitrogen). Membranes were blocked for 1 h using Odyssey blocking buffer (Li-Cor) diluted 1:1 in PBS. Primary abs for β-actin (1:5,000; Abcam) or the RSV F protein (motavizumab expressed from recombinant cDNA; 0.85 μg/ml) were diluted in blocking buffer diluted 1:1 with PBS + 0.1% Tween 20 (PBS-T), applied to membranes, and incubated overnight at 4°C. Membranes then were washed four times in PBS + 0.1% Tween for 5 min each. Secondary abs were diluted 1:2,500 (goat anti-human IRDye 680CW; Kirkegaard & Perry Labs Inc.) or 1:5,000 (goat anti-mouse IRDye 800CW; Li-Cor) in blocking buffer and added to each membrane for 60 min. Membranes were washed four times in PBS-T. Bands were imaged and quantitated using the Odyssey infrared imaging system. The quantitative signals from RSV F protein bands were normalized against those of β-actin in the same lane and used to generate an expression (exp) ratio that represented a comparison of expression of the mutant F protein to that of the *wt* F protein.

Flow cytometric assay for quantitative surface expression of RSV F. HEp-2 cells on 6-well plates were transfected with 0.4 μg of each plasmid encoding the *wt* RSV M, N, and P proteins and either RSV F *wt* or a mutant F construct using the Effectene transfection reagent (Qiagen). After 48 h, cells were treated with 20 mM EDTA in PBS to form a single-cell suspension. Cells were washed two times in wash buffer (2% FBS in PBS) and then incubated with palivizumab at 1 μg/mL for 30 min at RT. Cell were washed

again two times with wash buffer and immunostained with an Alexa Fluor goat anti-mouse 488 secondary ab at a final concentration of 2 μg/mL. Cells were washed two times in wash buffer and analyzed on a 5-laser custom LSR II flow cytometer (Becton Dickinson) in the Vanderbilt Medical Center Flow Cytometry Shared Resource. Data analysis was performed using the FlowJo software program (version 7.6.1). Weighted mean fluorescent intensity (MFI) was calculated by multiplying the raw mean fluorescent intensity by the frequency of positive cells. All flow cytometry data from Fig. 3, 4, and 5 were collected using the same negative and positive control samples in three independent experiments. Statistical analysis was performed using a Student *T*-test. P values less than 0.05 were considered significant.

RSV rescue system. The RSV *wt* strain A2 antigenomic cDNA was constructed by sequential ligation of RSV cDNA fragments and placed under control of T7 polymerase promoter in a BAC recombineering vector pKBS3. The RSV genome plasmid was constructed to contain a T7 termination sequence at the end, preceded by a hepatitis delta virus ribozyme motif that mediates self-cleavage to produce an authentic copy of the negative-sense RNA genome of RSV (85). Optimized RSV genes N, P, L, and M2-1 genes, the RSV A2 antigenome were transfected into BHK-T7 cells at 0.4 μg of N, P, and M2-1 and 0.2 μg of L, as previously described (49). The T7 polymerase is expected to transcribe the RSV antigenome, which undergoes auto-cleavage to remove the T7 termination sequence, and thus create the negative-sense single stranded RNA genome of RSV. N, P, L, and M2-1 are expressed under the CMV early-immediate promoter and form a replication complex to start transcription of the RSV negative-sense genome.

These transcripts are translated by host ribosomes and lead to the expression of viral proteins that contribute to the production of infectious virus. At day 3-6 post transfection, cell supernatant and cell lysates subjected to a freeze/thaw, are passed onto a fresh monolayer of HEp-2 cells.

VLP assay. A recent protocol developed for the generation of human metapneumovirus VLPs (R. G. Cox and J. V. Williams, unpublished results) was modified for the production of RSV VLPs. 293-F cells were transfected with plasmids encoding either vector alone or RSV M, N, P, and the indicated RSV F construct in equal amounts. Seventy-two hours after transfection, cell supernatants and pellets were separated and collected by using low-speed centrifugation. Cell pellets were resuspended in cell lysis buffer as described above. Cell supernatant was pelleted through a 20% sucrose cushion using a Sorvall Surespin 630 rotor at 26,000 rpm for 90 min. The resulting pellet was resuspended in equal volumes of cell lysis buffer with protease inhibitors (Sigma). Western blotting was performed as described above. The quantitative signals from RSV F, M, N, or P protein bands were corrected for background using vector alone and then normalized to the signal from *wt* F CT. Bars represent the means and standard deviations for three independent experiments. Statistical analysis was performed using Student *T*-test. All values less than 0.05 were considered significant.

Transmission electron microscopy (TEM). VLP transfections were prepared as described for the VLP assay with F CT *wt*. For RSV-infected samples, 293-F cells were inoculated at an MOI of 0.05 for 72 h. Cell supernatants were clarified and pelleted though 20%

sucrose in sterile MHN buffer (0.1 M $MgSO_4$, 50 mM HEPES, 150 mM NaCl). Pellets were resuspended in 20% sucrose in MHN, applied to formvar-carbon grids with 300 mesh Cu (Ted Pella Inc.), and stained with 1% aqueous sodium phosphotungstate acid (Electron Microscopy Sciences). Grids were imaged on a FEI Morgagni electron microscope operated at an acceleration voltage of 100 kV. Images were collected using a 1,000 × 1,000 active pixel charge-coupled-device (CCD) camera (AMT) at a magnification of 44,000x. Image contrast was enhanced in the Adobe Photoshop (CS5) software program using the levels adjustment. Shadow and highlight input sliders were adjusted to the beginning and end of the histogram curve to optimize tonal levels for the entire image; middle tones were not adjusted.

Results

Generation of F CT constructs. In the previous chapter, I established that virus-like filaments can be generated independent of viral infection by transfecting HEp-2 cells with cDNAs encoding F, M, N, and P (Figure 2-2). Consistent with RSV filaments formed during infection, virus-like filaments contained RSV proteins and were often kinked, clustered, and stained brightly for the F protein. Virus-like filaments were also distinct from host cell protrusions that contained F-actin (Figure 3-2 E-H). Thus, the filaments formed using the transfection-based procedure were similar to filaments formed during viral infection in both morphology and composition. We used the transfection-based filament formation assay as a tractable system with which to study the role of the F protein CT domain in viral assembly at the plasma membrane. I designed a panel of

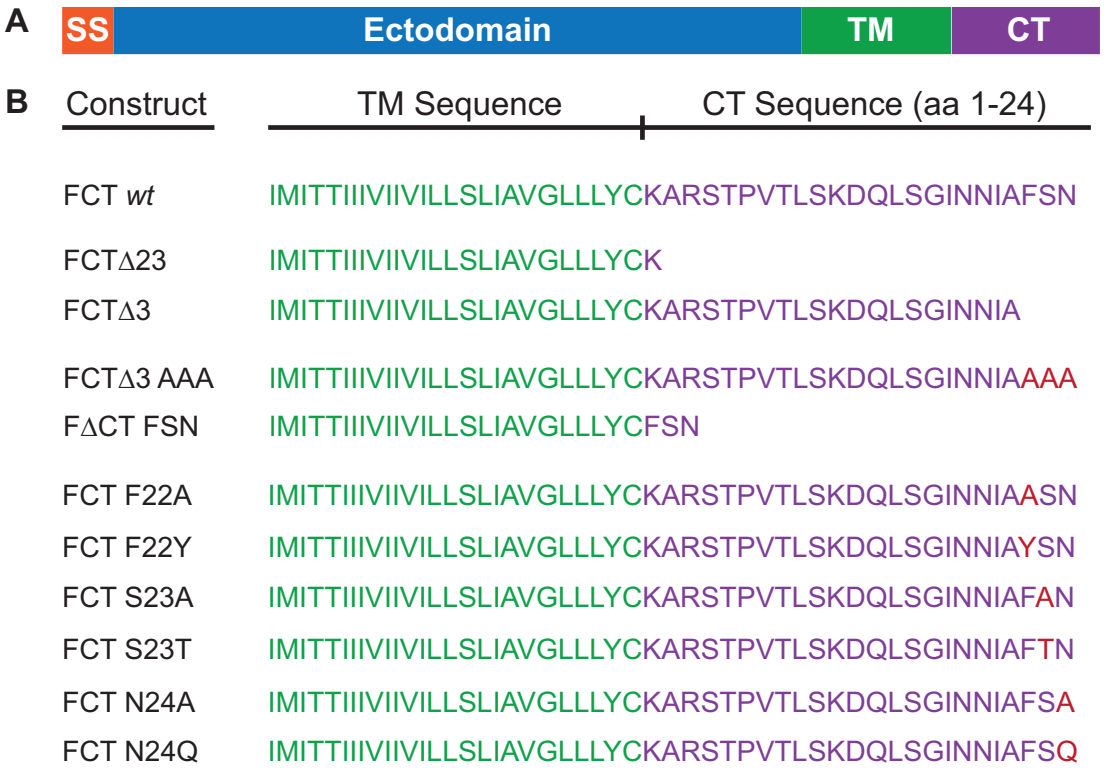

Figure 3-1. Schematic of F CT constructs. Panel A: F CT mutant constructs were generated using site-directed mutagenesis from F CT *wt* in the pcDNA3.1 vector. Functional regions are indicated by color: SS, signal sequence (orange); ectodomain (blue); TM, transmembrane domain (green); CT, cytoplasmic domain (purple). Panel B: Sequences of the TM and CT domain are indicated for each construct. Point mutations are indicated in red. We designated residue K as F CT residue 1. The schematic is not to scale.

altered cDNAs of the F protein gene in which the CT domain was truncated or otherwise mutated (Figure 3-1) using site directed mutagenesis. I then tested the effect of the tail mutations on virus-like filament formation at the cell surface using the transfection based assay. [8]

RSV F CT terminal residues Phe-Ser-Asn are required for filament formation. I asked here whether the CT domain was dispensable for viral assembly into filaments at the cell surface. When expressed alone, the F protein with an intact cytoplasmic tail (F CT *wt*) did not form virus-like filaments and localized to cellular projections that contained F-actin (Fig. 3-2 A-D). However, when coexpressed with M, N, and P, F CT *wt* was able to form virus-like filaments that were distinct from cellular projections containing F-actin (Fig. 3-2 E-H). Therefore, I used the presence of F-actin as a marker to distinguish virus-like filaments from cellular projections, since only the latter contained F-actin. In contrast to F CT *wt*, deletion of the terminal 3 amino acids from the F CT (residues Phe-Ser-Asn, or FSN) resulted in loss of virus-like filament formation and altered localization of the F protein only to F-actin-containing cellular protrusions (Fig. 3-2 I-L). This pattern of altered F staining at the cell surface was similar to the pattern of F CT *wt* when expressed alone in HEp-2 cells (*i.e.,* in the absence of the RSV N, P, and M proteins). Deletion of the three terminal amino acids of the CT domain resulted in the same phenotype of F distribution as deletion of the entire tail domain (Fig. 3-2 M-P). This F CT deletion construct was similar to the transmembrane-domain-plus-

[8] Figures 3-1 through 3-9 were previously published as part of an original manuscript. Shaikh *et al*. 2012. A critical phenylalanine residue in the respiratory syncytial virus fusion protein cytoplasmic tail mediates assembly of internal viral proteins into viral filaments and particles. mBio. 2012 Feb 7;3(1). pii: e00270-11. doi: 10.1128/mBio.00270-11. Print 2012

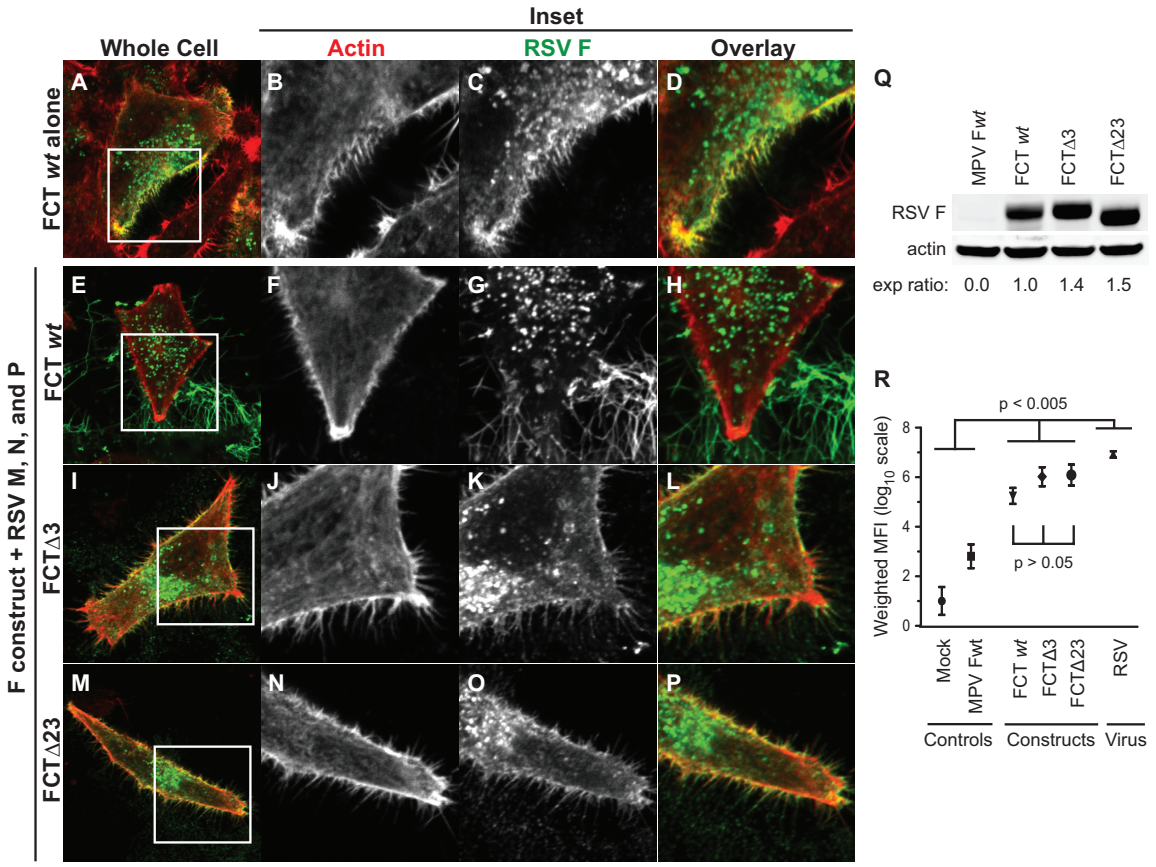

Figure 3-2: F CT terminal residues Phe-Ser-Asn are required for filamentous assembly at the cell surface. HEp-2 cells were transfected with F CT *wt* only (A to D) or with the indicated F CT construct and plasmids encoding RSV M, N, and P (E-P). Column 1 shows images of the whole cell (A, E, I, and M). Columns 2 to 4 (B to D, F to H, J to L, and N to P) show an enlargement of the corresponding inset in column 1. Column 2 shows actin staining only (B, F, J, and N); column 3 shows RSV F staining only (C, G, K, and O); and column 4 shows the overlay, with actin in red and RSV F in green (D, H, L, and P). (Q) Total cell lysate was collected from HEp-2 cells transfected with the indicated F CT construct, and RSV F or actin was detected by immunoblotting. The RSV F band was normalized against actin, and the expression (exp) ratio represents a normalization to results for F CT *wt*. (R) Total surface expression of RSV F was determined by flow cytometry using HEp-2 cells transfected with the indicated F CT construct and RSV M, N, and P. Data are plotted as means, and error bars represent standard deviations. Weighted MFI is mean fluorescence intensity (MFI) × the frequency of positive cells. MPV F *wt* is used as a specificity control.

one-anchor-residue ("TM+1") construct that we previously described (10) and is designated F CTΔ23. For each truncation construct, total cellular expression and total surface expression of the F protein were determined to be at levels equivalent to those of F CT *wt* (Fig. 3-2 Q and R, respectively). Therefore, reduced expression or trafficking of the mutant protein to the cell surface was not responsible for the failure of these CT truncation constructs to form virus-like filaments. These data indicate that the terminal CT residues Phe-Ser-Asn are required for assembly of RSV proteins into virus-like filaments.

Phe-Ser-Asn residues are sufficient for viral protein assembly into filaments at the cell surface. Based on the data presented in Figure 3-2, I next sought to determine whether the specific C-terminal residues Phe-Ser-Asn of F CT were necessary for filament formation when coexpressed with M, N, and P or, alternatively, if only the 24-amino-acid length of the CT domain determined filament formation. I mutated all three terminal residues to alanines (F CTΔ3 AAA) to test the hypothesis that a CT of a certain length was necessary for viral assembly. F CTΔ3 AAA was impaired for virus-like filament formation when coexpressed with RSV M, N, and P (Fig. 3-3 E-H) compared to F CT *wt* (Fig. 3-3 A-D). To determine if residues Phe-Ser-Asn were sufficient for virus-like filament formation, I deleted the entire F CT except for the terminal residues Phe-Ser-Asn (designated FΔCT FSN). FΔCT FSN formed virus-like filaments at the cell surface (Fig. 3-3 I-L) that were similar in length to F CT *wt* filaments (Fig. 3-3M), but the percentage of transfected cells with filaments was reduced 10-fold (Fig. 3-3N). These

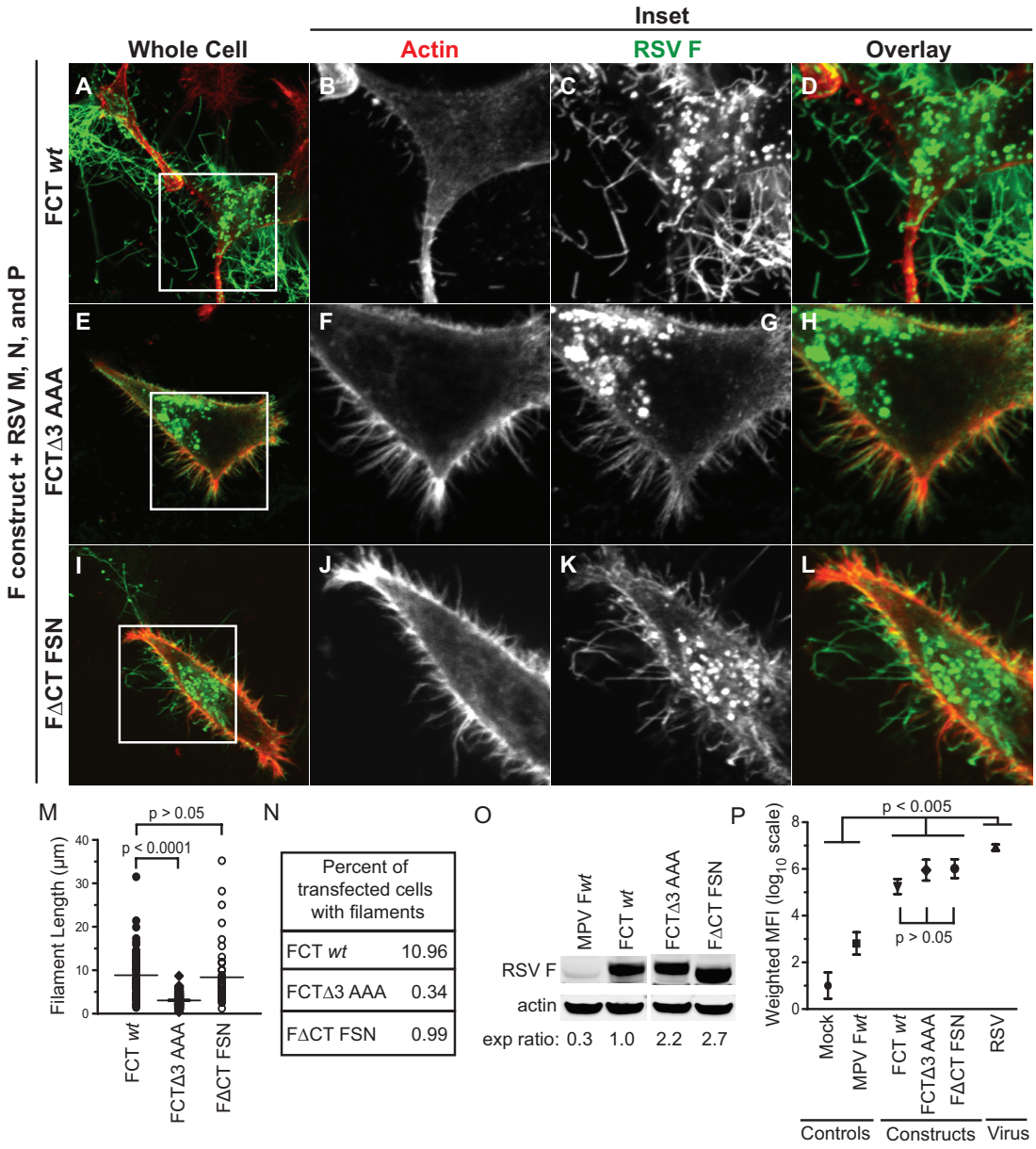
Inset
Whole Cell
Actin
RSV F
Overlay
F construct + RSV M, N, and P
FCT wt
FCTΔ3 AAA
FΔCT FSN
A
B
C
D
E
F
G
H
I
J
K
L
M
p > 0.05
p < 0.0001
Filament Length (μm)
40
30
20
10
0
FCT wt
FCTΔ3 AAA
FΔCT FSN
N
Percent of transfected cells with filaments
FCT wt 10.96
FCTΔ3 AAA 0.34
FΔCT FSN 0.99
O
MPV Fwt
FCT wt
FCTΔ3 AAA
FΔCT FSN
RSV F
actin
exp ratio: 0.3 1.0 2.2 2.7
P
p < 0.005
p > 0.05
Weighted MFI (log10 scale)
8
6
4
2
0
Mock
MPV Fwt
FCT wt
FCTΔ3 AAA
FΔCT FSN
RSV
Controls
Constructs
Virus

Figure 3-3. F CT residues Phe-Ser-Asn are sufficient for filamentous assembly at the cell surface. HEp-2 cells were transfected with the indicated F CT construct and RSV M, N, and P (A to L). Column 1 shows images of the whole cell (A, E, and I). Columns 2 to 4 (B to D, F to H, and J to L) show an enlargement of the corresponding inset in column 1. Column 2 shows actin staining only (B, F, and J); column 3 shows RSV F staining only (C, G, and K); and column 4 shows the overlay, with RSV F in green and actin in red (D, H, and L). (M and N) HEp-2 cells were transfected as described for panels A to L. Filament length was determined by measuring the lengths of individual filaments using Zeiss LSM software as described in Materials and Methods (M). Percent transfected cells was determined by counting RSV F-transfected cells with filaments and then dividing that number by the total number of RSV F-transfected cells (N). (O) Total cell lysate was collected from HEp-2 cells transfected with the indicated F CT construct, and RSV F and actin were detected by immunoblotting. The RSV F band was normalized against actin, and the expression (exp) ratio represents a normalization to F CT *wt*. (P) Total surface expression of RSV F was determined by flow cytometry using HEp-2 cells transfected with the indicated F CT construct and RSV M, N, and P. Data are plotted as means, and error bars represent standard deviations. Weighted MFI is mean fluorescence intensity (MFI) × the frequency of positive cells. MPV F *wt* is used as a specificity control.

data suggest that other residues in the CT or a minimum length of the CT is important for initiation of filament formation. The total cellular expression and total surface expression of F CTΔ3 AAA or FΔCT FSN were similar to those of F CT *wt*, again indicating that neither expression nor trafficking to the cell surface was impaired (Fig. 3-3O and 3-3P, respectively). These data suggest that the tri-peptide consisting of residues Phe-Ser-Asn is necessary and sufficient for assembly of viral structural proteins into virus-like filaments at the cell surface.

The Phe residue in the RSV F CT is necessary for filament formation. To determine if a specific residue of the F CT Phe-Ser-Asn motif was the determining factor for viral assembly into filaments, I designed F CT constructs that contained mutations of each of the three terminal residues individually. We compared the capacity of the mutant F CT constructs to form virus-like filaments when coexpressed with M, N, and P to that of F CT *wt* (Fig. 3-4 A-D). When the Phe residue was mutated to an alanine (F22A), virus-like filaments failed to form, and the F construct colocalized with cellular structures containing F-actin (Fig. 3-4 E-H). However, if either the Ser or Asn residue was mutated to an Ala, the mutant F CT constructs assembled into virus-like filaments, distinct from cellular structures containing F-actin (Fig. 3-4 I-L and 3-4 M-P, respectively). Total cellular expression and total surface expression of each of the F CT constructs with single amino acid mutations were equivalent to F CT *wt* levels, indicating that neither expression nor trafficking was impaired (Fig. 3-4Q and 3-4R, respectively). We also designed and tested F CT constructs with conserved mutations (F22Y, S23T, and N24Q). Figure 3-5 shows the effect of these mutations on filament formation. Mutation of Phe to

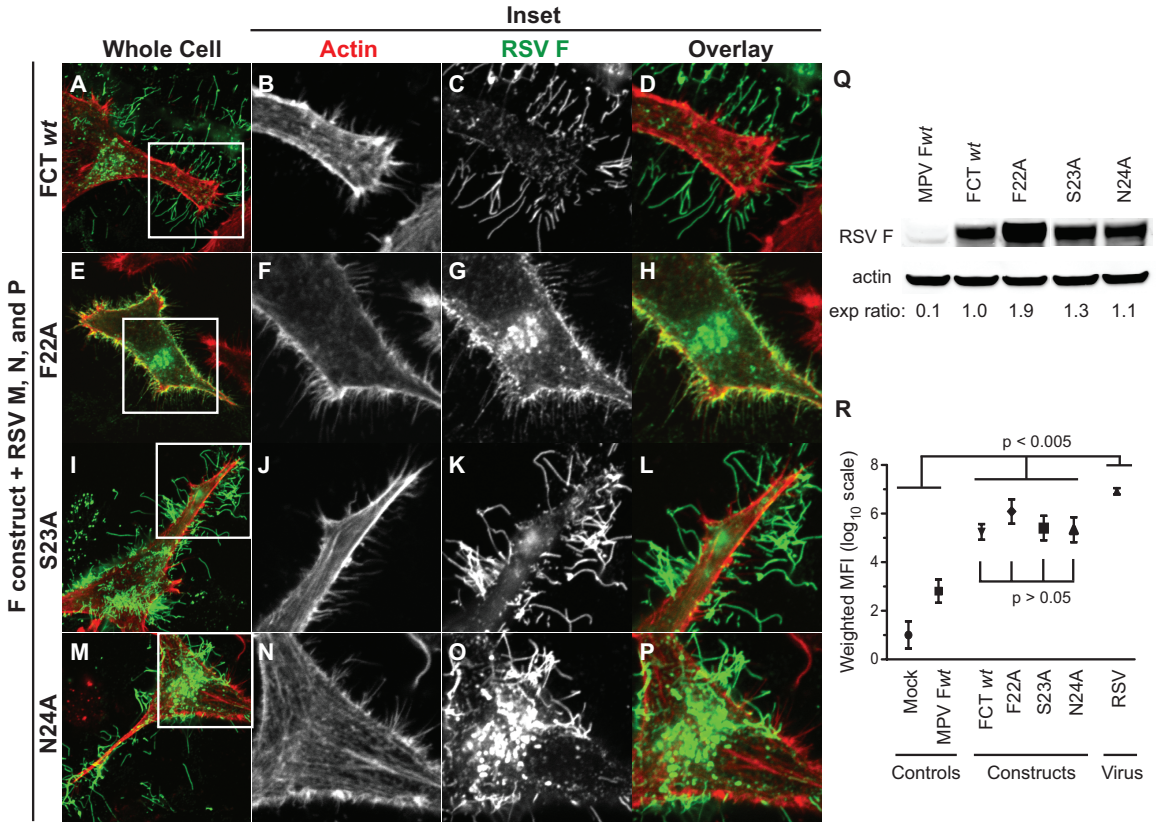

Figure 3-4. The Phe residue at position 22 in the RSV F CT is necessary for filamentous assembly at the cell surface. HEp-2 cells were transfected with the indicated F CT construct and RSV M, N, and P (A to P). Column 1 shows images of the whole cell (A, E, I, and M). Columns 2 to 4 (B to D, F to H, J to L, and N to P) show an enlargement of the corresponding inset in column 1. Column 2 shows actin staining only (B, F, J, and N); column 3 shows RSV F staining only (C, G, K, and O); and column 4 shows the overlay, with RSV F in green and actin in red (D, H, L, and P). (Q) Total cell lysate was collected from HEp-2 cells transfected with the indicated F CT construct, and RSV F or actin were detected by immunoblotting. The RSV F band was normalized against actin, and the expression (exp) ratio represents a normalization to F CT *wt*. (R) Total surface expression of RSV F was determined by flow cytometry using HEp-2 cells transfected with the indicated F CT construct and RSV M, N, and P. Data are plotted as means, and error bars represent standard deviations. Weighted MFI is mean fluorescence intensity (MFI) × the frequency of positive cells. MPV F *wt* is used as a specificity control.

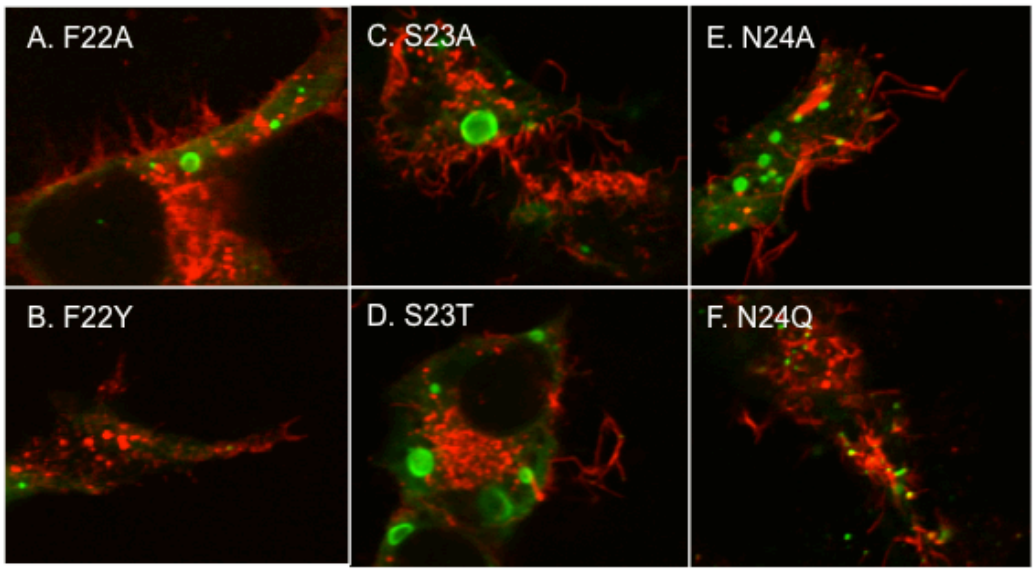

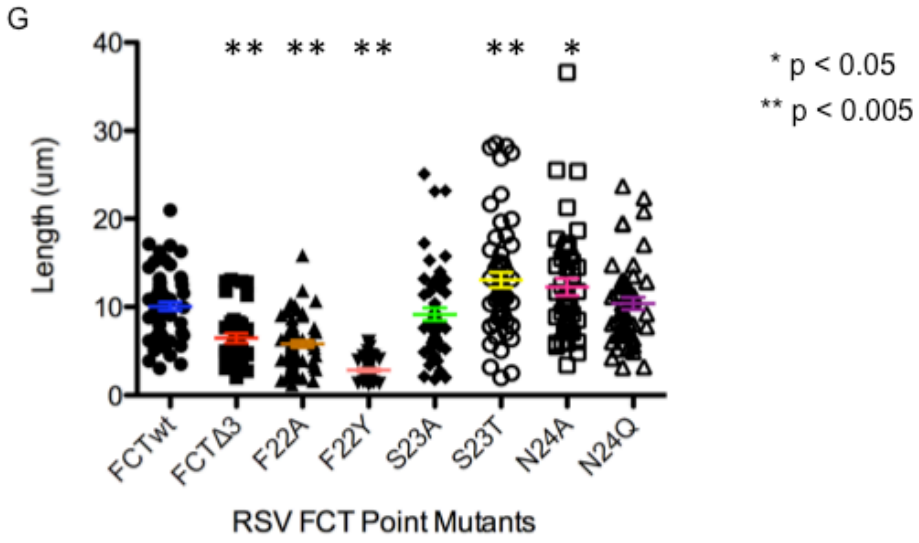

Figure 3-5. Conservative mutations in the F CT have similar results to alanine mutations. HEp-2 cells were transfected with the indicated F CT construct and RSV M, N, and P. RSV F and N were detected by indirect immunofluorescence (A-F). Filament length was determined by measuring the lengths of individual filaments using Zeiss LSM software as described in Materials and Methods (G)

Tyr (F22Y) did not retain the capacity to form virus-like filaments (Fig. 3-5B). Mutation of the Ser to Thr (S23T) or Asn to Gln (N24Q) resulted in F CT constructs are capable of forming filaments (Fig. 3-5D and 3-5F). The results from these conservative mutations were similar to the data described for the Ala point mutations in Figure 3-4. Finally, I also examined the length of virus-like filaments formed when these point mutations were introduced into the F CT (Figure 3-5G). Mutation of the Ser or Asn resulted in virus-like filament length that was at or greater than that of the *wt* F CT. Collectively, these data show that the Phe residue near the C-terminal end of F CT plays a key role in filamentous viral assembly at the plasma membrane.

A recombinant virus lacking residues Phe-Ser-Asn does not result in viable virus. Since the terminal residues, particularly the Phe residue, are essential for virus-filament formation, I introduced the F CTΔ3 mutation into a recombinant virus using a plasmid-based virus rescue system. Using a BAC recombineering approach developed by our collaborators Anne Hotard and Marty Moore at Emory University, I generated the mutant genomic cDNA and transfected the F CTΔ3 cDNA, along with helper plasmids encoding RSV N, P, L, and M2-1, into BHK cells that constitutively express T7 polymerase. Figure 3-6 shows that at 3 days after transfection, multiple syncytia could be seen, indicating that transcripts of F CTΔ3 were being made and expressed in these cells (indicated by the red arrows). However, when the supernatant or cell-associated fractions were harvested and passed onto a fresh monolayer of HEp-2 cells for expansion, virus was not recovered. Although the formation of syncytia normally indicates that virus is being generated, syncytia can also occur when the F protein is expressed. During the

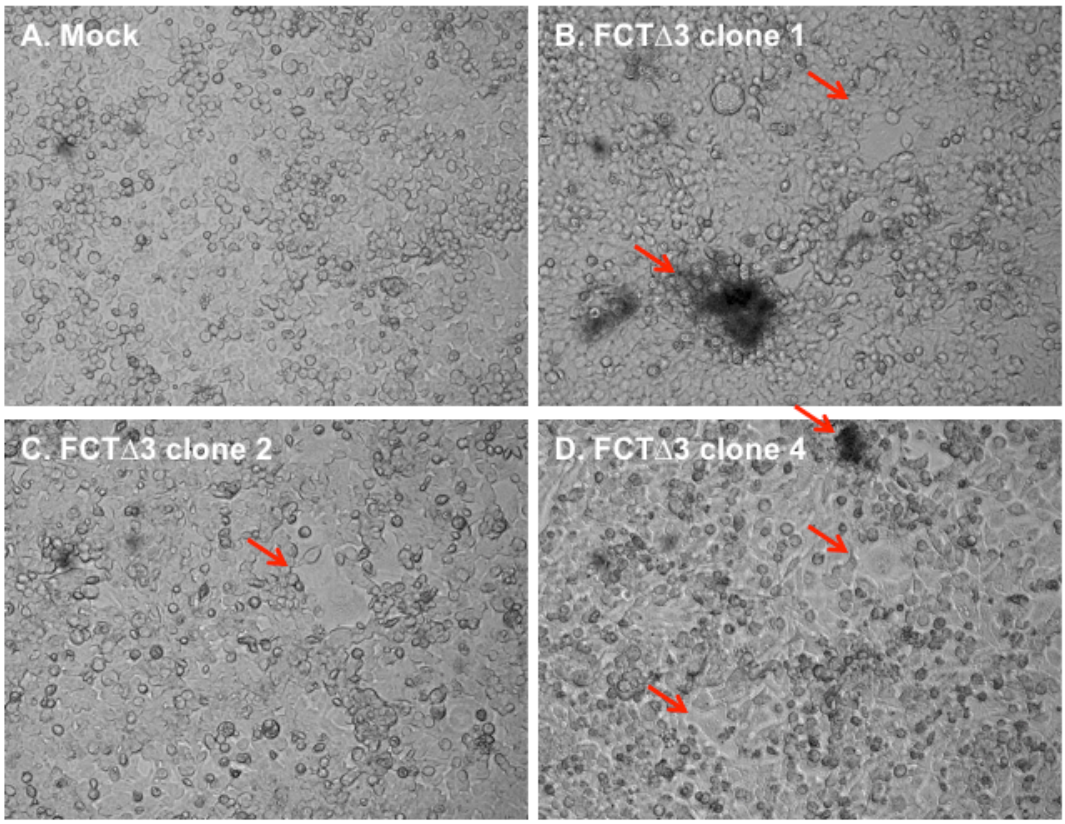

Figure 3-6. Transfection of genomic cDNA containing the F CTΔ3 mutation results in cell-to-cell fusion. BHK-T7 cells were transfected with plasmids encoding the F CTΔ3 A2 genomic cDNA and helper plasmids: N, P, L, and M2-1. AT 3 days post transfection, cells were imaged using phase contrast microscopy. Red arrows indicate syncytia.

initial transfection of the genomic construct into BHK cells, F transcript is likely generated, and the mutant F protein (F CTΔ3) is expressed at the cell surface, where it can mediate cell-to-cell fusion. However, the F CTΔ3 protein may be unable to mediate viral assembly and budding. Therefore, the fact that viable virus could not be generated from the rescue transfections suggests that alteration of the F CT in this way likely drastically affects viral assembly. [9]

Development of an RSV VLP assay in 293-F cells. Since a recombinant F CTΔ3 virus could not be recovered, I then sought to develop a VLP assay to determine the mechanism by which the F CT Phe residue affected viral assembly. Previously, I had developed a 293T-cell-based assay using metabolic labeling to detect VLPs (Figure 2-3). This assay, however, did not lend itself easily to screening many F CT constructs. In collaboration with Reagan Cox and John Williams at Vanderbilt University, I developed an RSV VLP assay using 293-F suspension cells. Figure 3-7A shows a general schematic of the assay. 293-F cells were used for their high growth rate, dense cell growth, and transfection efficiency, all of which have been limiting factors in previous efforts to develop VLP assays with conventional transformed epithelial cells lines, such as HEp-2 cells. Plasmids encoding F, M, N, and P were transfected into cells. At 72 hours post transfection, cells were pelleted using low-speed centrifugation. Cell lysates were collected, and the clarified supernatants were pelleted through a 20% sucrose cushion to remove free protein. The resulting pellet was resuspended in cell lysis buffer, and both cell lysates and supernatant pellets were separated by SDS-PAGE. Using this system,

[9] Images were collected with assistance from Reagan Cox in the laboratory of John Williams on a phase contrast microscope in the laboratory of Terence Dermody

sufficient quantities of VLPs were produced for protein quantification by immunoblotting using the Lycor Odyssey infrared imaging system rather than radiolabeling.

Next, I sought to determine the optimal combination of proteins to produce RSV VLPs. The F, M, N, and P proteins are the minimal requirements for passage of a minigenome construct consisting of the RSV leader and trailer sequences flanking a reporter gene (91). I had previously found that the F protein alone is insufficient for detectable VLPs using a radiolabeling assay (Figure 2-3). However, as described above, the previous assays were not optimal. Figure 3-7B shows the results obtained using supernatants harvested from transfection of 293-F cells with plasmids encoding vector only, F alone, F and M, F and N, or all four proteins: F, M, N, and P. The results show that while F alone is detectable in the supernatant, more F was present in the supernatant when M was coexpressed, and the most F was detectable when all four proteins are expressed. Furthermore, less M and N was incorporated into VLPs when only two proteins were present. In contrast, when all four proteins are expressed, internal proteins M, N, and P were efficiently incorporated into VLPs. The data from three independent experiments were quantified for each protein by raw I.K.K. counts using the Odyssey imaging software (Fig. 3-7 C-F).

At first glance, these date seem contradictory to the data presented in Figure 2-3. However, there are several caveats that need to be considered. First, the original data in the literature reflected the capacity of proteins to passage a minigenome not form VLPs. Second, VLP production in adherent 293-T cells was highly inefficient, requiring radiolabeling to detect VLPs. Third, 293-F cells are suspension cells that have been optimized for protein expression and therefore are very likely efficient at protein

secretion. Hence, the detection of F in the supernatant when it was expressed by itself may reflect the inherent capacity of the F protein to bud, the tendency of 293-F cells to secrete protein, or cell sheering. Thus, this system is unlikely to answer the question of what proteins are the minimum requirements for RSV budding, but it can still be used to determine the effect of F CT mutations on VLPs and incorporation of the internal virion proteins.

Since we found that F, M, N, and P are minimally required for filament formation independent of viral infection, we chose to express VLPs using all four proteins to recapitulate the minimum requirements for assembly into filaments. RSV VLPs were produced by transfecting 293F cells with plasmids encoding the indicated F construct and *wt* M, N, and P. TEM analysis of VLPs showed characteristic F-protein spikes (black arrows) on the surface of particles similar to those seen on RSV virion particles produced and imaged in the same manner (Fig. 3-8A and B). Second, the diameter of the VLPs was similar to that of RSV and within the usual range of diameter of virions grown in other cell types (4). In addition to structure, we also compared the protein composition of VLPs with that of native virus. Figure 3-8C shows a representative immunoblot comparing the level of each viral protein in the VLPs to that in virions. These data were quantified from three independent experiments and are presented as percentages of RSV virion protein levels (Fig. 3-8D). Compared with virus, the VLPs contained equivalent amounts of the F protein but less M, N, and P. Although the ratios of the F protein to internal proteins differed between VLPs and RSV, VLPs did still incorporate RSV internal proteins, thus allowing us to study the relative capacities of various F CT constructs to incorporate

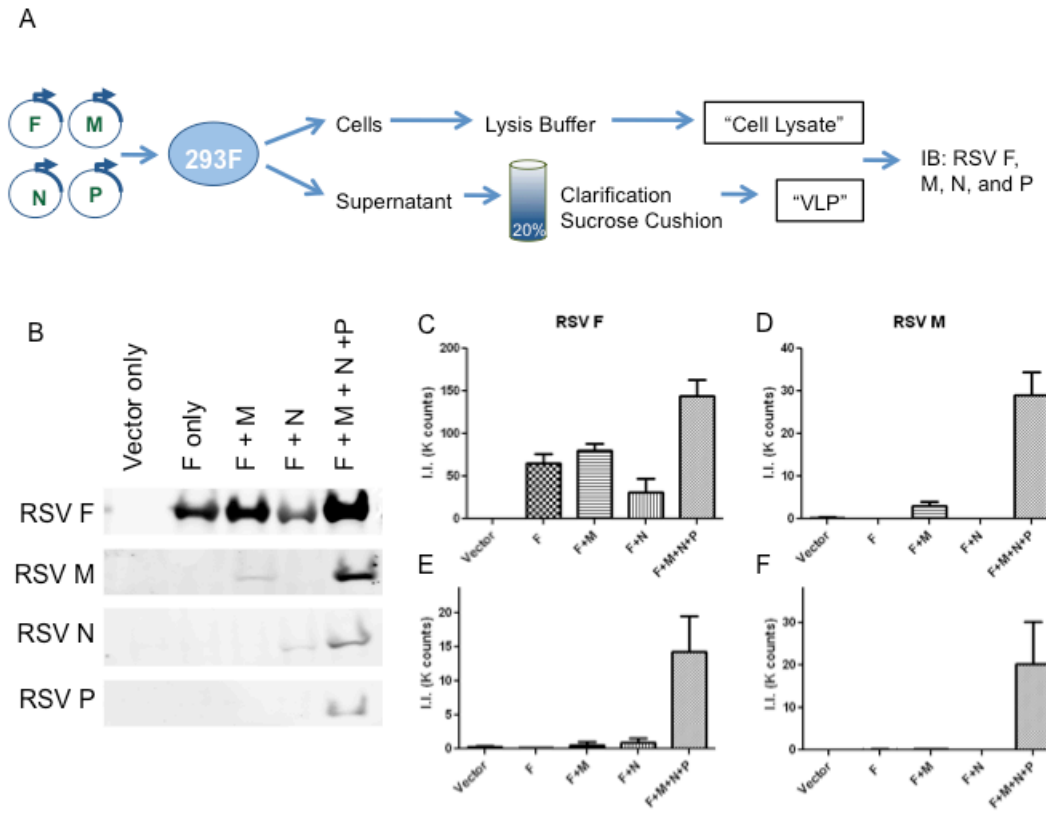

Figure 3-7. Establishment of the 293-F VLP assay. Panel A shows a schematic of the VLP assay. 293-F cells were transfected with the indicated plasmids. At 72 hours post transfection, cells were pelleted using low speed centrifugation. Cell lysates were collected and the clarified supernatants were pelleted through a 20% sucrose cushion to remove free protein. The resulting pellet was resuspended in cell lysis buffer, and both cell lysates and supernatant pellets were separated by SDS-PAGE. The indicated proteins were detected by immunoblot. Panel B shows a representative experiment of the cell supernatant fraction from the indicated transfections. Panel C shows a quantification of data from three independent experiments as shown in panel E (cell lysates in grey; VLPs in black). Data are plotted as means, and error bars represent standard deviations.

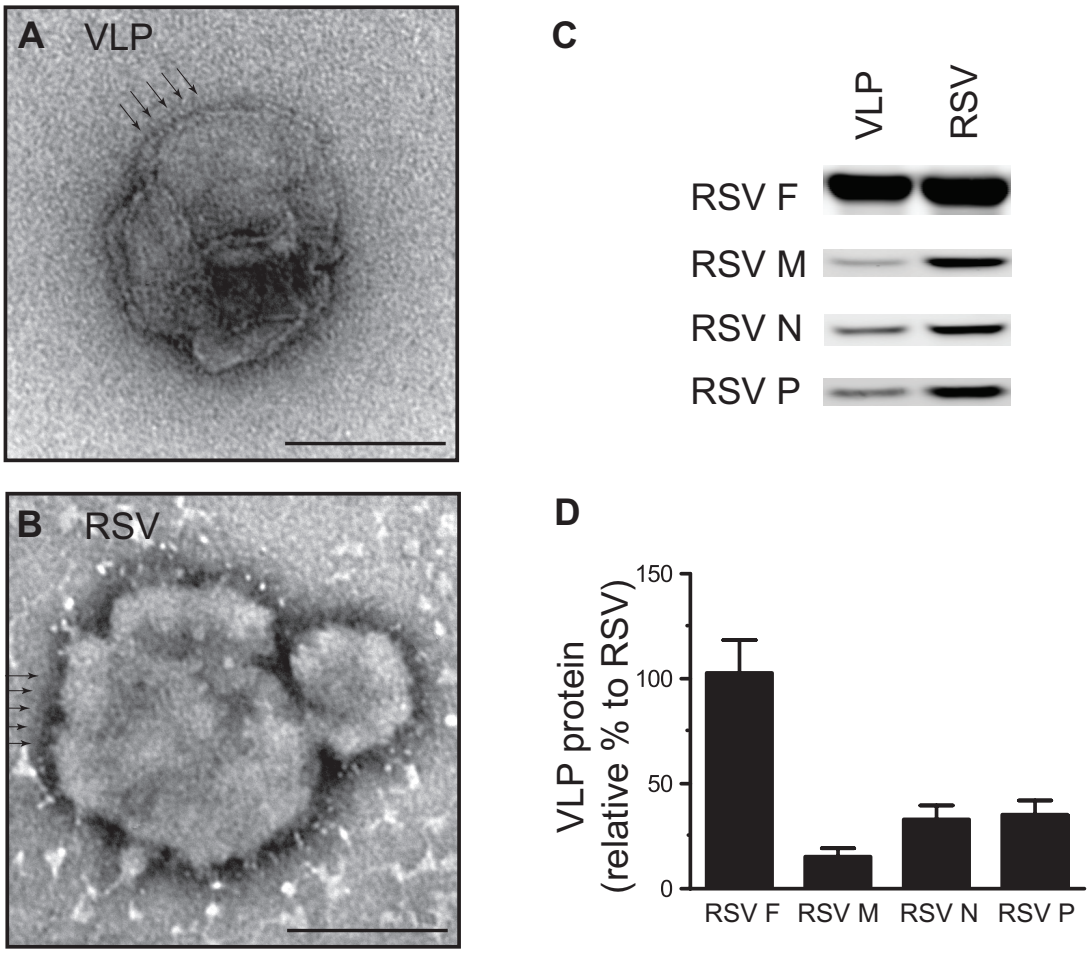

Figure 3-8. RSV VLPs generated from transfection of F, M, N, and P are similar to virions generated and collected in the same manner. 293-F cells were transfected with plasmids encoding RSV F CT *wt*, M, N, and P or infected with RSV at an MOI of 0.05. Panels A and B show transmission electron micrographs of a representative VLP and virion, respectively. Scale bars represent 100 nm. (C to D) Supernatants from RSV-infected or F CT *wt*-transfected cells were clarified and pelleted through a 20% sucrose cushion. Panel C shows a representative blot comparing protein levels in VLPs to RSV. Panel D shows a quantification of three independent experiments as shown in panel C. The indicated protein levels in VLPs were normalized to that of the corresponding protein in RSV.

internal virion proteins into budded vesicles. Several possibilities could explain the discrepancy of ratios. The VLPs may incorporate a higher proportion of F into each particle than M, N, and P, compared to those for virions, or there may be vesicles containing the F protein alone escaping into the supernatant. I favor the latter, since transfection of cDNA encoding the F protein alone led to a baseline transport of F into the supernatant (Fig 3-7B).

The Phe residue is required for incorporation of RSV M, N, and P into RSV VLPs. Next, I sought to determine why the F CT Phe residue is required for virus assembly into filaments. I hypothesized that the F CT is necessary for recruitment of an internal virion protein to filaments and therefore also would function in the generation of VLPs. After initial validation of the VLP system, I sought to determine how the F CT Phe residue affected VLP budding and the incorporation of internal virion proteins. I performed the VLP assay as described above and collected the cell pellets for total protein expression. Figure 3-9A shows immunoblots from a representative experiment. Data were normalized to the levels in the F CT *wt* sample, and the means and standard deviations from three independent experiments are shown in Fig. 3-9B. Compared with F CT *wt*, when residues Phe-Ser-Asn were deleted (F CTΔ3), or Phe was mutated to an Ala (F22A), there was a significant loss of RSV M, N, and P protein incorporation into VLPs. In contrast, point mutations of residue Ser23 or Asn24 (S23A or N24A, respectively) did not affect incorporation of RSV M, N, or P into VLPs. The F CTΔ3 and F22A constructs also induced less transfer of the F protein into the supernatant than the F CT *wt*, S23A, or N24A constructs, consistent with less budding of VLPs. These data show that the Phe

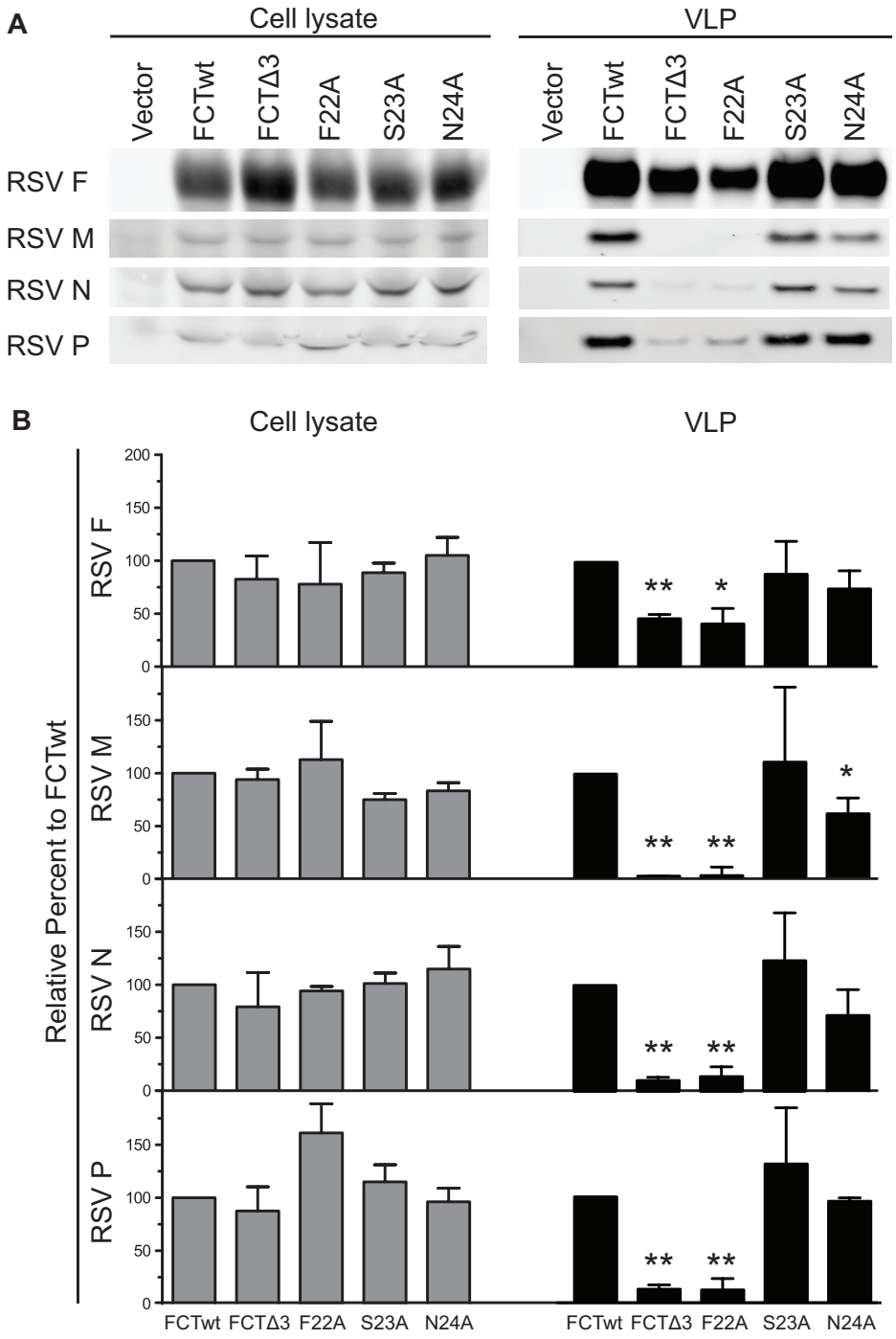

Figure 3-9. The Phe residue at position 22 in the RSV F CT is necessary for incorporation of internal virion proteins into VLPs. 293-F cells were transfected with plasmids encoding the indicated F CT construct and RSV M, N, and P. Panel A shows a representative experiment with indicated protein levels in cell lysates (left) or VLPs (right). Panel B shows a quantification of data from three independent experiments as shown in panel A (cell lysates in grey; VLPs in black). Data are plotted as means, and error bars represent standard deviations.

residue in the F CT is necessary for RSV M, N, and P incorporation into VLPs. Collectively, the data in this chapter show that the F CT mediates viral assembly through a C-terminal Phe residue in order to incorporate RSV M, N, and P into virus filaments at the cell surface prior to budding.

Mutations in the F CT Phe residue affect incorporation of M. Since mutations in the Phe residue resulted in loss of incorporation of all internal proteins, I next sought to determine which protein was involved. Since M, N, and P are thought to associate in the cytoplasm, it is reasonable that lost incorporation of all three proteins may be due to the fact that one protein is responsible for recruiting the others into VLPs. Since I previously showed that VLPs could be formed by expression of F and only one of the internal proteins (Figure 3-7), I performed the 293-F VLP assay using only two proteins, F and either M, N, or P. In addition, I used the F CT constructs to determine which one of the internal proteins was affected most by mutation in the F CT. Figure 3-10 shows the results from these experiments. When F+N or F+P VLPs were produced, there was no change in the amount of N or P incorporated with the different F CT constructs (Fig. 3-9B and 3-9C, respectively). However in the F+M VLPs, the amount of M varied with mutations in the F CT (Fig. 3-9A). Mutation of the Phe residue result in less M incorporated than with *wt* F CT. However, more M was incorporated with F CTΔ3 and with mutation in the Ser or Asn residues. The reason for this variation is unclear, but may include non-specific incorporation when other internal proteins are absent, and the fact that variations in the CTs of viral glycoproteins can often affect the amount of glycoprotein and internal proteins in VLPs (43). Further study of the interactions between

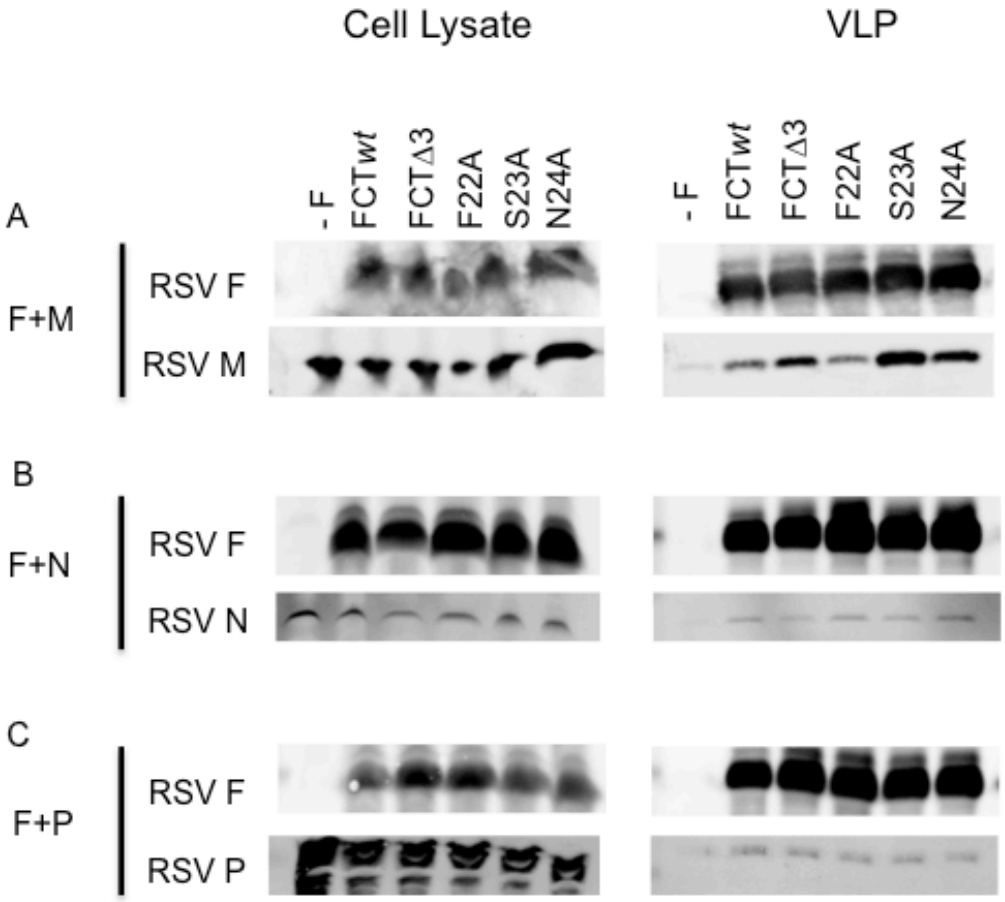

Figure 3-10. Incorporation of M into F+M VLPs is affected by mutations in the F CT. 293-F cells were transfected with plasmids encoding the indicated F CT construct and RSV M, N, or P. Cell lysate and cell supernatants were harvested as described for Figure 3-7. Immunoblots from representative experiments for indicated proteins are shown. Panel A represents VLPs generated with the indicated F CT construct and M. Panel B represents VLPs generated with the indicated F CT construct and N. Panel C represents VLPs generated with the indicated F CT construct and P.

the F CT and internal virion proteins is necessary to fully understand the mechanism that drives incorporation of internal virion proteins into filaments and VLPs.

Discussion

The RSV F CT domain plays a critical role in viral replication, but the mechanism by which the F CT functions in assembly and budding has not been well characterized. In this study, I found that a single Phe residue in the F CT at amino acid position 22 mediates assembly of virus-like filaments, incorporation of RSV internal proteins into VLPs, and subsequent budding of VLPs from cells. The finding that a single amino acid residue in the F CT can control both assembly and budding is remarkable. I studied the role of RSV proteins in assembly of filaments independent of viral infection by expressing proteins from plasmids, and I found that filament formation requires the F, M, N, and P proteins. This assembly process likely is driven by interactions of these viral proteins with each other or collectively with host proteins. Using cDNA-based expression of F proteins with alterations in the F CT, I determined the key residue in the F CT is required for assembly of virus-like filaments containing the four minimally required structural proteins, F, M, N, and P. Furthermore, I used a VLP budding assay under the same protein expression conditions to reveal that the F CT coordinates assembly through its capacity to incorporate M, N, and P into particles. These data provide a direct link between F CT coordination of viral assembly into filaments and budding of viral particles. Alternatively, the formation of filaments and virus particles may be two different outcomes of essentially the same assembly process, with the Phe residue serving in a critical role for both processes.

The specific mechanisms that govern F CT-mediated assembly, however, are still not well defined. Our data show that expression, trafficking, and surface expression of F are not affected by mutations in the F CT. This finding is consistent with findings of previous studies indicating that the TM domain of F is responsible for targeting the protein to the apical surface (5). Localization to specific lipid microdomains in the plasma membrane also appears to depend on an unidentified domain in the ectodomain (17). Therefore, it is likely that the F CT Phe residue I identified is critical for a protein-protein interaction. A simple explanation may be that this residue directly interacts with one of the internal virion proteins, such as M, or a complex of these proteins. On the other hand, the F protein is a trimer, and the F CT is located in close proximity to the plasma membrane. It may be that the hydrophobic Phe residue confers a specific conformation to the cytoplasmic portion of the trimer. Finally, the possibility of an interaction with a host protein or complex of proteins cannot be excluded. Future studies will focus on elucidating the specific protein-protein interactions mediated by the F CT and how these interactions lead to the incorporation of other viral proteins into filaments.

Coordination of RSV assembly by the F CT is consistent with many other studies indicating that paramyxovirus glycoprotein cytoplasmic tails are crucial to both assembly and budding (13). For RSV and human metapneumovirus (HMPV), members of the Pneumovirus subfamily, the G protein is dispensable for viral replication *in vitro* (18, 19). Although the F CT may be sufficient, optimal incorporation of viral proteins and RNA might require both F and G, since residues in the RSV G protein CT are thought to be important for interactions with M (20). However, for the *Paramyxoviridae* subfamily, the requirement of glycoprotein CTs varies with each virus. For measles virus and Sendai

virus assembly, the F protein CT is required. Newcastle disease virus F and HN glycoproteins interact with different internal viral proteins, M and N, respectively. In contrast, the F and HN CTs of parainfluenza virus 5 serve somewhat redundant functions (13). The lack of a common theme for the role of CT domains in paramyxoviruses may simply indicate that many questions about the specific mechanisms of viral assembly remain unanswered, and further investigation into the RSV F CT may contribute to general knowledge regarding glycoprotein CT-mediated assembly for other paramyxoviruses.

In addition to viral protein incorporation, the formation of RSV particles at the cell surface requires viral interactions with the host cell membrane. The viral membrane first must be deformed outward as an extension of the cell membrane. Then, the particle must elongate by incorporation of additional membrane to create long filaments. Finally, a scission event must occur to release the viral particle from the cell membrane. All of these processes are energy intensive and require complex coordination of surface proteins and nucleocapsids containing RNA and viral proteins (21). Many viruses usurp endosomal sorting complexes required for transport (ESCRT) machinery to accomplish the task of outward bud formation and membrane scission using late domains found in viral proteins (13). Viral budding using late domains requires the AAA ATPase Vps4. However, inhibition of Vps4 does not affect RSV budding (6), and like other ESCRT-independent viruses, RSV may use viral protein-mediated pushing and pulling forces to initiate membrane bending at lipid microdomains in order to exit the cell (21). RSV assembles into filaments at lipid microdomains (22, 23). The RSV F protein associates with detergent-resistant membranes (DRMs), as do the RSV M, N, P, M2-1, and L

proteins during viral infection (17, 23–25). Furthermore, the M protein associates with lipid microdomains in the presence of the F protein (26). Our data suggest that the Phe residue in the F CT is critical for F-protein interactions with internal virion proteins to provide both the pulling and pushing forces required to bend the membrane to form filaments, presumably at lipid microdomains. Our data also provide some insight about how the F CT mediates initial membrane bending and filament elongation. The capacity of a shortened CT with only residues Phe-Ser-Asn to form virus-like filaments was reduced by 10-fold. However, once the filament formation process was initiated, the shortened CT was able to induced filaments that elongated to lengths comparable to those generated by F CT *wt*. These data suggest that other residues, or a minimum length, of the CT is important for initiation of outward bud formation.

Manipulation of the plasma membrane also likely involves a variety of host proteins that function at the cell surface. Many cellular structures extending outward from the cell surface depend on actin polymerization (*e.g.*, microvilli, filapodia, lamellipodia, and membrane ruffles), and lipid microdomains have been linked to the cortical actin network (27). In fact, disruption of actin-associated signaling pathways affects filament formation, and β-actin and actin-related proteins are found in the same sucrose gradient-purified fractions as RSV (15, 28–32). However, actin polymerization is dispensable for filament formation, and F-actin is excluded from viral filaments (15). While actin and actin-related proteins likely are involved in aspects of RSV assembly, our data support the hypothesis that the process by which viral proteins extend the cell membrane outward to form filaments is distinct from the process used by actin-based cellular structures. Exclusion of cellular proteins from viral filaments also suggests a mechanism allowing

specific sorting of viral and host proteins into filaments, a process that likely is highly regulated and involves interactions among viral proteins, host proteins, and lipid microdomains.

Despite these studies, the mechanism by which RSV assembles and buds is still poorly understood. Viral protein-protein and protein-lipid interactions likely play a significant role, and further investigation could yield insight into what motifs mediate these interactions for both viral and cellular proteins. Further study of RSV assembly and budding will contribute to general understanding of how ESCRT pathway-independent viruses can exit the cell and how viral surface and internal proteins contribute to egress. Finally, understanding the mechanisms that drive RSV assembly and budding could lead to targeted development of novel antiviral drugs for prophylactic or therapeutic use against RSV infection.

Chapter Summary

Since the data from chapter II indicate that viral filamentous assembly is largely driven by viral proteins themselves, I sought to define those viral determinants in this chapter. These data identify specific residues in the F CT that are important for viral assembly into filaments. Furthermore, the data indicate that the mechanism by which the Phe residue in the F CT mediates filament formation is through incorporation of internal virion proteins though the mechanism remains unknown. Finally, I show that the M protein is a likely target of the F CT, although a direct protein interaction is not shown and may be mediated by host proteins. Collectively, these data indicate that the F CT is a driving force behind viral assembly into filaments.

Chapter IV

VIRUS INTERACTIONS WITH THE HOST CELL

Introduction

In addition to viral determinants, many host proteins are implicated in virus assembly and budding. Disruption of apical recycling endosome (ARE) proteins myosin Vb and Rab11-family interaction protein 1 (FIP1) results in decreased production of viral progeny (9). Additionally, inhibition of Rab11-FIP2 causes increased cell-associated infectious virus and longer viral filaments on infected polarized MDCK cells, suggesting a defect in membrane scission to produce free virions (97). Lipids and lipid-associated proteins are implicated in RSV assembly (62). RSV proteins associate with detergent-resistant membranes and co-localize with lipid microdomain markers (13, 28, 62).

In the previous chapter, I showed that the F CT, and specifically a Phe located three residues from the C terminus of F CT, is critical for viral assembly into filaments. However, the mechanism by which the F CT coordinates viral assembly and budding is not clear, and the role of host factors in viral replication is unclear. In this chapter, I describe the use of several approaches to investigate RSV interactions with the host cell. First, I test whether the F CT facilitates viral assembly through interaction with host factors by validating the results from a Y2H screen. Second, I examine how host factors may affect the function of the M protein and its role in viral assembly and budding using a Y2H screen host gene expression, knockdown cell lines, and pharmacologic inhibitors. Third, I test the role of an exosome pathway in viral budding using chemical inhibitors to

neutral sphingomyelinase. Finally, I further investigate the role of ARE proteins in viral replication using a mouse model. These studies further elucidate the function of host proteins in RSV replication.

Materials and methods

Cell culture and *wt* RSV virus preparations. HEp-2 cells (ATCC CCL-23) were maintained in Opti-MEM I medium (Invitrogen) containing 2% (vol/vol) fetal bovine serum (FBS), 1% (vol/vol) l-glutamine, 2.5 μg/ml amphotericin B, and 1% (vol/vol) penicillin-streptomycin. Human bronchial epithelial cells (HBE σ16) were maintained in 10% vol/vol) FBS, 1% (vol/vol) l-glutamine, 2.5 μg/mL amphotericin B, and 1% (vol/vol) penicillin-streptomycin. Transfections were performed using the Effectene transfection reagent (Qiagen) for HEp-2 cells. The RSV *wt* strain A2 was expanded in HEp-2 cells, and RSV/GFP (kindly provided by MedImmune) was expanded in Vero cells.

RSV infections and viral titration. For filament visualization, HEp-2 cell monolayers on 12-mm micro-cover glasses (no. 2; VWR) were inoculated at a multiplicity of infection (MOI) of 1.0 and incubated for 24 h. For quantification of viral yield in the presence of inhibitors and in knockdown cell lines, HEp-2 cell monolayers were inoculated at various MOIs (see assay for details). Cells were then washed and medium was added containing either vehicle, indicated inhibitor, or normal media for knockdown cell lines. At time of harvest, cell supernatant was harvested and normalized for volume. The samples were then clarified of cellular debris by centrifugation in a microcentrifuge at 13,000 rpm for

10 min. The resulting supernatant was designated as supernatant virus. The cell monolayer was resuspended in an equal volume of medium, scraped, and freeze/thawed 3x using a dry ice/ethanol bath and a 37 °C water bath. The samples then were clarified of cellular debris by centrifugation in a microcentrifuge at 13,000 rpm for 10 min. The resulting solution was designated cell-associated virus.

Identification of proteins that interact with RSV F protein cytoplasmic tail by yeast two-hybrid (Y2H) screening. Bait cloning and Y2H screening were performed by Hybrigenics, S.A., Paris, France. A cDNA encoding the RSV strain A2 F cytoplasmic tail was synthesized and then PCR-amplified and cloned in a Y2H vector optimized by Hybrigenics. The bait construct was checked by sequencing the entire insert, and was subsequently transformed in the L40ΔGAL4 yeast strain (30). Fresh human lung tissue was obtained from the healthy margins of a lung resection, and then disrupted and total RNA extracted. A human normal lung random-primed cDNA library containing ten million independent fragments was generated then transformed into the Y187 yeast strain and used for mating. High mating efficiency was obtained by using a specific mating method (70-72). The screen was first performed on a small scale to adapt the selective pressure to the intrinsic property of the bait. Neither toxicity nor auto-activation of the bait was observed. Then, the full-scale screen was performed in conditions ensuring a minimum of 50 million interactions tested, in order to cover five times the primary complexity of the yeast-transformed cDNA library (76). 270 million interactions were tested for interaction with RSV F cytoplasmic tail. After selection on medium lacking leucine, tryptophan, and histidine, 45 positive clones were picked, and the corresponding

prey fragments were amplified by PCR and sequenced at their 5′ and 3′ junctions. Sequences then were filtered and constructed as contigs, as described previously (29), and compared to the latest release of the GenBank database using BLASTN (1). A Predicted Biological Score (PBS) was attributed to assess the reliability of each interaction, as described previously (29). Briefly, the PBS relies on two different levels of analysis. First, the local score took into account the redundancy and independency of prey fragments, as well as the distributions of reading frames and stop codons in overlapping fragments. Second, the global score took into account the interactions found in all the screens performed at Hybrigenics using the same library. In addition, potential false-positives were flagged by a specific "E" PBS score. This designation was assigned by discriminating prey proteins containing "highly connected" domains, previously found several times in screens performed on libraries derived from the same organism. The PBS scores correlate positively with the biological significance of interactions (76, 100).

Generation of shRNA lentiviruses and cell populations with knockdown of gene expression. Five human GIPZ lentiviral shRNAmir constructs were obtained from the Vanderbilt Genomic Sciences Resource Core (filamin A (FLNA), alpha clone V2LHS_131780, positive GAPDH control, and negative non-silencing and empty vector controls). Lentiviruses were produced using the Open Biosystems Trans-Lentiviral GIPZ Packaging System (Thermo Scientific) in HEK 293T cells according to kit instructions. Briefly, cells were transfected with pGIPZ lentiviral vector and packaging mix. Supernatant was collected at 48 and n 72 hours post transfection, clarified at 3,000 rpm for 20 min at 4° C, and filtered using a 0.45 μm PES filter unit. Filtered supernatant was

concentrated using ultracentrifugation at 23,000 rpm for 2 hours. Pellet was resuspended in serum-free DMEM. Transduction efficiency was determined using flow cytometry and GFP expression levels in HEp-2 cells in the presence of 10 μg/mL polybrene (Millipore). Transduced HEp-2 cells were selected for expression using 5 μg /mL puromycin. Expression levels and viral titers were determined from the resulting heterogeneous population.

Quantitative analysis of total cell lysate in knockdown populations. HEp-2 cells transduced with indicated lentivirus were grown under puromycin selection. Cell lysates were harvested using a single detergent lysis buffer (50 mM Tris-HCl, 150 mM NaCl, 1% Triton X-100, pH 8.0) containing 1:200 dilution of mammalian protease inhibitor cocktail (Sigma). Lysates were separated on 4-12% NuPAGE Bis-Tris gels and transferred to nitrocellulose membranes (Invitrogen). Membranes were blocked for one hour using Odyssey blocking buffer (Li-Cor) diluted 1:1 in PBS. Primary antibodies for β -actin (Abcam, 1:5,000), FLNA (Abcam, 1:500), or GAPDH (Millipore, 1:500) were diluted in blocking buffer diluted 1:1 with PBS + 0.1% Tween-20. Secondary antibodies were diluted at 1:5,000 (goat anti-mouse IRDye 800CW and donkey anti-goat IRDye700, Li-Cor) in blocking buffer. Bands were imaged using the Odyssey Infrared Imaging System.

Fixation and immunostaining. Cells were fixed with 3.7% (*wt*/vol) paraformaldehyde in phosphate-buffered saline (PBS) for 10 min. Cells were permeabilized with 0.3% (*wt*/vol) Triton X-100 and 3.7% paraformaldehyde in PBS for 10 min at room temperature (RT). After fixation, cells were blocked in 3% (*wt*/vol) bovine serum albumin (BSA) in PBS for

60 min, followed by addition of primary antibody (Ab) in the blocking solution for 60 min. Cells were then washed three times in PBS, and species-specific IgG Alexa Fluor (Invitrogen) was added at a dilution of 1:1,000 in block solution for 60 min to detect primary Abs. Cells were washed three times in PBS and fixed on glass slides using the Prolong Antifade kit (Invitrogen). All steps were performed at RT. Images were obtained on a Zeiss inverted LSM510 confocal microscope using a 63×/1.40 Plan-Apochromat oil lens. Anti-RSV M (clone B135), anti-RSV P protein (clone 3_5), and anti-RSV N protein (clone B130) monoclonal Abs were a kind gift of Earling Norrby and Ewa Bjorling. An anti-RSV F protein humanized mouse monoclonal ab (palivizumab; MedImmune) was obtained from the Vanderbilt Pharmacy. F-actin was visualized using rhodamine phalloidin, and To-Pro-3 iodide was used to visualize the nucleus (Invitrogen).

Myristoylation inhibitor assays. HEp-2 cells were plated in 48 well plates and inosculated with *wt* RSV at an MOI=1.0 for 1 hour. Cells were then incubated in normal growth media or media containing either GW4869 (Calbiochem) or spiroepoxide (Axxora LLC) at 100 μM. At 72 h.p.i., supernatant and cell-associated virus was harvested.

nSMase inhibitor assays. HBE-σ16 or Caco-BBE cells were plated in 48 well dishes (Costar). Once cell monolayers were confluent cells medium was exchanged for serum-free medium containing either DMSO, 10 μM GW4869 in DMSO (Calbiochem), or 10 μM spiroepoxide in DMSO (Axxora). 16 hours post-treatment cells were infected with RSV at an MOI of 1.0 for 1 hour in normal growth medium. Infectious medium was

aspirated and replaced by medium containing either the same inhibitor or DMSO. 72 h.p.i., supernatant- and cell-associated virus was collected and tittered.[10]

Rab25 mouse studies. Mice were inoculated intranasally with 10^6 pfu RSV *wt* strain A2. On day 4 after inoculation, mice were sacrificed by CO2 inhalation. The lungs were harvested for virus quantification by plaque assay. Lung tissues were ground using a glass homogenizer in 3 mL of HBSS (Hanks Balanced Salt Solution) medium. Homogenates were clarified by centrifugation in a tabletop centrifuge at 2,000 rpm at 4 °C for 10 min, and supernatants were used to determine viral titers (65).

Results

Filamin A localizes to viral filaments. Since I had previously shown that the F CT is essential for viral assembly, we sought to determine whether host factors function in viral filamentous assembly though interactions with the F CT. Hybrigenics performed a Y2H screen using a custom human lung tissue cDNA library and probed with a peptide corresponding to the *wt* F CT as bait. The results from this screen are summarized in Table 4-1. I sought to screen candidate F CT-interacting proteins by microscopy to determine if any localized to viral structures in infected cells. HEp-2 cell culture monolayers were either mock-infected or infected with *wt* RSV and incubated for 24 hours in complete growth medium. Cells were fixed and immunostained for RSV F to mark viral filaments and the indicated host protein. Figure 4-1 shows the localization of these proteins in mock- or RSV-infected cells. Several proteins did not distribute to

[10] These methods were developed by Thomas Utley and are described in his thesis entitled, "Investigations in the assembly and budding of respiratory syncytial virus."

filaments. Glutamate-ammonia ligase (GLUL) was seen throughout the cell in punctate granules, but did not localize to viral filaments in RSV-infected cells (Fig. 4-1 A-D). Four and a half LIM domains 2 (FHL2) protein exhibited a diffuse pattern throughout the cytoplasm, but it also failed to co-localize with RSV F in viral filaments (Fig. 4-1 E-H). In contrast, although filamin A (FLNA) also localized diffusely throughout the cytoplasm, it specifically co-localized with RSV F in viral filaments (Fig. 4-1 I-L).

To confirm this co-localization, HEp-2 cell culture monolayers were mock-infected or infected with *wt* RSV that also encodes a GFP protein (RSV/GFP) to mark infected cells (Fig. 4-1 M-P). Compared to neighboring uninfected cells, filamin A in infected cells appeared to localize brightly to virus-induced structures at the cell surface that were kinked and clustered in a manner consistent with viral filaments. GFP, which typically diffuses throughout the cytoplasm when expressed in cells, was excluded from these structures, indicating that protein sorting into viral filaments is specific, and cytoplasmic diffusion alone is not sufficient for filamin A incorporation into viral assembly structures.

Knockdown of filamin A gene expression does not affect viral replication. Since filamin A exhibited the greatest degree of localization with viral filaments of any cytoskeleton-related proteins examined, I studied its role in assembly and budding. I inhibited expression of filamin A to determine if reduction of expression inhibited the efficiency of viral replication in infected cells. To reduce filamin A gene expression, I generated lentiviruses that express an shRNA hairpin directed against filamin A. HEp-2 cell culture monolayers were transduced with the filamin A shRNA lentivirus (FLNA)

Gene Name	Frame	Y2H Fragments	Description
C1orf43	??	antisense	HepC NSSA Transactivated
COL6A2	IF		Collagen α2 (type IV) chain
DD5	IF		E3 ubiquitin protein ligase, HECT family
DGAT1	??	antisense	Diacylglycerol O-acyltransferase homolog 1
FAM114A2	??	antisense, 3′ UTR	Family with sequence similarity 114, member A2
FHL2	IF		Four and a half LIM domains 2: translational regulation
FLNA var1	IF		Filamin A; associated with actin cytoskeleton
GLUL	IF		Glutamate-ammonia ligase
GOLGA8A	??	antisense, 3′ UTR	Golgi autoantigen, golgi matrix protein
HLA-DRB5	IF		Major histocompatibility complex, class II, DRβ5
HPGD	??	antisense, 3′ UTR	Hydroxyprostaglandin dehydrogenase 15-(NAD)
HSPA5	IF		Heat shock 70 kDa protein 5 (glucose-regulated protein, 78kDa)
LPL	??	antisense, 3′ UTR	Lipoprotein lipase
RBM12	IF	3′ UTR, IF stop codon	RNA binding motif protein 12
RPL23A	??	antisense	Ribosomal protein L23a
SERPINF1	IF	IF stop codon	Serpin peptidase inhibitor, clade F
SGK269	??	antisense, 3′ UTR	Sugen kinase 269
SNRP70	IF		Small nuclear ribonucleoprotein 70 kDa polypeptide (RNP antigen)
SP140	IF		SP140 nuclear body protein
SRP9	IF	antisense, 3′ UTR	Signal recognition particle 9 kDa
TBC1D15	IF		TBC1 domain family, member 15; GTPase activating protein
TGFβ3	IF		Transforming growth factor β3

Table 4-1. Summary of candidate proteins from F CT Y2H screen of a custom lung cDNA library The Y2H screen was performed by Hybrigenics (Paris, France) using the *wt* F CT peptide fused to LexA at the N-terminus as bait to screen a custom human lung cDNA library. The candidate proteins are listed by their gene name along with a description of the gene and associations. The cDNA fragment also was analyzed for being in frame (IF), unknown frame (??), and whether the interaction was with an antisense strand (antisense) or in the 3′ UTR (3′ UTR).

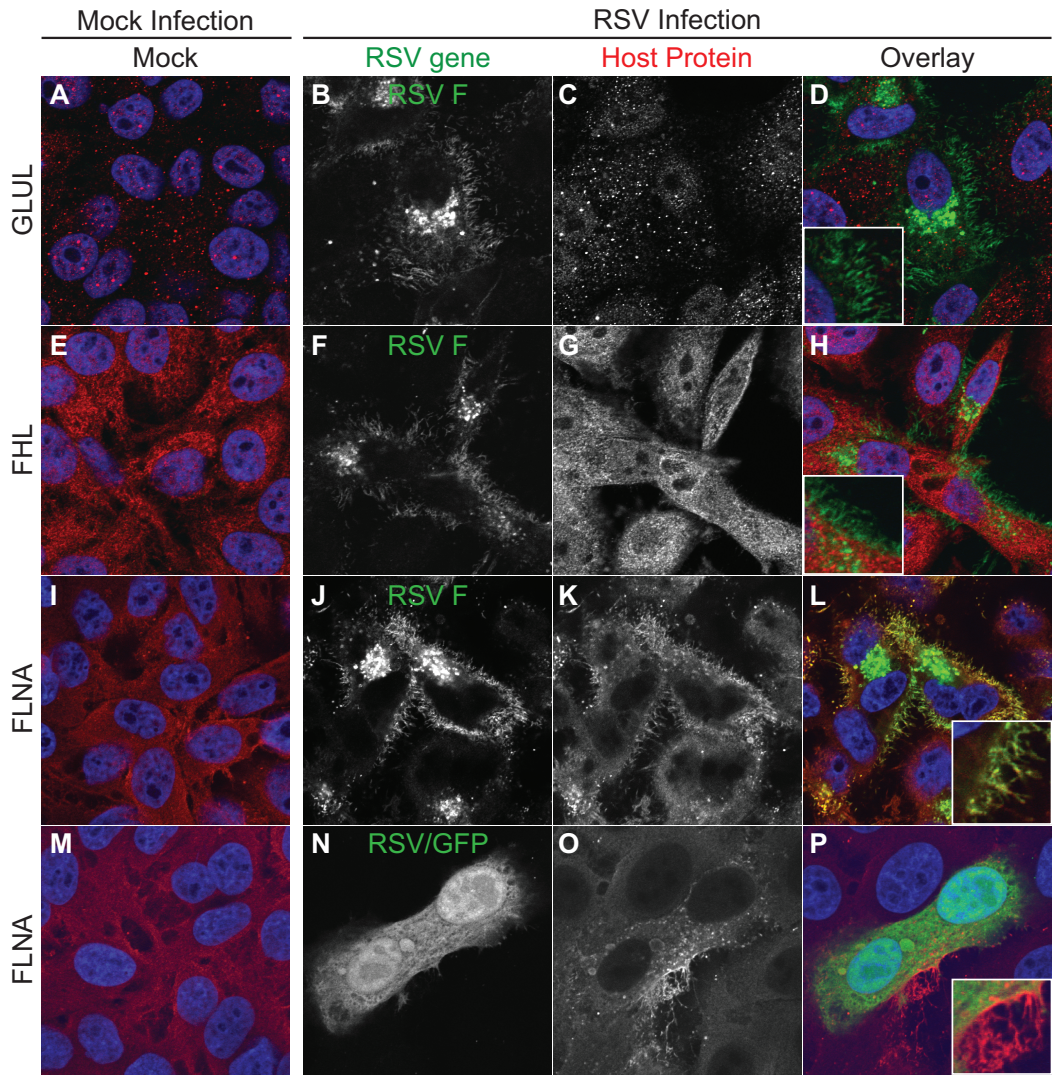

Figure 4-1. Cellular localization of candidate proteins from an F CT Y2H screen. HEp-2 cells were inoculated with RSV strain A2 at than MOI=1.0 and incubated for 24 hours. RSV F and the indicated cellular proteins were detected by indirect immunofluorescence. Column 1 (panels A, E, I, and M) shows mock infected cells, and columns 2-4 show RSV infected cells. Column 2 (panels B, F, J, and N) shows the indicated RSV protein; column 3 (panels C, G, K, and O) shows the indicated cellular proteins; and column 4 (panels D, H, L, and P) shows the overlay with the RSV protein in green and the cellular protein in red.

or with control lentiviruses encoding no shRNA (empty), an shRNA that is non-silencing (N.S.), or an shRNA directed against the housekeeping gene GAPDH. Cells were selected for shRNA expression using puromycin, and the resulting puromycin-resistant cell lines were screened for protein knockdown and viral replication. Figure 4-2A shows that transduction of cells with the filamin A shRNA lentivirus caused a >99% knockdown of expression of the protein. As a parallel control, GAPDH expression was inhibited in cells transduced with GAPDH shRNA. Transduction with empty vector or non-silencing lentiviruses did not affect the expression of either GAPDH or filamin A.

Since the knockdown of filamin A was efficient, I next infected these lentivirus-transduced cells with *wt* RSV strain A2 at an MOI=0.05 to determine the effect of filamin A knockdown on viral replication at 72 hours post-infection (h.p.i). Figures 4-2B and 4-2C show that neither supernatant nor cell-associated viral titer, respectively, were affected by the knockdown of filamin A. In addition to filamin A, I also tested whether other proteins from the yeast two hybrid F CT interaction screen were required for efficient viral replication by expressing shRNA against each protein delivered by lentiviruses, as described for filamin A. Expression of shRNA was confirmed by GFP expression from a second reading frame, but total viral yield at 72 h.p.i. was not affected (Table 4-2). Collectively, these data suggest that although filamin A protein localizes to viral filaments, it is not required for viral replication.

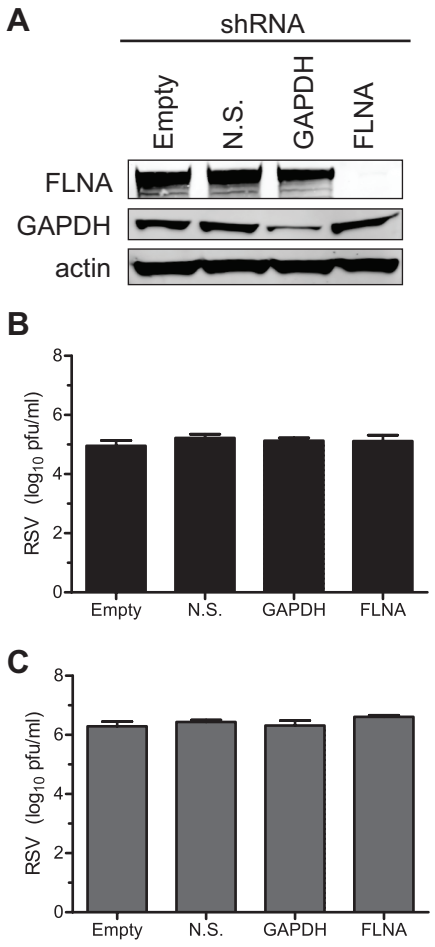

Figure 4-2. Viral titers in FLNA knockdown cells. HEp-2 cells were transduced with a lentivirus encoding an shRNA directed against the indicated protein. After selection, cell lysates were harvested and filamin A, GAPDH, and actin were detected by immunoblot (A). The same cells then were infected with RSV stain A2 at an MOI=0.05 for 72 hours. Both cell-associated (B) and supernatant virus (C) yields were quantified by a plaque assay.

Gene Name	Antibody	shRNA	Results
FHL2	+	+	No co-localization with RSV F; shRNA does affect on viral titers
FLNA, var 1	+	+	Co-localization with RSV F in viral filaments; shRNA does affect on viral titers
GLUL	+	+	No co-localization with RSV F; shRNA does affect on viral titers
SRP9	+	+	Antibody did not detect protein by IF; shRNA does not affect viral titers
TBC1D15	+	+	Antibody did not detect protein by IF; shRNA does not affect viral titers

Table 4-2. Summary of results: available antibodies and shRNAs for candidate proteins from F CT Y2H screen. The available reagents for the F CT Y2H candidate genes are summarized. For genes with available antibodies, HEp-2 cells were inoculated with RSV *wt* strain A2 at an MOI=1.0 for 24 hours. At 24 hours, cells were fixed, and RSV F and the indicated cellular protein were detected by indirect immunofluorescence. For genes with available shRNA lentivirus constructs, HEp-2 cells were transduced with each lentivirus construct. A heterogeneous population was selected using puromycin, and expression of the shRNA was confirmed by concomitant expression of GFP. Cells were then infected with RSV strain A2 at an MOI=0.05 for 72 hours and both supernatant and cell associated virus yields were determined by plaque assay. The results for localization to viral filaments marked by RSV F and affect of shRNA expression on viral yields is summarized.

PICALM localizes to viral inclusion bodies. In addition to an F CT Y2H screen, Hybrigenics also performed a Y2H screen with the M protein using the same custom lung cDNA library. The results of this screen are summarized in Table 4-3. I chose to test five proteins from this list based on protein function and the availability of antibodies. Syntaxin 18, (STX18) is a SNARE protein that localizes to the ER membrane and is a component of the SNARE complex, which often function in fusing membranes (90). Phosphatidylinositol binding clathrin assembly protein (PICALM) recruits clathrin and adaptor protein complex 2 (AP2) to cell membranes at sites of coated-pit formation and clathrin-vesicle assembly (16). Optineurin (OPTN) is a protein implicated in glaucoma that interacts with Rab8 and myosin VI at the Golgi apparatus (19). Guanine nucleotide-binding proteins (GNAL) are G proteins and may be involved in signaling pathways (98). Finally, AP3µ1 is the cargo recognition subunit of the adapter protein 3 complex that is involved in endosomal and lysosomal sorting (74). Figure 4-3 shows HEp-2 cells that have been mock-inoculated or inoculated with *wt* RSV at an MOI=1.0 and incubated for 24 hours. RSV M and the indicated cellular protein were detected by indirect immunofluorescence. The results show that AP3µ1 (Figure 4-3A and 4-3B) localized diffusely throughout the cell and did not localize exclusively with M. OPTN did co-localize with the M protein, but also was present diffusely throughout the cell (Figure 4-3C and 4-3D). PICALM colocalized with M, largely in discrete granules that resembled RSV inclusion bodies (Figure 4-3E and 4-3F). The only available antibodies for STX18 and GNAL did not detect the respective proteins by immunofluorescence.

Gene Name	Frame	Y2H Fragments	Description
AP3μ1	IF	3′ UTR IF SC	Cargo recognition subunit of AP3; Involved in endosomal sorting
GMEB1	IF	IF SC	
GNAL	IF		G protein; signal transduction within olfactory neuroepithelium
GTF2H1	IF		
HLA-DRB1	IF		
OPTN	IF		Binds myosin VI at the golgi; Co-localizes with Rab8
PICALM	IF	IF SC	Clathrin assembly protein
RBM41	IF	IF SC	
SNRP70	IF		
STX18	IF		Component of a SNARE complex; Localizes to ER membrane
ZNF91-like	IF		
HSP22	IF	IF SC	
Protein kinase H11	IF	IF SC	
Surfactant pulmonary associated protein C	OOF		

Table 4-3. Summary of candidate proteins from M Y2H screen of a custom lung cDNA library. The Y2H screen was performed by Hybrigenics (Paris, France) using an Mopt peptide fused to LexA at the N-terminus as bait to screen a custom human lung cDNA library. The candidate proteins are listed by their gene name along with a description of the gene and associations. The cDNA fragment also was analyzed for being in frame (IF), out of frame (OOF), and whether the interaction was in the 3′ UTR (3′ UTR) or contained an in frame stop codon (IF SC).

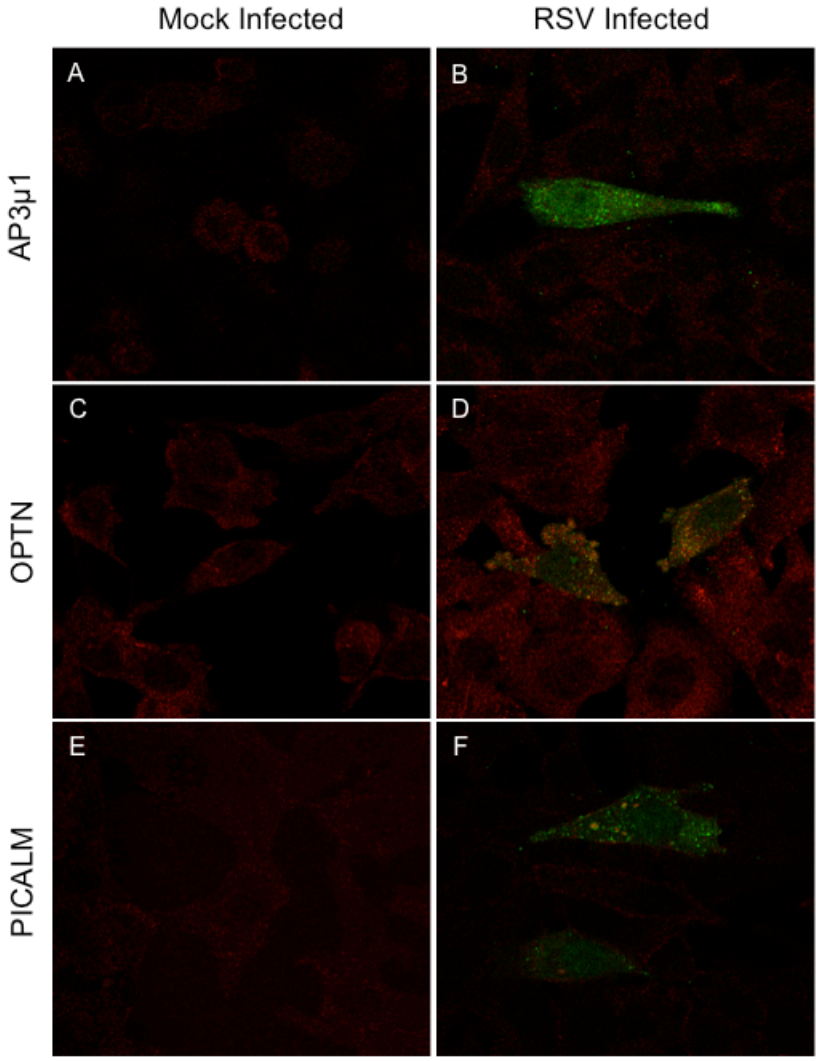

Figure 4-3. Cellular localization of candidate proteins from an M Y2H screen. HEp-2 cells were inoculated with RSV strain A2 at than MOI=1.0 and incubated for 24 hours. RSV M and the indicated cellular proteins were detected by indirect immunofluorescence. RSV M is shown in green and the cellular gene in red. Column 1 (panels A, C, and E) shows mock infected cells, and columns 2 (panels B, D, and F) shows RSV-infected cells.

Since PICALM appeared to localize to viral inclusion bodies, I repeated the above experiment and stained for RSV N and P, which mark RSV inclusion bodies. Figure 4-4 shows the PICALM does indeed colocalize with RSV N and P in inclusion bodies (Fig. 4-4G and 4-4J, respectively). Next, I attempted to knockdown PICALM by transfecting cells with a pool of siRNAs directed against PICALM (Dharmacon) to determine if PICALM plays a role in viral replication. As controls, I also used siRNAs to GAPDH or a non-specific siRNA as described previously. Transfection with siRNAs resulted in a 25-50% knockdown of PICALM, and the non-specific siRNAs did not affect PICALM expression (Fig. 4-4K and 4-4L). Since inclusion bodies are thought to function as viral transcription and replication sites, I tested whether PICALM knockdown, although incomplete, had an effect on viral transcripts at 18 h.p.i. using RT-PCR with probes directed against the F protein. There was, however, no affect on viral transcripts PICALM siRNA treated cells versus untreated or non-specific siRNA treated cells. These data show that although PICALM localized to viral inclusion bodies, the protein may not play a significant role in viral transcription. Further studies would be necessary to determine if PICALM is important for another part of the viral life cycle.

OPTN knockdown does not affect viral replication. In addition to testing PICALM for affect on viral replication, I also tested the effect of OPTN knockdown on the ability of RSV to replicate in human bronchial epithelial (HBEσ16) cells. For another project, Thomas Utley and Josh Heck in the Crowe laboratory had created an OPTN knockdown cell line, along with control untreated and non-targeting (N.T.) cell lines, using a lentivirus to deliver an shRNA construct under G418 selection. Using these cell lines,

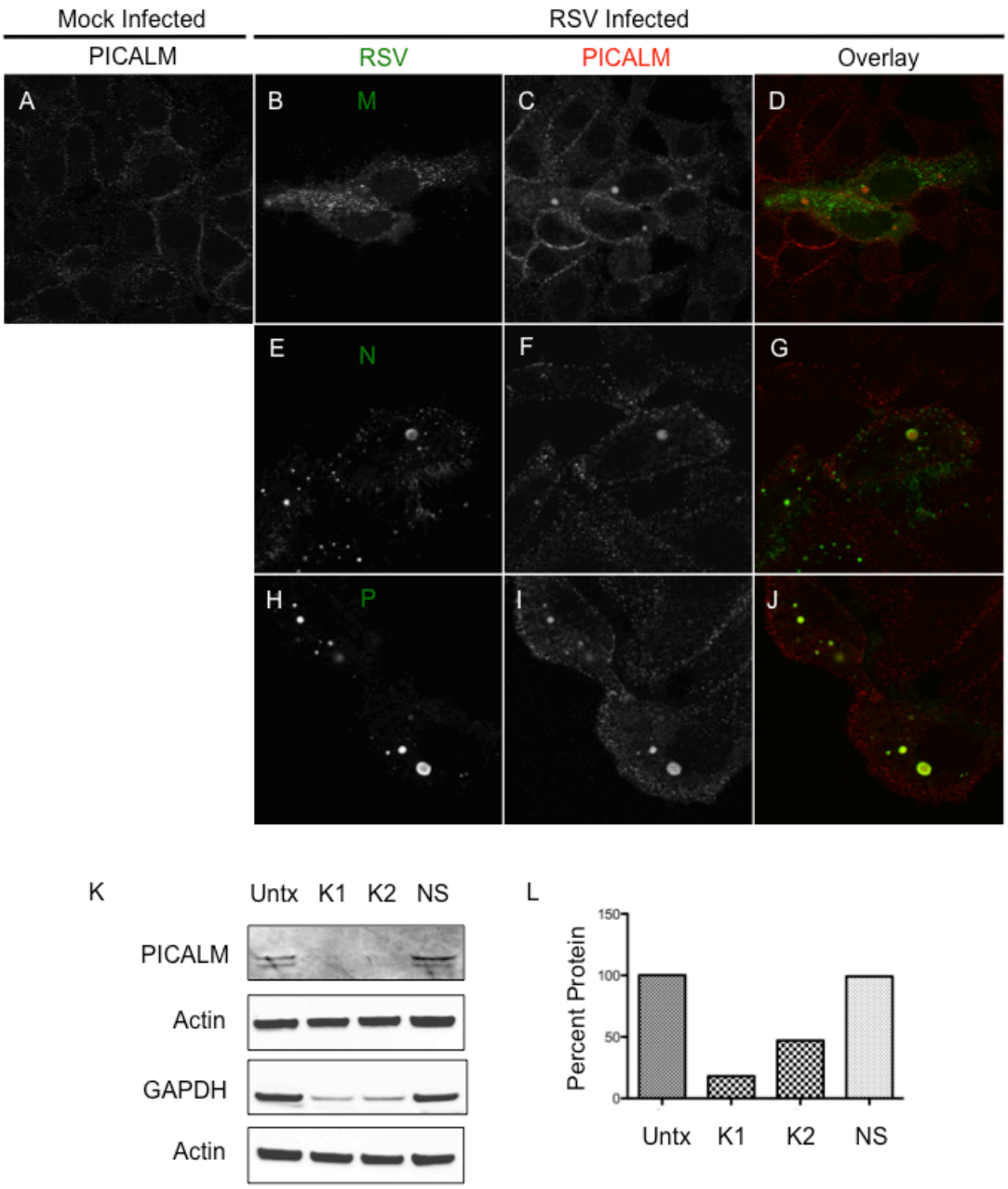

Figure 4-4. PICALM localized with N and P in viral inclusion bodies. Panels A-J. HEp-2 cells were inoculated with RSV at an MOI=1.0 for 24 hours. RSV M, N, P, and PICALM were detected using indirect immunostaining. Mock infected cells immunostained for PICALM are shown in column 1 (panel A). Columns 2-4 show RSV infected cells. Column 2 (panels B, E, and H) shows the indicated RSV protein staining. Column 3 (panels C, F, and I) shows PICALM staining. Column 3 (panels D, G, and J) show the overlay with the RSV protein in green and PICALM in red. Panel K and L: HEp-2 cells were left untreated or transfected with a pool of siRNA constructs directed against PICALM, GAPDH, or non-specific (NS) siRNA. Proteins were detected by immunoblot (K) and quantified (L) as a percentage of untreated protein level.

I inoculated HBEσ16 cells at an MOI=1.0 for 2, 3, and 6 days and quantified supernatant and cell-associated virus at each time point. Figure 4-5 shows that RSV replication was lower in OPTN shRNA-expressing cells, compared to untreated or N.T shRNA-expressing cells in both the supernatant (Fig. 4-5A) and cell-associated fractions (Fig. 4.6B). However, these data were not statistically significant. Therefore, although OPTN is a candidate for interaction with the M protein by Y2H, the results indicate that it does not play a significant role in viral replication.

Inhibition of myristoylation does not affect viral replication. In addition to a Y2H screen with the M protein, I also performed a motif analysis of the M protein using PredictProtein software (data not shown). The results suggest that the M protein is myristoylated, which would explain its capacity to associate with membranes (44). To test this hypothesis, I treated HEp-2 cells with two small molecule myristoylation inhibitors, DL-2-hydroxymyristic acid (2OHM) and 13-oxamyristic acid (13OM), that affect replication of other viruses (22). HEp-2 cells were inoculated with RSV at an MOI=1.0, and incubated in normal growth media or media containing the indicated inhibitor. At 72 h.p.i., both supernatant and cell-associated virus were harvested seperately. Figure 4-6 shows that inhibition of cellular myristoylation did not affect viral replication. These data do not exclude the possibility that the M protein is myristoylated, especially since no positive control is used for these inhibitors. However, these data suggest that myristoylation may not be critical for viral replication.

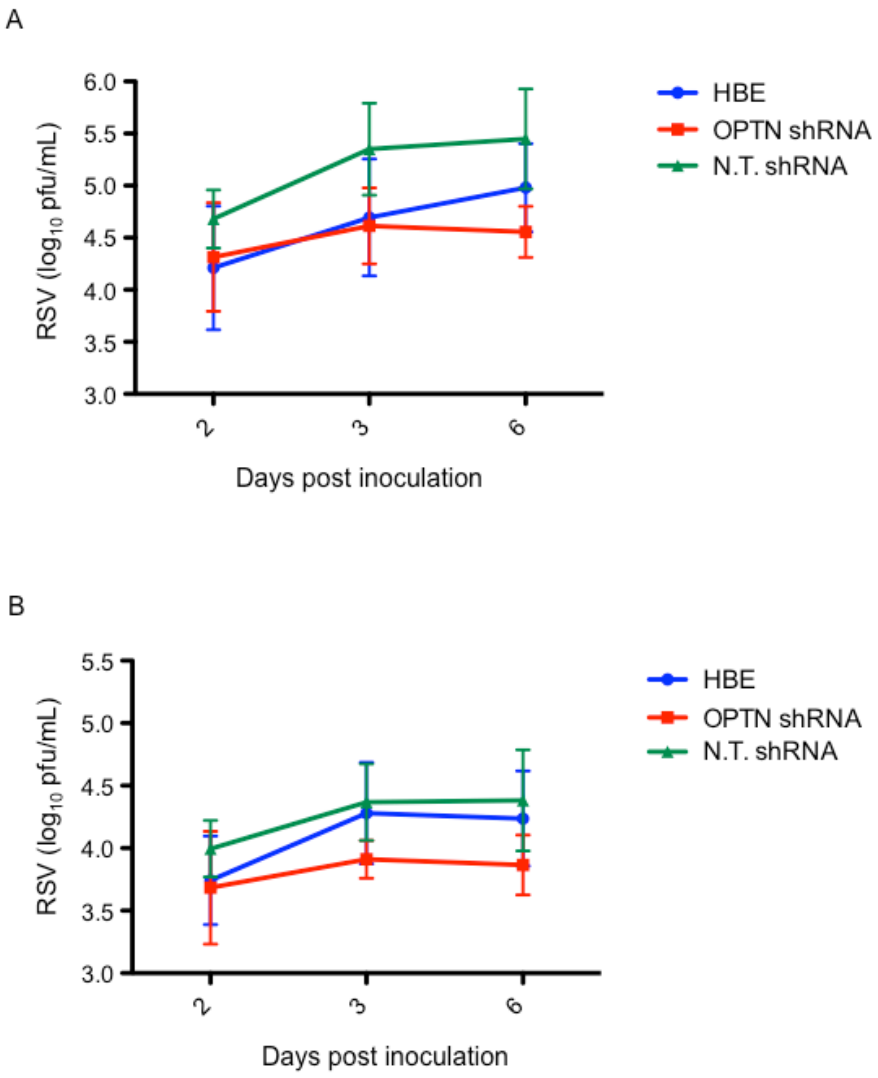

Figure 4-5. Viral titers in OPTN knockdown cells. HBEσ16 cells that stably expressed the indicated shRNA were infected with RSV at an MOI=1.0 for 2, 3, or 6 days. Viral supernatants (A) and cell-associated (B) titers were determined using a plaque assay.

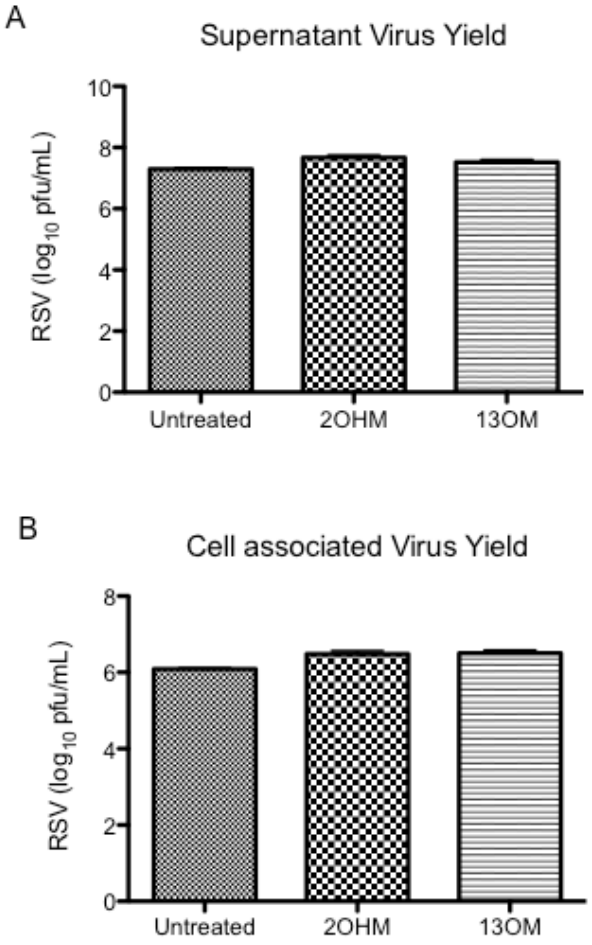

Figure 4-6. Myristoylation inhibitors do not affect RSV replication. HEp-2 cells were inoculated with *wt* RSV at an MOI=1.0. Cells were left in normal growth media (untreated) or incubated with inhibitor. Viral supernatants (A) and cell-associated (B) titers were determined using a plaque assay.

Inhibition of exosomes does not affect viral replication. Finally, in addition to Y2H screens and motif analysis, I also sought to replicate findings that RSV may use exosomes in order to bud from host cells. Previous work in the Crowe laboratory by Thomas Utley in the Crowe laboratory found that inhibition of neutral sphingomyelinase (nSMase) using two chemical inhibitors results in diminished supernatant but not cell-associated viral titers. Since the RSV budding mechanism is ESCRT-independent (97), the mechanism by which RSV performs that final membrane scission step is unknown. The exosome mechanisms of membrane scission involve conversion and placement of lipids to create the membrane curvature required to form exocytic vesicles. Formation of ceramide, a cone-shaped lipid, by nSMase is sufficient to produce exocytic vesicles (46, 93). Therefore, it is plausible that RSV recruits nSMase to enrich viral filaments in ceramide and thereby produce membrane scission. HBEσ16 cells were treated with medium containing DMSO only, GW4869, or spiroepoxide. After treatment, cells were inoculated with RSV at an MOI=1.0 for one hour and again incubated in medium containing either vehicle or inhibitor. Supernatant and cell-associated virus was quantified at 72 h.p.i.. Figure 4-7 shows a representative experiment in which there was little effect on RSV replication in the presence of inhibitor. Supernatant virus yield, which represents the budded fraction, was reduced by 0.5 $\log_{10}$ pfu/mL in the presence of GW4869 but unaffected by spiroexpoxide (Fig. 4-7A). Cell-associated virus yield was unaffected in the presence of either inhibitor (Fig. 4-7B). These data are contradictory to the results obtained previously. These experiments were repeated six times, with varying levels of RSV replication. However, the original results could not be replicated nor was an assay readily available to test whether the inhibitors were working properly.

In addition to inhibitor studies, I also examined the localization of endogenous and GFP-tagged nSMase2 in HBEσ16 cells. Cells were inoculated with RSV at an MOI=1.0, incubated for 24 or 72 hours, and immunostained for F or nSMase2 (Fig. 4-8 A-H). Cells expressing GFP-nSMase2 were transfected with a plasmid encoding GFP fused to nSMase2, a gift from Motohiro Tani that was previously validated (87), 24 hours prior to inoculation (Fig. 4-8 I-L). The results show that endogenous nSMase localizes to viral filament marked by F at both 24 and 72 h.p.i. (Fig. 4-8 A-H). However, a GFP-nSMase2 fusion protein did not localize to viral filaments. It is possible that the GFP tag interferes with the localization of nSMase2 in viral filaments the antibody may be cross-reactive with other cellular proteins. The data from these localization studies are similar to those obtained previously, but are not consistent with the inhibitor data. The source of this discrepancy is unknown, and further studies of the exosome pathway are required to conclusively determine whether it is involved in RSV budding.

RSV replication is not affected by knockout of Rab25 in a mouse model. Finally, I attempted to determine if knockout of ARE proteins, such as Rab25, affects the ability of RSV to replicate in mice (17). Previous studies in the Crowe laboratory by Sean Brock and Thomas Utley indicated that the ARE is important for viral assembly and budding (9, 97). Our collaborator at Vanderbilt, Jim Goldenring, kindly supplied us with Rab25 knockout (KO) mice on a C57/BL6 background. With the help of Sunny Mok, Rab25 KO mice, along with age-matched controls, were infected with 10^6 PFU RSV intranasally under anesthesia. At 6 days post infection, mice were euthanized and the lungs were harvested and processed for viral titers. Figure 4-8 shows the viral titers in homogenized

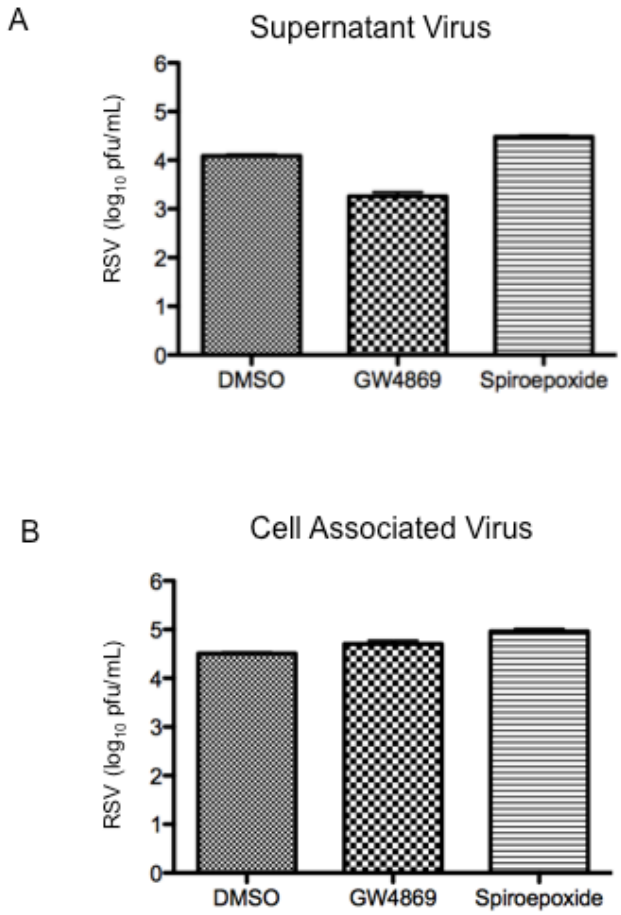

Figure 4-7. Viral titers with nSMase inhibitors. HBEσ16 cells were pretreated with either vehicle or inhibitor for 16 hours and then inoculated with RSV at an MOI=1.0. After inoculation, cells were again treated with either vehicle or inhibitor for 72 hours. Viral supernatants (A) and cell-associated (B) titers were determined using a plaque assay.

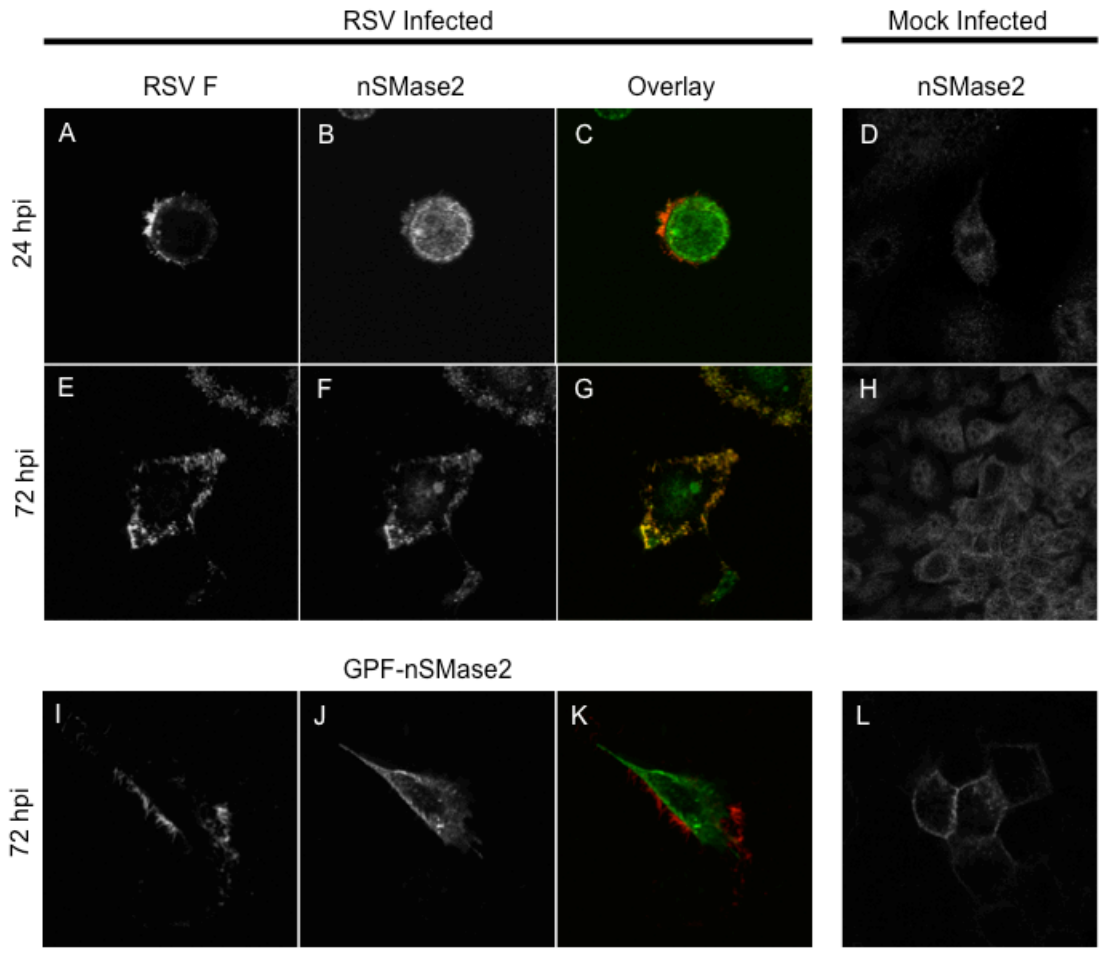

Figure 4-8. nSMase localization in RSV-infected cells. HBEσ16 cells were inoculated with RSV and incubated for 24 or 72 hours. Cells expressing GFP-nSMase2 were transfected 24 hours prior to virus inoculation. RSV F was detected by indirect immunofluorescence and nSMase2 was detected with either indirect immunofluorescence (A-H) or by GFP fluorescence (I-L).

mouse lung tissue. RSV replication was reduced in Rab25 KO mice by approximately 0.5 $\log_{10}$ pfu/mL. However, the differences were not significant. Although Rab25 and the ARE clearly affect viral replication, apparently Rab25 function could be compensated *in vivo* by other ARE proteins. Furthermore, RSV produces titers in mice of only $4x10^4$ pfu/mL, which is much lower than those obtained from human cell lines. Therefore, the limitations of the mouse model for RSV experiments may make it difficult to interpret the role of Rab25 in RSV replication.

Discussion

Mechanisms of RSV assembly and budding are of interest since it appears to use an unconventional pathway that is independent of host proteins of the multi-vesicular body apparatus (97). A number of viruses coopt the host cytoskeleton and related proteins to accomplish assembly and budding (88). I had determined previously that the RSV F CT coordinates filament formation, and here we show data suggesting that the F CT interacts with the host protein filamin A. We found this interaction interesting because it may function in anchoring emerging viral filaments to the cytoskeleton and therefore might allow some mechanical advantage needed to deform host cell membrane and elongate the viral filaments. Indeed, some of the images in chapter II in the setting of depolymerized actin suggested that the base of filaments might be transiently associated with actin. Comprehensive Y2H and proteomic studies done previously in the Crowe laboratory by Thomas Utley revealed that cytoskeletal elements are abundant in the apical region of polarized cells, but we found that the dominant apical cytoskeleton-associated proteins did not localize to filaments (see Chapter II for details). Even filamin

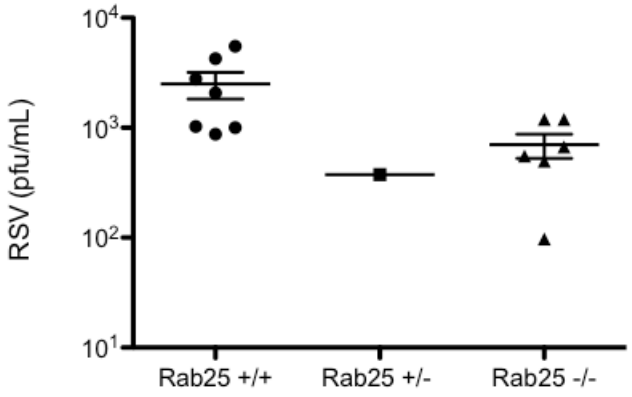

Figure 4-9. RSV replication in Rab25 knockout mice. Rab25 knockout mice and age-matched controls on a C57/BL6 background were inoculated with 10^6 pfu RSV intranasally. At six days post infection, mouse lungs were collected and homogenized. Viral titers were determined by plaque assay.

A, the sole host protein that we confirmed to be located reliably in filaments, was not required for viral replication, suggesting that an F CT-filamin A interaction is not necessary for viral assembly into filaments.

While inhibition of filamin A expression did not affect viral replication, these data do not necessarily exclude a role for filamin A in viral replication. Filamin A is part of a larger family of filaments that connect the cortical actin network to the plasma membrane. Given the interaction of F CT and filamin A, the protein may still function in anchoring the F protein to the cortical actin network or to certain lipid microdomains, thereby localizing F to the appropriate location in the plasma membrane for assembly. It is possible that in the absence of filamin A, other members of the filamin family are able to substitute for filamin A.

Secondly, I performed a series of studies of the M protein. Viral M proteins are thought to provide a major component of the structure for viral particles. A recent study examining viral filaments by scanning electron microscopy showed that in the absence of the M protein, short filament-like structures with F and G were observed on the cell surface (64). These data suggest that while the viral glycoproteins are sufficient for the initial outward bud formation, elongation of filaments is driven by the M protein. The M proteins of other viruses oligomerize into higher order structures (32), and it is possible that oligomerization of the RSV M protein is responsible for elongation of the structure of viral filaments. To determine if host proteins are involved in this process, I screened a number of candidate proteins that were found to interact with the M protein by a Y2H screen. Although the function and localization of some of these candidates appeared promising, such as association of PICALM with viral inclusion bodies, none were found

to be required for viral replication. Furthermore, I also examined the mechanism by which the M protein associates with membranes. The data in this chapter suggest that this process is not dependent on myristoylation, and after these studies were performed, the crystal structure of the M protein was solved. The membrane-association properties of the M protein are likely attributed to large patches of basic residues on the surface of the M protein that span across both the N- and C-terminal domains that interact with phospholipids (66).

Finally, although many studies were performed to elucidate interactions of host proteins with F and M, the mechanism by which RSV performs the final scission event is still unknown. RSV budding appears to be independent of ESCRT and nSMase, suggesting that host proteins may not function in viral budding. The influenza M2 protein localizes to the neck of viral filaments and may mediate membrane scission through an amphipathic helix in the cytoplasmic tail (78). It is therefore possible for viruses to accomplish membrane scission with assistance from the host, and further study of viral proteins may elucidate the requirements for RSV budding.

Chapter summary

In chapters II and III, I showed that viral proteins, and specifically a Phe residue in the F CT, may be the driving factors for viral assembly into filaments. However, many viruses interact with the host cell. In this chapter, I used the results of two Y2H screens to show that RSV assembly and budding is independent of many host proteins. These data are summarized in Table 4-4. These data show that although host proteins may be involved in viral processes, these proteins are not critical to viral replication. However,

Candidates	Colocalization Results	Protein Knockdown Results
Approach: F CT Y2H Screen		
GLUL	VF - no colocalization	No effect on viral replication shRNA expression confirmed by GFP
FHL	VF - no colocalization	No effect on viral replication shRNA expression confirmed by GFP
FLNA	Colocalization with VF	No effect on viral replication Knockdown confirmed by IB
SRP9	Antibody did not work	No effect on viral replication shRNA expression confirmed by GFP
TBC1D15	Antibody did not work	No effect on viral replication shRNA expression confirmed by GFP
Approach: M Y2H screen		
AP3µ1	VF - no colocalization	N/A
OPTN	Colocalization with M in cytoplasm	shRNA expressing cell line – no effect on RSV titers
PICALM	Colocalization with IBs	siRNA does not affect viral RNA levels Knockdown confirmed by IB
STX18	Antibody did not work	N/A
GNAL	Antibody did not work	N/A
Approach: exosome data validation		
nSMase2	Endogenous protein colocalization with VF GFP-nSMase2 does not colocalize with VF	Inhibition by GW4869 and spiroexpoxide has minor affect on supernatant virus
Approach: ARE protein validation		
Rab25	N/A	Knockout in mice has no effect on viral replication in lungs

Table 4-4: Summary of investigated RSV host interactions. Candidate genes and proteins were examined for localization with viral structures and proteins by indirect immunofluorescence, shRNA/siRNA protein knockdown approaches, knockdown cell lines, and knockout mouse models. VF = viral filaments, IB = inclusion bodies.

there are many caveats to these experiments, including the fact that the function of these host proteins may be compensated by other cellular proteins. Certainly, RSV relies on host proteins for replication (15, 57, 58), and many more proteins have been shown to associate with viral structures (75). Therefore, further studies of RSV interactions with the host cell are required to define critical factors for viral replication. Collectively, these data indicate that RSV proteins interact with many host factors but may have evolved to accomplish efficient replication independent of these interactions. Alternatively, the data might indicate that these interactions are artificial results of the screening method.

Chapter V

SUMMARY AND FUTURE DIRECTIONS

Thesis summary

As described in chapter I, the viral and host determinants of RSV assembly and budding have not been well characterized. In this thesis, I demonstrate that assembly of viral filaments at the cell surface is driven by viral proteins and specifically depends on the F CT to incorporate internal virion proteins into filaments. I also show data about a number of host factors that participate in RSV assembly and budding.

I first attempted to characterize viral filamentous assembly at the cell surface. RSV filaments were shown to contain viral structural proteins and genomic RNA and were therefore considered to be sites of viral assembly prior to budding. The minimum viral protein requirements for filaments were determined to be F, M, N, and P, which resulted in formation of virus-like filaments at the cell surface and budded VLPs that could be detected in the cell supernatant. Formation of these filaments did not depend on host cell cytoskeletal rearrangements. In fact, both F-actin and tubulin were absent from viral filaments. However, disruption of the cytoskeleton did affect the efficiency of filament formation. Actin or actin-associated proteins may be involved in anchoring filaments below the plasma membrane. Overall, however, these data indicate that viral filaments are distinct from host cytoskeleton-based protrusions at the cell surface.

In addition to the composition of viral filaments, my data show that the components of viral filaments suggest there is a mechanism for specific sorting of

cytosolic and membrane proteins into these viral assembly structures. A number of actin-associated cytosolic proteins were excluded from viral filaments, as was cytosolic GFP expressed after transfection. RSV assembly is thought to occur at lipid rafts, but both raft and non-raft membrane proteins were excluded from viral filaments. These data suggest that viral filaments are the result of specific protein sorting at both the plasma membrane and the cell interior. Therefore, viral assembly into filaments may depend on direct interactions between viral proteins.

Since viral proteins appeared to be the driving factors of filamentous assembly, I next sought to determine the viral determinants of the assembly process by focusing on the capacity of the F CT to coordinate internal virion protein assembly into viral filaments. A critical residue near the C terminus of the F CT was found to be required for the formation of virus-like filaments independent of infection. The terminal three residues, Phe-Ser-Asn, were both necessary and sufficient for filament formation. Furthermore, mutation of the Phe residue or deletion of the terminal three residues resulted in a reduced number of VLPs, and the VLPs that formed did not incorporate internal virion proteins into budded particles. These data provide a link between viral requirements of assembly into filaments and the generation of budded cell-free particles. Finally, M protein incorporation into VLPs most strongly correlated with filamentous assembly, suggesting that the F CT may interact with the M protein to facilitate RSV assembly and budding.

Finally, I examined host factors that may participate in RSV assembly and budding using a Y2H screen with the F CT and the M protein as bait for interaction with proteins expressed from a custom human lung cDNA library. The Y2H screen identified filamin

A, PICALM, and OPTN, as proteins that potentially interacted with RSV proteins. Filamin colocalized with F in viral filaments. Knockdown of filamin A indicated that it is dispensable for viral replication. Secondly, I found that PICALM localized to viral inclusion bodies, which are thought to be sites of viral transcription and replication. However, knockdown of PICALM did not disrupt RSV transcription. Third, OPTN colocalized with the M protein. However, knockdown of OPTN did not affect viral replication. In addition to Y2H screens, I also studied the role of the ARE in RSV replication using a mouse model. Knockout of Rab25 in mice resulted in a modest reduction of viral replication. The data from Y2H screens and other proteomics-based approaches indicate that a number of host proteins are associated with viral structures but not critical for viral replication. Collectively, these data indicate that RSV proteins interact with many host factors but may have evolved to accomplish efficient replication independent of these interactions.

Finally, I examined viral budding. RSV budding is known to be ESCRT-independent, but the mechanism by which the final membrane scission event occurs is unknown. Previous data in the Crowe laboratory had suggested that RSV may use an exosome pathway to exit the cell. In trying to validate those preliminary data, I found that although endogenous nSMase2 colocalized with F in viral filaments, chemical inhibition of the exosome pathway only modestly effected budding. These data suggest that RSV does not utilize this exosome pathway to exit from the cell and may depend on unknown host exocytic pathways. Additionally, it may be that viral proteins themselves are able to perform the final scission step, as has been shown for influenza virus (79). RSV budding is thought to depend on both glycoprotein pulling and internal protein pushing forces

acting in concert, perhaps driven by viral glycoprotein interactions with internal virion proteins.

The data presented in this thesis allow us to propose a model for RSV filament assembly and budding (Fig. 5-1). First, although viral proteins are able to coat host structures at the cell surface, filamentous assembly is distinct from actin-based cellular protrusions and incorporates viral proteins at specific lipid microdomains. However, actin or actin-associated proteins may play a role in anchoring filaments below the plasma membrane. Viral glycoproteins appear to be sufficient for the initial outward bud formation (64). The F CT, and specifically the Phe residue at the C terminus, may then be necessary for elongation of this bud by mediating the incorporation of internal virion proteins. This task may be accomplished by F CT interactions with the M protein. RSV M is then able to recruit the RNP complex, possibly through direct interactions with other viral or host proteins. As the filament elongates, viral proteins and RNA continue to be incorporated. Eventually, the viral filament undergoes a membrane scission event, which allows it to separate from the host cell and become a free virion. This scission event is independent of ESCRT and exosome budding, but further studies are needed to determine the specific mechanism.

Future directions

Although this thesis presents data that help define both the viral and host determinants of RSV assembly and budding, there are many questions that remain unanswered. The F CT is critical for viral assembly into filaments, but the exact mechanism is unknown. Although the M protein is implicated as a potential interacting

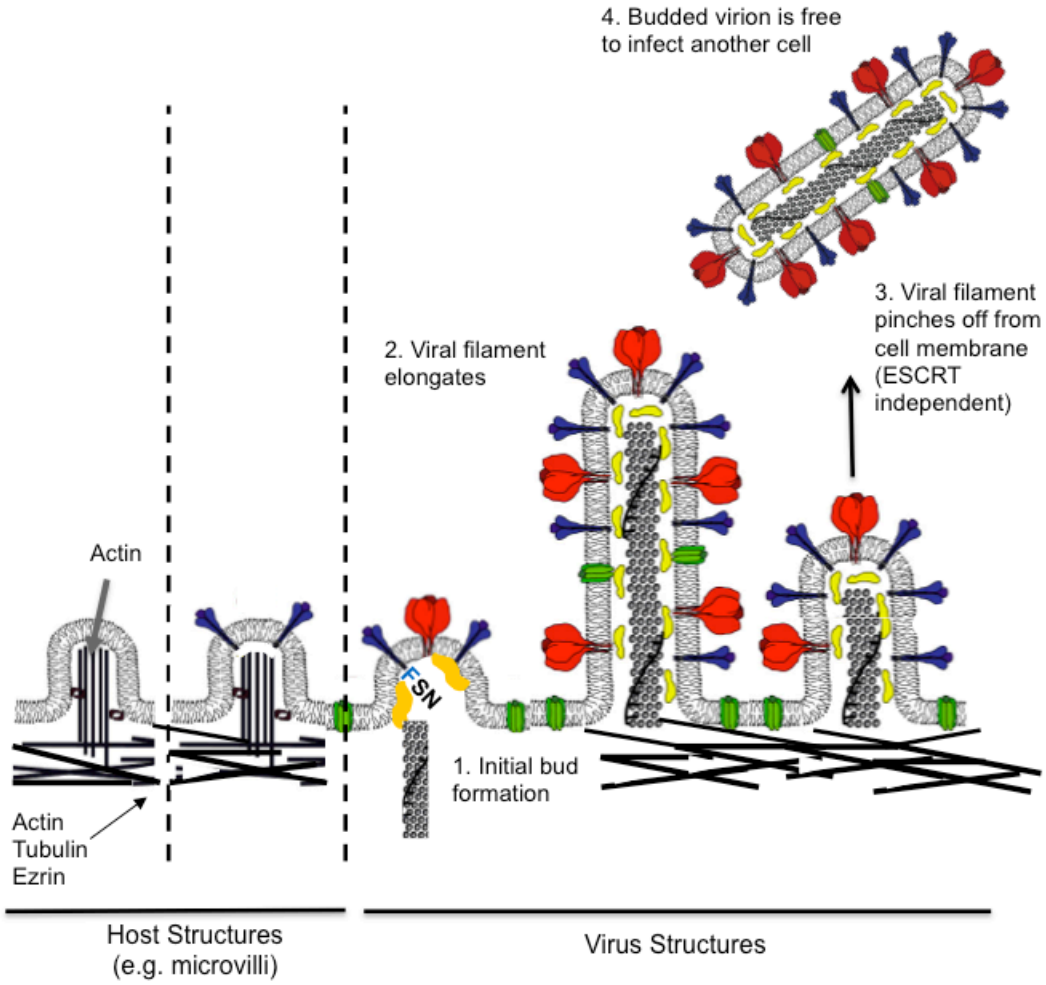

Figure 5-1. Model of RSV assembly and budding. Viral and host structures are indicated below the plasma membrane. RSV F (blue), G (red), SH (green) are depicted on the surface of filaments as transmembrane proteins, while M (yellow) and the viral RNP complex (black) are shown on the interior of viral filaments. Viral assembly steps: (1) initial bud formation, (2) viral filament elongation, (3) viral filament pinches off from cell membrane in an ESCRT independent manner, and (4) the budded virion is free to infect another cell.

partner, a direct interaction has not been shown. In fact, it has been difficult to show direct protein interactions of viral glycoproteins with internal virion proteins. Previous work in the literature has been limited to VLP assays, colocalization studies by indirect immunofluorescence, and association with lipid microdomains. Likely, the limitation of showing a direct interaction by immunoprecipitation is due to a weak or transient interactions. The host membrane, a complex of viral proteins, or viral protein oligomers may also be required. F does not immunoprecipitate with M, N, or P, though the use of chemical crosslinkers could allow the stabilization of a transient interaction. Y2H screens also have not been successful at detecting viral protein-protein interactions.

Several approaches could be used to determine direct viral protein interactions, such as ELISAs or fluorescence resonance energy transfer (FRET) using F CT mutants that are both capable and incapable of mediating filamentous assembly. FRET, however, is limited by the fact that the fluorescent tags required for the assay would have to be placed at the C terminus of the F CT and therefore may disrupt the function of the protein in viral assembly. A second approach to determining direct viral protein interactions might include the use of peptides to mimic the F CT. These peptides could be used in direct immunoprecipitation studies, ELISAs, and potentially used in structure studies with the M or N proteins, for which the structures have already been solved. These studies could potentially indicate critical residues in the M or N protein that might interact with the F CT. A critical limiting factor in demonstrating direct protein interactions, however, is the potential weak or transient nature of these interactions. The nature of these interactions may require nuclear magnetic resonance (NMR)-based assays, which is more amenable to determining weak protein interactions by looking for

chemical shift perturbations to protein-protein interfaces. NMR may be able to detect small changes in protein conformation and could be combined with studies of F CT mutants that are functional or non-functional in viral assembly. Third, classic immunoprecipitation studies coupled with mass spectrometry could be used to determine weak interactions, due to the sensitivity of mass spectrometry. Fourth, additionally Y2H screens could be performed using both *wt* and mutant F CT constructs against an M or N library to determine if the Phe residue is critical for interactions with other viral proteins. These studies would elucidate the mechanism by which the F CT is able to mediate incorporation of internal virion proteins into filaments and VLPs.

Although viral assembly into filaments may be driven largely by direct viral protein-protein interactions, it is not possible to exclude host factors. Viral assembly and budding occurs at specific lipid microdomains, but most viral lipid studies have centered on detergent insolubility. To determine if lipids play a role in RSV assembly, it may be necessary to determine what types of lipids are incorporated into virions. Due to its pleomorphic nature, however, RSV is difficult to purify from cell-derived vesicles of similar size using centrifugation gradients. However, it may be possible to immunoprecipitate virions using antibodies to viral glycoproteins and then perform mass spectrometry to define the lipid species in the resulting purer virion population. Insight into the lipids that RSV selectively incorporates into virions may help determine the specific microdomains at which viral assembly occurs. Furthermore, as lipid microdomains continue to become better defined, the localization of viral proteins and viral assembly at specific locations in the plasma membrane may become better determined.

Finally, the question of whether viral filaments become free virus has not been answered. Although I attempted some live imaging experiments of viral filaments with limited success, further studies are needed to determine definitively whether viral filaments become free virions. Live-cell imaging is often limited by photobleaching, but recent advances have produced fluorescent proteins can be imaged for longer periods of time. These photo-stable probes could be used to label vRNA or viral proteins to allow visualization of viral filaments for extended periods of time, thereby also allowing determination of budding kinetics. Live-cell imaging may also lead to information regarding the mechanism by which RSV performs the final membrane scission step.

Currently, RSV is thought to be independent of host cell exocytic mechanisms. It is plausible that viral proteins are capable of mediating membrane scission by using amphipathic helices to perform membrane, though these helices have not been identified in RSV proteins. Studies involving giant unilaminar vesicles may be able to decipher whether viral proteins are sufficient for budding and further study of host cell exocytosis mechanisms may help determine if RSV relies on host machinery to bud from infected cells. Moreover, these studies may be able to answer how the F or M biophysically drives filament formation. Membrane curvature could be initiated by the presence of the F protein, in which a large ectodomain drives membrane curvature outward to create the larger leaflet while the smaller cytoplasmic domain can accommodate the smaller, inner leaflet. Elongation may be driven by oligomerization of the M protein with itself or as it interactions with the RNP complex. Furthermore, the effect of various lipid compositions could be tested in such a system. These studies may elucidate the biophysical mechanism by which F and other viral proteins drive bud initiation, elongation, and scission.

APPENDIX A

Appendix A

A STABALIZED RESPIRATORY SYNCYTIAL VIRUS REVERSE GENETICS SYSTEM AMENABLE TO RECOMBINATION MEDIATED MUTAGENESIS

Anne L. Hotard, Fyza Y. Shaikh, Sujin Lee, Michael N. Teng, James E. Crowe Jr., and Martin L. Moore

The following work is presented as part the manuscript indicated above that is in preparation by Hotard *et al*. and is intended for submission to *Cell Reports*. Figures A1 and A2 represent the data I contributed to this manuscript.

ABSTRACT

We describe the first example of combining bacterial artificial chromosome (BAC) mutagenesis via recombineering for reverse genetics for an RNA virus. A BAC-based respiratory syncytial virus (RSV) rescue system was established in which RSV antigenomic cDNA was stabilized in a BAC vector. We efficiently generated RSV mutants by recombination-mediated BAC mutagenesis. Together with codon-optimized helper expression plasmids, BAC-RSV is a stable, versatile reverse genetics platform of a *Pneumovirus*.

RESULTS

In order to determine if katushka can be used at a marker for infected cells expressing RSV F, we inoculated HEp-2 cells with rA2-line19F and rA2-kline19F at an MOI=3.0. At 24 h.p.i. cells were immunostained for cell surface RSV F and analyzed using flow cytometry (Fig. A1 A-C). For both rA2-line19F and rA2-kline19F infected cells, 97-98% of the cells were positive for RSV F surface expression (Fig A1 D). In rA2-kline19F infected cells, 92% of the cells were positive for kaushka, with a more varied levels of expression than RSV F staining (Fig. A1 C). The expression of katushka did not affect the level of RSV F expressed on the cell surface.

In order to test the whether expression of katushka affected the formation of viral filaments and cellular syncytia, we inoculated HEp-2 cells with rA2-line19F and rA2-kline19F and immunostained cells using an anti-RSV F antibody and TO-PRO-3. At 24 h.p.i., cells infected with both recombinant viruses show viral filaments at the cell surface as well as a pattern of peri-nuclear staining consistent with F expression in the secretory pathway (Fig. A2 A-C and D-F). Katushka is expressed diffusely throughout the cell as well as near the plasma membrane. At 48 h.p.i, cellular syncytia containing multiple nuclei are present (Fig. A2 G-H). These syncytia also express katushka and viral filaments marked with RSV F.

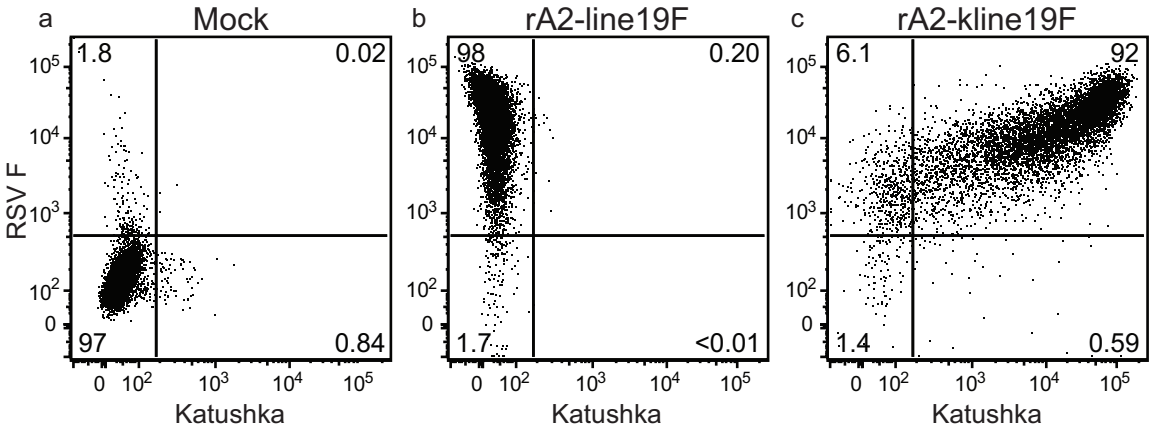

d

Co-expression of RSV F and Katushka reporter gene			
Virus	Mean percent of cells expressing indicated marker +/- SD		
	F	Katushka	F and Katushka
Mock	00.94 +/- 0.75	00.31 +/- 0.47	00.01 +/- 0.01
rA2-line19F	97.34 +/- 0.86	00.18 +/- 0.03	00.17 +/- 0.03
rA2-kline19F	98.01 +/- 0.19	92.05 +/- 0.86	91.50 +/- 0.78

Figure A1. Cell surface expression of RSV F protein in cells inoculated with recombinant virus expressing Katushka is similar to that caused by recombinant virus lacking the marker. HEp-2 cell culture monolayers were inoculated with indicated virus at MOI=3 and incubated for 24 hours. RSV F protein was detected using indirect immunostaining. Panels A to C show scatter plots from representative samples with a percentage of total cells detected as indicated for each quadrant. Panel D shows the mean percentage of cells expressing the indicated markers +/- standard deviation, from triplicate samples in a representative experiment.

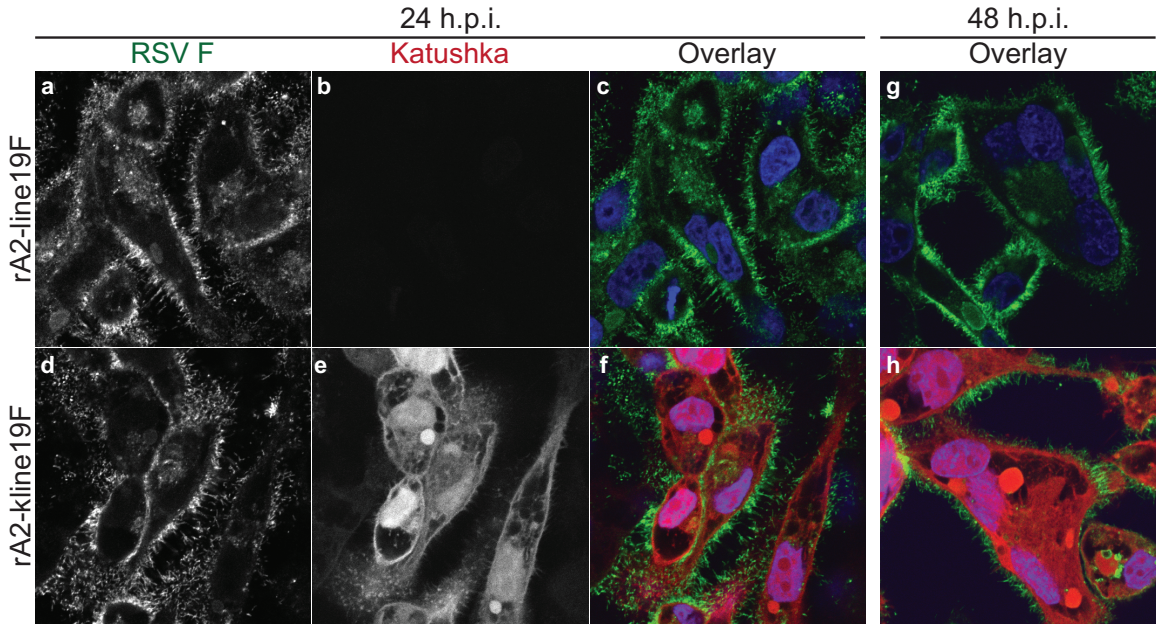

Figure A2. RSV filament formation induced by recombinant virus expressing Katushka protein is similar to that caused by recombinant virus lacking the marker. HEp-2 cell monolayer cultures were inoculated with indicated virus at MOI=1.0 and incubated for 24 hours. RSV F protein was detected using indirect immunostaining and cell nuclei were detected using TO-PRO-3 iodide stain. Panels A to C and D to F show infected cells 24 hours after inoculation. Panels A and D show RSV F only; panels B and E show Katushka only; panels C and F show an overlay with RSV F in green, Katushka in red, and nuclei in blue. Panels G to H show cells inoculated with the indicated virus after 48 hours.

APPENDIX B

Appendix B

INTRACELLULAR NEUTRALIZATION OF A VIRUS USING A CELL-PENETRATING MOLECULAR TRANSPORTER

Gopal Sapparapu, Artez L. Sims, Fyza Y. Shaikh, Eva M. Harth, James E. Crowe, Jr.

The following work is presented as part the manuscript indicated above that is in preparation by Sapparapu *et al*. and is intended for submission to *Nature Biotechnology*. Figures B1 represent the data I contributed to this manuscript.

ABSTRACT

We report here a new method for delivery of small recombinant antibody fragments into virus-infected cells using a dendrimer-based molecular transporter (MT). The construct penetrated virus-infected cells efficiently and inhibited virus replication. This approach provides a novel approach for the immediate delivery of inhibitory antibodies directed to virus proteins that are exposed only in the intracellular environment. This approach circumvents the need for the current and rather complicated expression of inhibitory antibodies in cells following gene transfer.

RESULTS

We tested whether the MT-conjugated scFv was able to penetrate cells (Fig. B1). The unconjugated scFv, unconjugated MT, or MT-conjugated scFv was applied to

MA104 intestinal cell culture monolayers, then the location of the scFv molecules was investigated by laser scanning confocal microscopy using both conventional x-y images and reconstructions of stacks of x-y plane images to analyze distribution in the x-z and y-z planes. The cytoplasm of cells was marked with a CellTracker dye, the plasma membranes were marked with a fluorescent wheat germ agglutinin (WGA), and the His_{10} labeled scFv was detected using nickel conjugated to a fluorescent dye optimized for 647 nm detection (Ni-NTA-647). Only the MT-conjugated scFv was detected inside cells; neither the dye alone nor unconjugated scFv were detected in cells. The fluorescence assay detection showed the antibody fragment to be within the confines of the treated cells in both x-y, x-z, and y-z planes. The antibody distributed throughout the cell to some degree, but was concentrated in discrete foci at the time points tested.

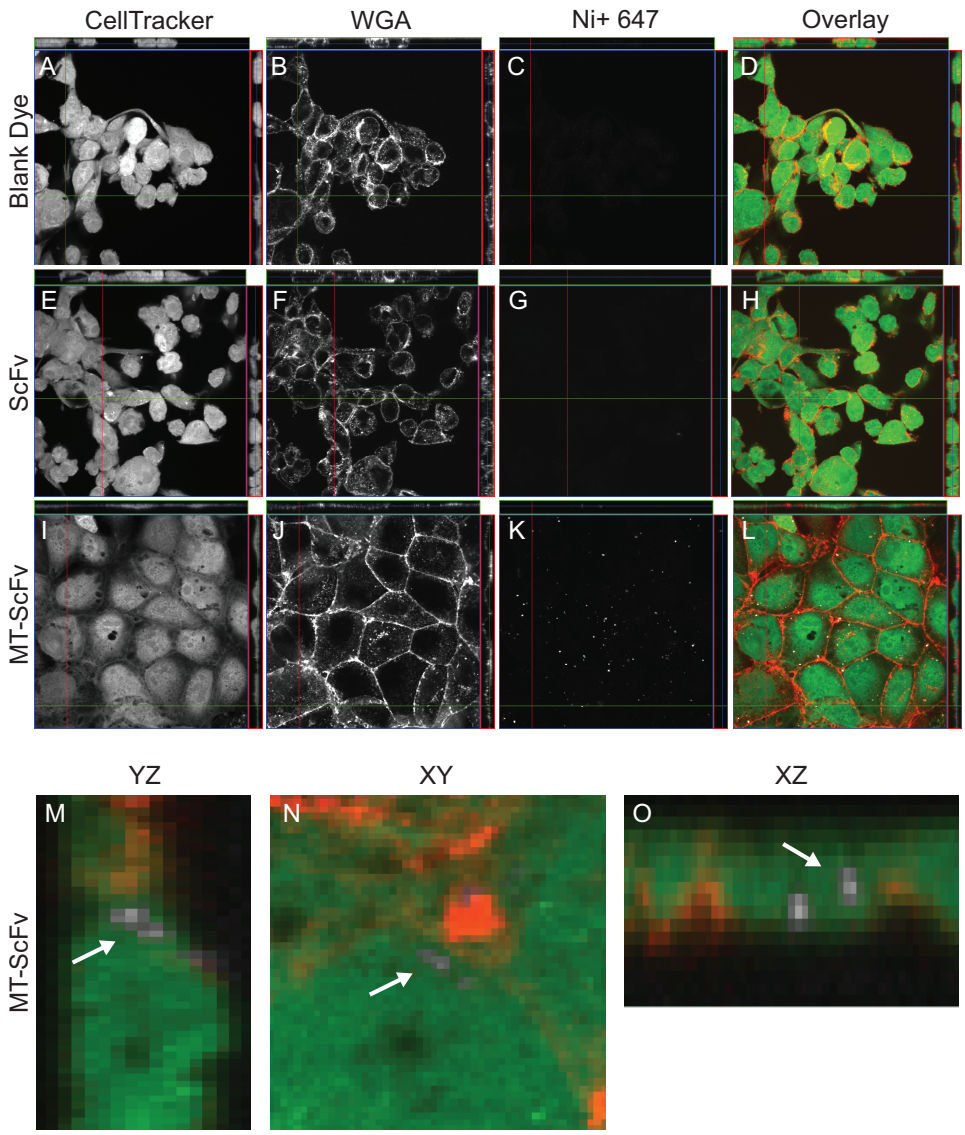

Figure B1. Intracellular localization of molecular transporter-conjugated rotavirus-specific single chain variable fragment (ScFv). MA104 rhesus monkey kidney cells were loaded with CellTracker Green CMFDA, then treated with Ni^{+}-647 dye alone, ScFv complexed with Ni^{+}-647 dye, or MT-ScFv complexed with Ni^{+}-647 dye. Cells were fixed and treated with wheat germ agglutinin (WGA) conjugated to Alexa Fluor 555 and imaged using laser scanning confocal microscopy. Column 1 (panels A, E, and I) shows the CellTracker; column 2 (panels B, F, and J) shows WGA; column 3 (panels C, G, and K) shows the Ni^{+}-647 dye; and column 4 (panels D, H, and L) shows the overlay with the CellTracker in green, WGA in red, and the Ni^{+}-647 in white. Panels M-O: Cells were treated as described for panels A-L with MT-ScFV complexed with Ni^{+}-647 dye. YZ (M) and XZ (O) planes were reconstructed form the XY (N). White arrows indicate the location of a same Ni^{+}-647 dye.

APPENDIX C

A Critical Phenylalanine Residue in the Respiratory Syncytial Virus Fusion Protein Cytoplasmic Tail Mediates Assembly of Internal Viral Proteins into Viral Filaments and Particles

Fyza Y. Shaikh, Reagan G. Cox, Aaron W. Lifland, et al.
2012. A Critical Phenylalanine Residue in the Respiratory Syncytial Virus Fusion Protein Cytoplasmic Tail Mediates Assembly of Internal Viral Proteins into Viral Filaments and Particles . mBio 3(1): .
doi:10.1128/mBio.00270-11.

RESEARCH ARTICLE

A Critical Phenylalanine Residue in the Respiratory Syncytial Virus Fusion Protein Cytoplasmic Tail Mediates Assembly of Internal Viral Proteins into Viral Filaments and Particles

Fyza Y. Shaikh,[a] Reagan G. Cox,[a] Aaron W. Lifland,[b] Anne L. Hotard,[c] John V. Williams,[a,d] Martin L. Moore,[c] Philip J. Santangelo,[b] and James E. Crowe, Jr.[a,d,e]

Departments of Pathology, Microbiology and Immunology[a] and Pediatrics[d] and The Vanderbilt Vaccine Center,[e] Vanderbilt University Medical Center, Nashville, Tennessee, USA; Department of Pediatrics, Emory University and Children's Healthcare of Atlanta, Atlanta, Georgia, USA[c]; and Department of Biomedical Engineering, Georgia Institute of Technology and Emory University, Atlanta, Georgia, USA[b]

ABSTRACT **Respiratory syncytial virus (RSV) is a single-stranded RNA virus in the *Paramyxoviridae* family that assembles into filamentous structures at the apical surface of polarized epithelial cells. These filaments contain viral genomic RNA and structural proteins, including the fusion (F) protein, matrix (M) protein, nucleoprotein (N), and phosphoprotein (P), while excluding F-actin. It is known that the F protein cytoplasmic tail (FCT) is necessary for filament formation, but the mechanism by which the FCT mediates assembly into filaments is not clear. We hypothesized that the FCT is necessary for interactions with other viral proteins in order to form filaments. In order to test this idea, we expressed the F protein with cytoplasmic tail (CT) truncations or specific point mutations and determined the abilities of these variant F proteins to form filaments independent of viral infection when coexpressed with M, N, and P. Deletion of the terminal three FCT residues (amino acids Phe-Ser-Asn) or mutation of the Phe residue resulted in a loss of filament formation but did not affect F-protein expression or trafficking to the cell surface. Filament formation could be restored by addition of residues Phe-Ser-Asn to an FCT deletion mutant and was unaffected by mutations to Ser or Asn residues. Second, deletion of residues Phe-Ser-Asn or mutation of the Phe residue resulted in a loss of M, N, and P incorporation into virus-like particles. These data suggest that a C-terminal Phe residue in the FCT mediates assembly through incorporation of internal virion proteins into virus filaments at the cell surface.**

IMPORTANCE **Respiratory syncytial virus (RSV) is a leading cause of bronchiolitis and pneumonia in infants and the elderly worldwide. There is no licensed RSV vaccine and only limited therapeutics for use in infected patients. Many aspects of the RSV life cycle have been studied, but the mechanisms that drive RSV assembly at the cell surface are not well understood. This study provides evidence that a specific residue in the RSV fusion protein cytoplasmic tail coordinates assembly into viral filaments by mediating the incorporation of internal virion proteins. Understanding the mechanisms that drive RSV assembly could lead to targeted development of novel antiviral drugs. Moreover, since RSV exits infected cells in an ESCRT (endosomal sorting complexes required for transport)-independent manner, these studies may contribute new knowledge about a general strategy by which ESCRT-independent viruses mediate outward bud formation using viral protein-mediated mechanisms during assembly and budding.**

Received 29 December 2011 **Accepted** 5 January 2012 **Published** 7 February 2012

Citation Shaikh FY, et al. 2012. A critical phenylalanine residue in the respiratory syncytial virus fusion protein cytoplasmic tail mediates assembly of internal viral proteins into viral filaments and particles. mBio 3(1):e00270-11. doi:10.1128/mBio.00270-11.

Editor Anne Moscona, Weill Medical College, Cornell University

Address correspondence to James E. Crowe, Jr., james.crowe@vanderbilt.edu.

Respiratory syncytial virus (RSV) is a leading cause of serious viral lower respiratory tract illness in infants and the elderly worldwide. The virus is a member of the *Paramyxoviridae* family, and the genome consists of a single-stranded, negative-sense RNA molecule that encodes 11 proteins. The virion contains three glycoproteins: the fusion (F) protein, attachment glycoprotein (G), and small hydrophobic (SH) protein. The F protein is sufficient for mediating viral entry into cells *in vitro*. The G protein plays a role in viral attachment, and the SH protein is thought to inhibit apoptosis (1). RSV also contains six internal structural proteins: the matrix (M) protein, nucleoprotein (N), phosphoprotein (P), large (L) polymerase protein, and two isoforms of matrix protein 2 (M2-1 and M2-1). The M protein provides structure for the virus particle. RSV N, P, and L form the ribonucleoprotein (RNP) complex, which encapsidates the RSV genome and functions as the RNA-dependent RNA polymerase. M2-1 and M2-2 are accessory proteins that control transcription and replication (2).

Viral proteins traffic to the apical surface of polarized epithelial cells, where they assemble into virus filaments at the plasma membrane (3). However, the mechanisms that drive assembly into filaments and budding are not well understood. Generation of nascent RSV genomic RNA appears to occur in discrete cytoplasmic inclusion bodies that contain the RSV N, P, L, and M2-1 and -2 proteins but not the F, G, or SH protein (4). It is suspected that the

RNP complexes form in the inclusions and then traffic to the apical membrane, where they meet with the surface glycoproteins F, G, and SH arriving from the Golgi apparatus through the secretory pathway (5). RSV proteins and viral RNA assemble into virus filaments at the cell surface. These filaments are thought to contribute to cell-cell spread of the virus and morphologically resemble the filamentous form of virions seen in electron microscopy (EM) studies of virus produced in polarized cells (6). Live imaging has shown these structures to be dynamic, with rotation and directional movement (7, 8). Filament formation can also be modulated by alterations in the function of host proteins, including myosin Vb and Rab11a family interacting proteins 1 and 2. Budding occurs in a Vps-4-independent manner (6, 9), resulting in pleomorphic particles ranging from 150 to 250 nm in diameter for spherical forms and up to 10 μm long in filamentous forms (10).

Previously, we showed that the F protein traffics to the apical surface in the absence of any other viral protein or viral RNA and that the F-protein cytoplasmic tail (FCT) was completely dispensable for apical trafficking (5). It is unlikely, however, that a paramyxovirus would retain such a domain if it did not play some role in replication or pathogenesis, and indeed other investigators showed that a virus lacking the FCT had a 100- to 1,000-fold decrease in viral titers in a multicycle growth curve. This mutant virus was unable to form filaments at the cell surface but was capable of accomplishing cell-cell fusion (11, 12). Furthermore, the cytoplasmic tail (CT) of many paramyxovirus glycoproteins has been shown to be important for assembly and budding (11, 13).

Since the FCT is required for efficient replication but is not required for fusion or trafficking, we hypothesized that the FCT coordinates the assembly of viral proteins into filaments at the cell surface. In this study, we demonstrate that a key phenylalanine (Phe) residue in the FCT is critical for RSV assembly into filaments at the cell surface. Moreover, when Phe was mutated, RSV F was unable to recruit RSV M, N, and P efficiently into virus-like particles (VLPs). These studies indicate that the FCT, and specifically a Phe residue at amino position 22 of the FCT, is responsible for recruitment of internal viral proteins into filamentous structures at the cell surface for efficient assembly and subsequent budding.

RESULTS

RSV infection induced virus filaments that contain RSV F, M, N, and P. We first tested whether the cell surface filaments induced by RSV infection of epithelial cells contained all of the expected RSV structural proteins. HEp-2 cell monolayer cultures were inoculated with RSV wild-type (wt) strain A2 and incubated in complete growth medium for 24 h. The cell monolayers were then fixed and immunostained for the RSV F, M, N, or P protein or host cell filamentous actin (F-actin). In addition, we also stained cells for the presence of RSV genomic RNA using a fluorescently conjugated probe designed to hybridize to RSV gene start sequences (14). Figure 1 shows RSV filaments protruding from the cell membrane (A to P). Morphologically, these filaments often were clustered and kinked, and they stained brightly with antibodies to the RSV F protein. The filamentous structures contained RSV F, M, N, P, and viral RNA, indicating that both structural and genomic components are present. Thus, these filaments likely are virions assembling at the plasma membrane prior to budding.

Since RSV filaments might resemble host cell protrusions that contain cytoskeletal proteins, we next sought to distinguish viral filaments from cell projections simply decorated with the RSV F protein. Previous work in the field has shown that F-actin is not found in viral filaments (15). Therefore, we visualized F-actin using phalloidin to distinguish viral filaments from host structures containing F-actin (e.g., microvilli, filapodia, lamellipodia, and membrane ruffles). Figure 1Q to T show that viral filaments, marked by the presence of the RSV F protein, did not contain F-actin. Viral filaments also did not contain either tubulin or ezrin (data not shown). Although the viral and host filamentous structures often occurred in the same regions of the plasma membrane, viral filaments were distinct from the cell projections that contained cytoskeletal proteins. These data are consistent with previously published data that provide evidence for specific RSV protein sorting into viral filaments (6).

RSV virus-like filaments can be generated independent of viral infection. We next sought to determine the minimal requirements for RSV filament formation by transfecting combinations of plasmids encoding RSV proteins. Transfection of cDNAs encoding the RSV F, M, N, and P genes into HEp-2 cells induced formation of virus-like filaments that resembled viral filamentous structures formed during infection. Figure S1 in the supplemental material shows a representative image of filaments formed when these four RSV structural proteins were expressed in HEp-2 cells. Consistent with RSV filaments formed during infection, virus-like filaments contained RSV proteins and were often kinked, clustered, and stained brightly for the F protein (see Fig. S1A to D). RSV F was found to be necessary for virus-like filament formation (see Fig. S1E to H), and in fact, exclusion of any single gene of the four during transfection eliminated filament formation (data not shown). Thus, the filaments formed using the transfection-based assay were similar to filaments formed during viral infection in both morphology and composition. We used the transfection-based filament formation assay as a tractable system with which to study the role of the F protein CT domain in viral assembly at the plasma membrane.

RSV FCT terminal residues Phe-Ser-Asn are required for filament formation. We and others have shown that the FCT domain is not required for F-protein trafficking to the cell surface (5, 12). We asked here whether the CT domain was dispensable for viral assembly into filaments at the cell surface. We designed a panel of altered cDNAs of the F protein gene in which the CT domain was truncated or otherwise mutated (Fig. 2). We tested the effect of the tail mutations on virus-like filament formation at the cell surface using the transfection-based assay characterized in Fig. S1 in the supplemental material. When expressed alone, the F protein with wild-type cytoplasmic tail (FCT wt) did not form virus-like filaments and localized to cellular projections that contained F-actin (Fig. 3A to D). However, when coexpressed with M, N, and P, FCT wt was able to form virus-like filaments that were distinct from cellular projections containing F-actin (Fig. 3E to H). Therefore, we used the presence of F-actin as a marker to distinguish virus-like filaments from cellular projections, since only the latter contained F-actin. In contrast to FCT wt, deletion of the terminal 3 amino acids from the FCT (residues Phe-Ser-Asn, or FSN) resulted in a loss of virus-like filament formation and altered localization of the F protein only to F-actin-containing cellular protrusions (Fig. 3I to L). This pattern of altered F staining at the cell surface was similar to the pattern of FCT wt when it was expressed alone in HEp-2 cells (i.e., in the absence of the RSV N, P, and M proteins). Deletion of the three terminal amino acids of the

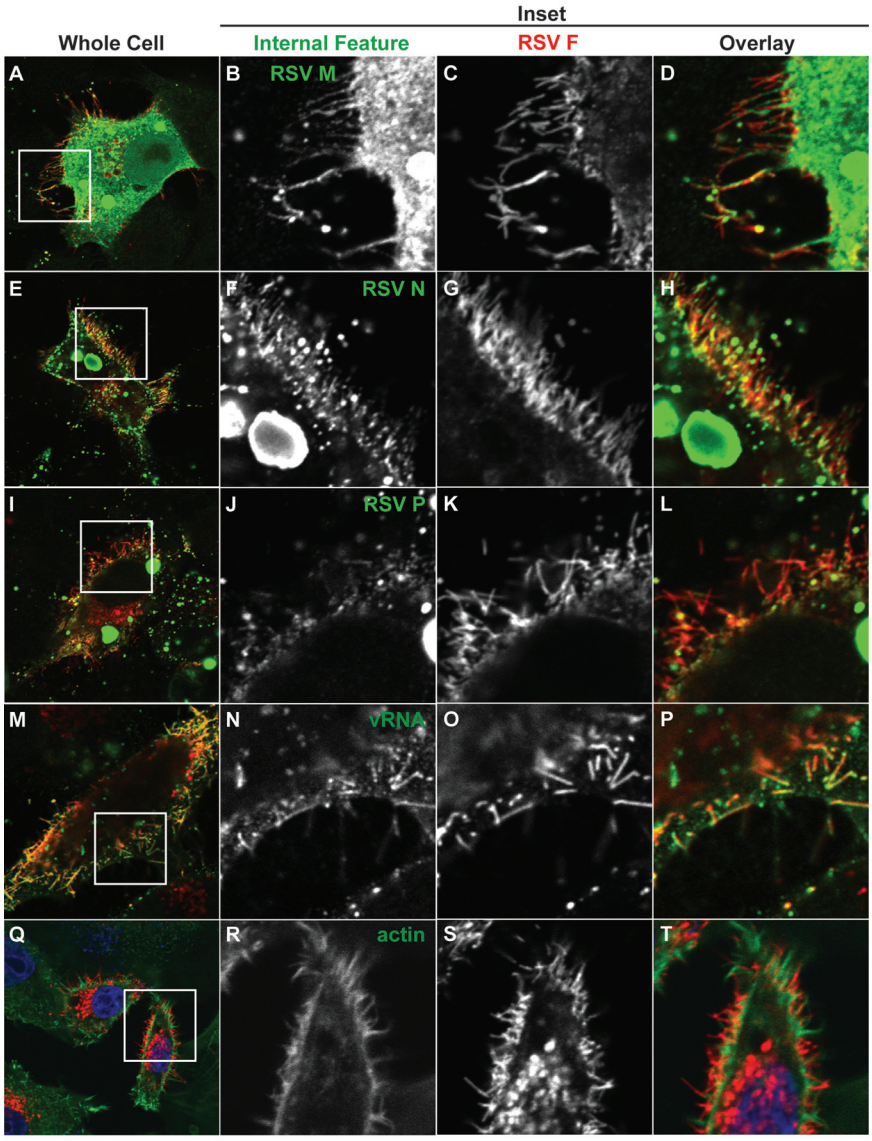

FIG 1 RSV F, M, N, P, and viral RNA localize to viral filaments during infection. HEp-2 cells were inoculated with RSV strain A2 at a MOI of 1.0 and incubated for 24 h. RSV F, M, N, and P were detected by indirect immunofluorescence; viral RNA (vRNA) was detected using an RNA probe specific to the RSV genomic gene start sequences; actin was detected using phalloidin. Column 1 (A, E, I, M, and Q) shows the entire cell. Panels B to D, F to H, J to L, N to P, and R to T show an enlargement of the inset shown in column 1. Column 2 (B, F, J, N, and R) shows RSV M, N, P, vRNA, or phalloidin staining only; column 3 (C, G, K, O, and S) shows RSV F only; and column 4 (D, H, L, P, and T) shows the overlay, with RSV F in red and RSV M, N, P, vRNA, or actin in green.

CT domain resulted in the same phenotype of F distribution as deletion of the entire tail domain (Fig. 3M to P). This FCT deletion construct was similar to the transmembrane-domain-plus-one-anchor-residue ("TM+1") construct that we previously described (5) and is designated FCTΔ23. For each truncation construct, total cellular expression and total surface expression of the F protein were measured at levels equivalent to those of FCT wt (Fig. 3M and N, respectively). Therefore, reduced expression or trafficking of the mutant protein to the cell surface did not play a role in the failure of these CT truncation constructs to form virus-like filaments. These data indicate that the terminal CT residues Phe-Ser-Asn are necessary for assembly of RSV proteins into virus-like filaments.

Phe-Ser-Asn residues are sufficient for viral protein assembly into filaments at the cell surface. Based on the data presented in Fig. 3, we next sought to determine if the specific residues Phe-Ser-Asn on the C terminus of FCT were necessary for filament formation when coexpressed with M, N, and P or alternatively if only the 24-amino-acid length of the CT domain determined filament formation. We mutated all three terminal residues to alanines (FCTΔ3 AAA) in order to test the hypothesis that a CT of a certain length was necessary for viral assembly. FCTΔ3 AAA was impaired for virus-like filament formation when coexpressed with RSV M, N, and P (Fig. 4E to H) compared to results for FCT wt (Fig. 4A to D). In order to determine if residues Phe-Ser-Asn were sufficient for virus-like filament formation, we deleted the entire FCT except for the terminal residues Phe-Ser-Asn (designated FΔCT FSN). FΔCT FSN formed virus-like filaments at the cell surface (Fig. 4I to L) that were similar in length to FCT wt filaments (Fig. 4M), but the percentage of transfected cells with filaments was reduced 10-fold (Fig. 4N). These data suggest that other residues in the CT or a minimum length of the CT may be important for initiation of filament formation. The total cellular expression and total surface expression of FCTΔ3 AAA or FΔCT FSN were similar to those of FCT wt, again indicating that neither expression nor trafficking to the cell surface was impaired (Fig. 4O and P, respectively). These data suggest that residues Phe-Ser-Asn are necessary and sufficient for assembly of viral structural proteins into virus-like filaments at the cell surface.

The Phe residue in the RSV FCT is necessary for filament formation. In order to determine if a particular residue of the FCT Phe-Ser-Asn motif was the determining factor for viral assembly into filaments, we designed FCT constructs that contained mutations of each of the three terminal residues individually. We compared the abilities of the mutant FCT constructs to form virus-like filaments when coexpressed with M, N, and P to that of FCT wt (Fig. 5A to D). When the Phe residue was mutated to an alanine (F22A), virus-like filaments failed to form, and the F construct colocalized with cellular structures containing F-actin (Fig. 5E to H). However, if either the Ser or Asn residue was mutated to an alanine, the mutant FCT constructs were able to assemble into virus-like filaments, distinct from cellular structures containing F-actin (Fig. 5I to L and 5M to P, respectively). Total cellular

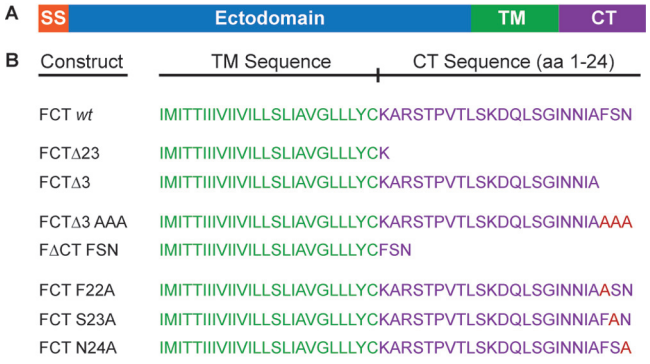

FIG 2 Schematic of FCT constructs. (A) FCT mutant constructs were generated using site-directed mutagenesis from FCT wt in the pcDNA3.1 vector. Functional regions are indicated by color: SS, signal sequence (orange); ectodomain (blue); TM, transmembrane domain (green); CT, cytoplasmic domain (purple). (B) Sequences of the TM and CT domain are indicated for each construct. Point mutations are indicated in red. We designated residue K as FCT residue 1. The schematic is not to scale.

expression and total surface expression of each of the FCT constructs with single amino acid mutations were equivalent to FCT wt levels, indicating that neither expression nor trafficking was impaired (Fig. 5Q and R, respectively). We also designed and tested FCT constructs with conservative mutations (F22Y, S23T, and N24Q). The results were similar to the data described for the alanine point mutations in Fig. 5 (data not shown). Collectively, these data show that the Phe residue near the C-terminal end of FCT plays a key role in filamentous viral assembly at the plasma membrane.

The Phe residue is required for incorporation of RSV M, N, and P into RSV VLPs. Next, we sought to determine why the FCT Phe residue was necessary for virus assembly into filaments. We first introduced the FCTΔ3 mutation into a recombinant virus using a plasmid-based virus rescue system, but this mutant virus could not be rescued, likely due to the drastic effect on assembly. We then developed a VLP assay to determine whether the FCT Phe

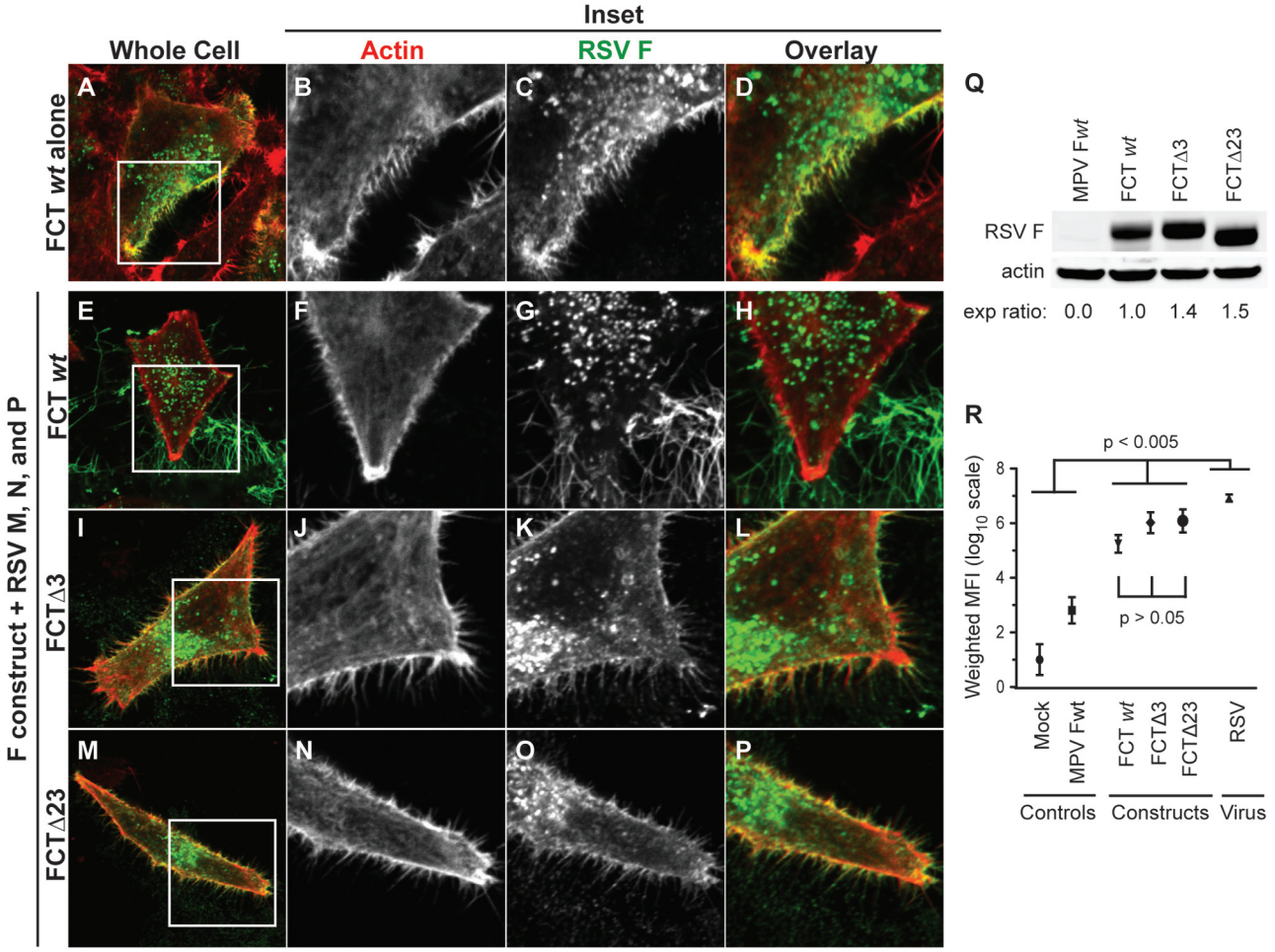

FIG 3 **FCT** terminal residues Phe-Ser-Asn are required for filamentous assembly at the cell surface. HEp-2 cells were transfected with FCT wt only (A to D) or with the indicated FCT construct and plasmids encoding RSV M, N, and P (E-P). Column 1 shows images of the whole cell (A, E, I, and M). Columns 2 to 4 (B to D, F to H, J to L, and N to P) show an enlargement of the corresponding inset in column 1. Column 2 shows actin staining only (B, F, J, and N); column 3 shows RSV F staining only (C, G, K, and O); and column 4 shows the overlay, with actin in red and RSV F in green (D, H, L, and P). (Q) Total cell lysate was collected from HEp-2 cells transfected with the indicated FCT construct, and RSV F or actin was detected by immunoblotting. The RSV F band was normalized against actin, and the expression (exp) ratio represents a normalization to results for FCT wt. (R) Total surface expression of RSV F was determined by flow cytometry using HEp-2 cells transfected with the indicated FCT construct and RSV M, N, and P. Data are plotted as means, and error bars represent standard deviations. Weighted MFI is mean fluorescence intensity (MFI) × the frequency of positive cells. MPV F wt is used as a specificity control.

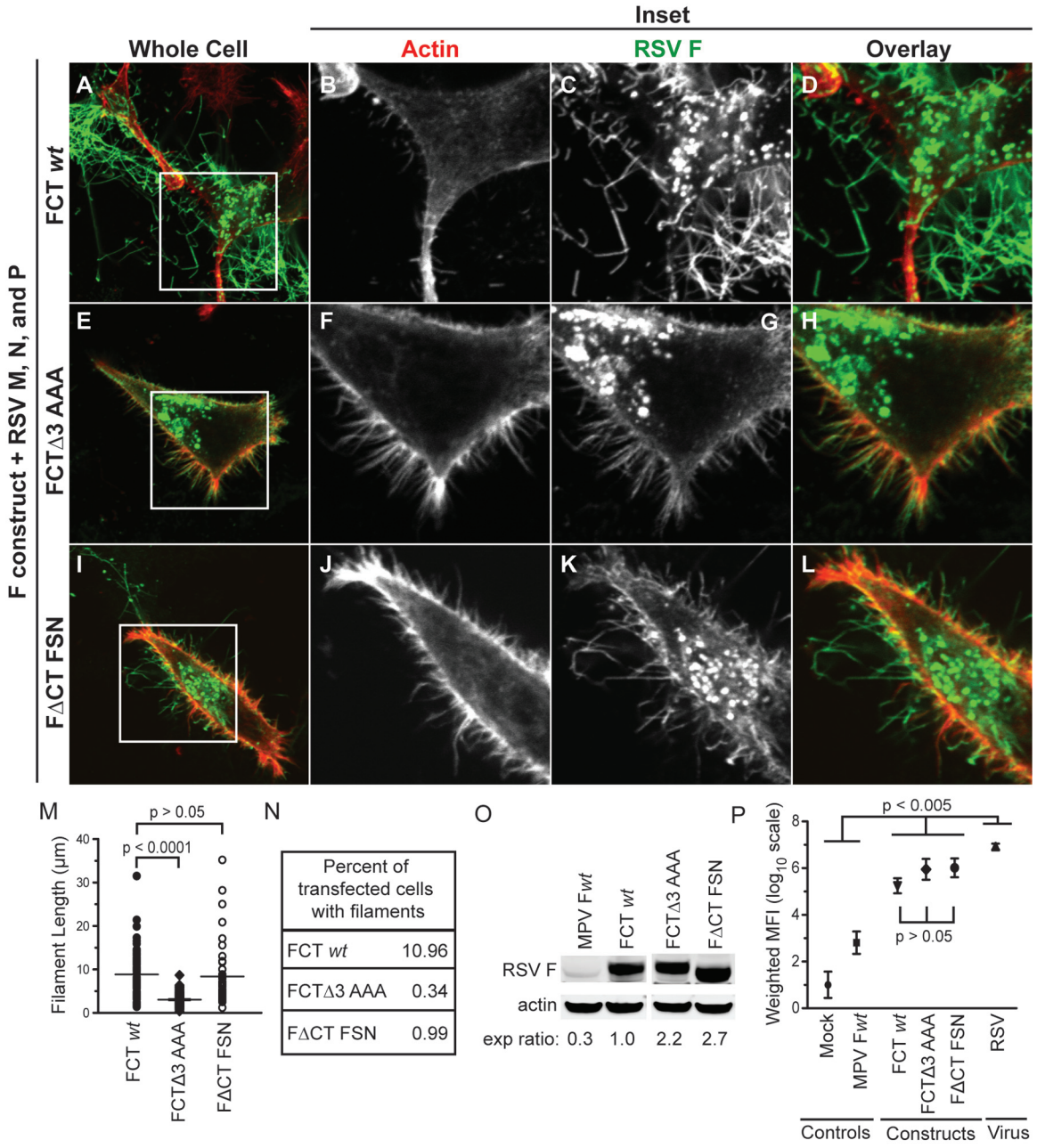

FIG 4 FCT residues Phe-Ser-Asn are sufficient for filamentous assembly at the cell surface. HEp-2 cells were transfected with the indicated FCT construct and RSV M, N, and P (A to L). Column 1 shows images of the whole cell (A, E, and I). Columns 2 to 4 (B to D, F to H, and J to L) show an enlargement of the corresponding inset in column 1. Column 2 shows actin staining only (B, F, and J); column 3 shows RSV F staining only (C, G, and K); and column 4 shows the overlay, with RSV F in green and actin in red (D, H, and L). (M and N) HEp-2 cells were transfected as described for panels A to L. Filament length was determined by measuring the lengths of individual filaments using Zeiss LSM software as described in Materials and Methods (M). Percent transfected cells was determined by counting RSV F-transfected cells with filaments and then dividing that number by the total number of RSV F-transfected cells (N). (O) Total cell lysate was collected from HEp-2 cells transfected with the indicated FCT construct, and RSV F and actin were detected by immunoblotting. The RSV F band was normalized against actin, and the expression (exp) ratio represents a normalization to FCT wt. (P) Total surface expression of RSV F was determined by flow cytometry using HEp-2 cells transfected with the indicated FCT construct and RSV M, N, and P. Data are plotted as means, and error bars represent standard deviations. Weighted MFI is mean fluorescence intensity (MFI) × the frequency of positive cells. MPV F wt is used as a specificity control.

residue determined the ability of the F protein to assemble internal virion proteins into VLPs. 293-F cells were used for their high growth rate, dense cell growth, and transfection efficiency, all of which have been limiting factors in previous efforts to develop VLP assays with conventional transformed epithelial cells lines, such as HEp-2 cells (data not shown). Using this system, sufficient VLPs were produced for relative protein quantification by immunoblotting using the Lycor Odyssey infrared imaging system. Second, previous work in the field has shown that F, M, N, and P are the minimal requirements for passage of a minigenome construct

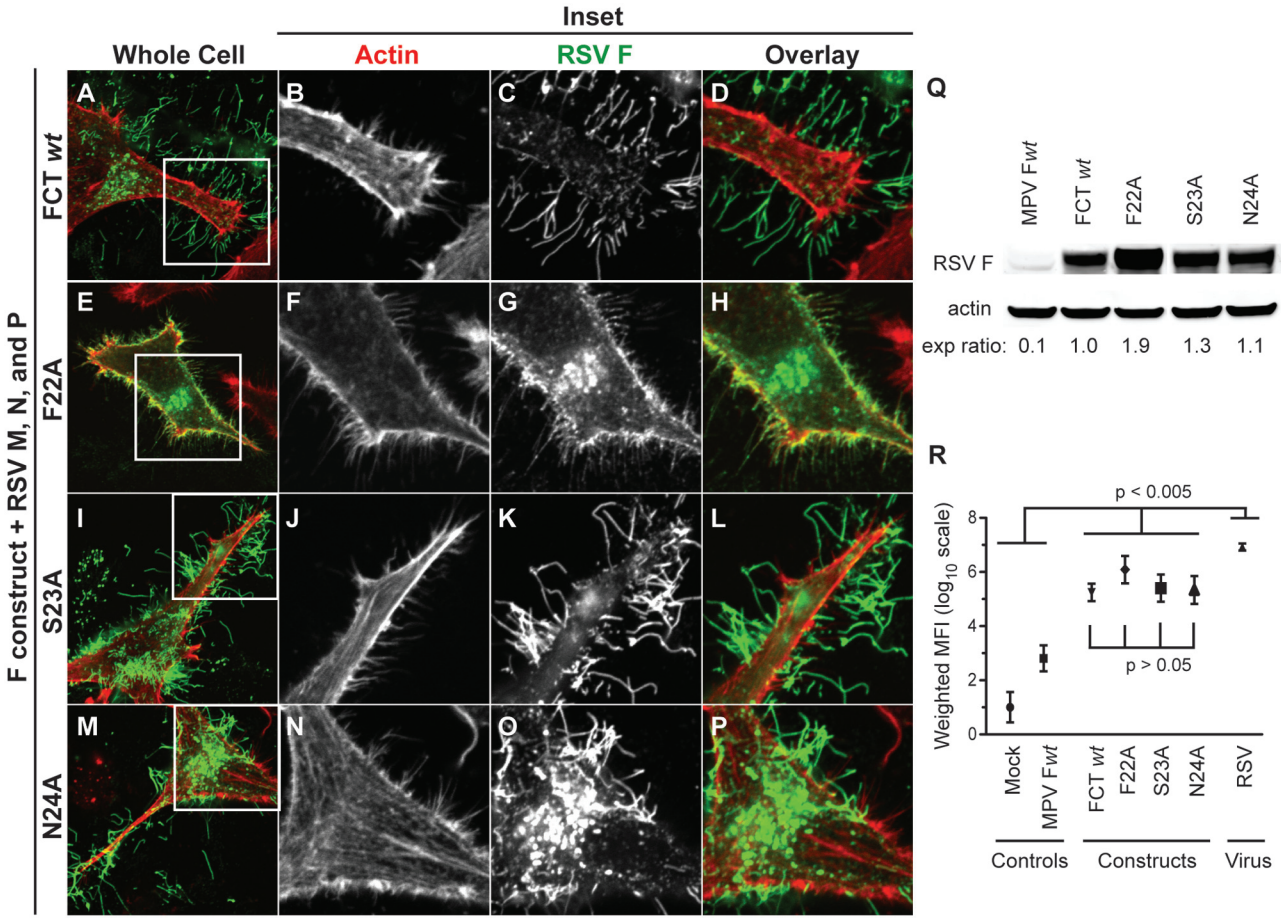

FIG 5 The Phe residue at position 22 in the RSV FCT is necessary for filamentous assembly at the cell surface. HEp-2 cells were transfected with the indicated FCT construct and RSV M, N, and P (A to P). Column 1 shows images of the whole cell (A, E, I, and M). Columns 2 to 4 (B to D, F to H, J to L, and N to P) show an enlargement of the corresponding inset in column 1. Column 2 shows actin staining only (B, F, J, and N); column 3 shows RSV F staining only (C, G, K, and O); and column 4 shows the overlay, with RSV F in green and actin in red (D, H, L, and P). (Q) Total cell lysate was collected from HEp-2 cells transfected with the indicated FCT construct, and RSV F or actin were detected by immunoblotting. The RSV F band was normalized against actin, and the expression (exp) ratio represents a normalization to FCT wt. (R) Total surface expression of RSV F was determined by flow cytometry using HEp-2 cells transfected with the indicated FCT construct and RSV M, N, and P. Data are plotted as means, and error bars represent standard deviations. Weighted MFI is mean fluorescence intensity (MFI) × the frequency of positive cells. MPV F wt is used as a specificity control.

consisting of the RSV leader and trailer sequences flanking a reporter gene (16). Since we found that these proteins are also the minimum requirements for filament formation independent of viral infection, we choose to express VLPs using all four proteins to recapitulate the minimum requirements for assembly and budding.

RSV VLPs were produced by transfecting cells with plasmids encoding the indicated F construct and wt M, N, and P. TEM analysis of VLPs showed characteristic F-protein spikes (black arrows) on the surface of particles similar to those seen on RSV virion particles produced and imaged in the same manner (Fig. 6A and B). Second, the diameter of the VLPs was similar to that of RSV and within the usual range of diameter of virions grown in other cell types (10). In addition to structure, we also compared the protein composition of VLPs with that of virus. Figure 6C shows a representative immunoblot comparing the level of each viral protein in the VLPs to that in virions. These data were quantified from three independent experiments and are presented as percentages of RSV virion protein levels (Fig. 6D). Compared to virus, the VLPs contained equivalent amounts of the F protein but less M, N, and P. Although the ratios of the F protein to internal proteins differed between VLPs and RSV, VLPs did still incorporate RSV internal proteins, thus allowing us to study the relative abilities of various FCT constructs to incorporate internal virion proteins into budded vesicles. Several possibilities could explain the discrepancy of ratios. The VLPs may incorporate a higher proportion of F into each particle than M, N, and P, compared to those for virions, or there may be vesicles containing the F protein alone escaping into the supernatant. We favor the latter, since transfection of cDNA encoding the F protein alone led to a baseline transport of F into the supernatant (data not shown).

After initial validation of the VLP system, we sought to determine how the FCT Phe residue affected VLP budding and the incorporation of internal virion proteins. We performed the VLP assay as described above and collected the cell pellets for total protein expression. Figure 6E shows immunoblots from a representative experiment. Data were normalized to the

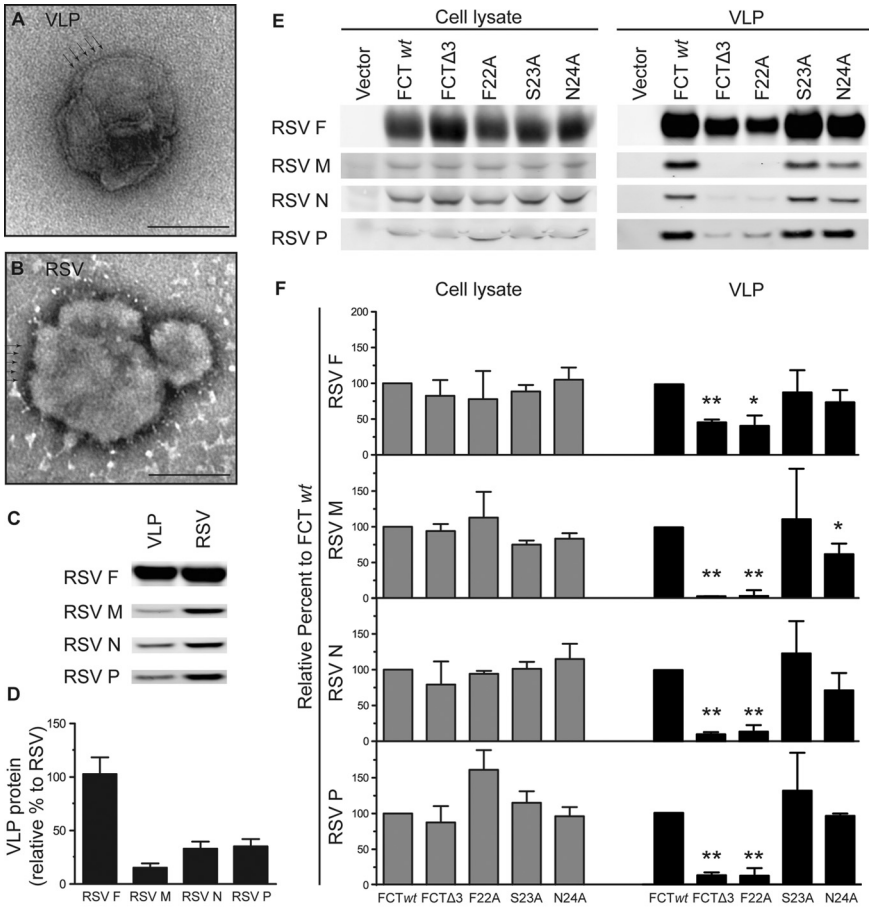

FIG 6 The Phe residue at position 22 in the RSV FCT is necessary for incorporation of internal virion proteins into VLPs. 293-F cells were transfected with plasmids encoding RSV FCT wt, M, N, and P or infected with RSV at an MOI of 0.05. Panels A and B show transmission electron micrographs of a representative VLP and virion, respectively. Scale bars represent 100 nm. (C to D) Supernatants from RSV-infected or FCT wt-transfected cells were clarified and pelleted through a 20% sucrose cushion. Panel C shows a representative blot comparing protein levels in VLPs to RSV. Panel D shows a quantification of three independent experiments as shown in panel C. The indicated protein levels in VLPs were normalized to that of the corresponding protein in RSV. For panels E and F, 293-F cells were transfected with plasmids encoding the indicated FCT construct and RSV M, N, and P. Panel E shows a representative experiment with indicated protein levels in cell lysates (left) or VLPs (right). Panel F shows a quantification of data from three independent experiments as shown in panel E (cell lysates in grey; VLPs in black). Data are plotted as means, and error bars represent standard deviations.

levels in the FCT wt sample, and the means and standard deviations from three independent experiments are shown in Fig. 6F. Compared to FCT wt, when residues Phe-Ser-Asn were deleted (FCTΔ3) or Phe was mutated to an alanine (F22A), there was a significant loss of RSV M, N, and P protein incorporation into VLPs. In contrast, point mutations of residue Ser or Asn (S23A or N24A, respectively) did not affect incorporation of RSV M, N, or P into VLPs. The FCTΔ3 and F22A constructs also induced less transfer of the F protein into the supernatant than the FCT wt, S23A, or N24A constructs, consistent with less budding of VLPs. These data show that the Phe residue in the FCT is necessary for RSV M, N, and P incorporation into VLPs. Collectively, the data in this report show that the FCT mediates viral assembly through a C-terminal Phe residue in order to incorporate RSV M, N, and P into virus filaments at the cell surface prior to budding.

DISCUSSION

The RSV FCT domain is known to play a critical role in viral replication, but the mechanism by which the FCT functions in assembly and budding has not been well characterized. In this study, we determined that a single critical Phe residue in the FCT at amino acid position 22 mediates assembly of virus-like filaments, incorporation of RSV internal proteins into VLPs, and subsequent budding of VLPs from cells. The finding that a single amino acid residue in the FCT can control both assembly and budding is remarkable. We studied the role of RSV proteins in assembly of filaments independent of viral infection by expressing proteins from plasmids, and we found that filament formation requires the F, M, N, and P proteins. This assembly process likely is driven by interactions of these viral proteins with each other or collectively with host proteins. Using cDNA-based expression of F proteins with alterations in the FCT, we determined the key residue in the FCT that is required for assembly of virus-like filaments containing the four minimally required structural proteins, F, M, N, and P. Furthermore, we used a VLP budding assay under the same protein expression conditions to reveal that the FCT coordinates assembly through its ability to incorporate M, N, and P into particles. These data provide a direct link between FCT coordination of viral assembly into filaments and budding of viral particles. Alternatively, the formation of filaments and virus particles may be two different outcomes of essentially the same assembly process, with the Phe residue serving in a critical role for both processes.

The specific mechanisms that govern FCT-mediated assembly, however, are still not well defined. Our data show that expression, trafficking, and surface expression of F are not affected by mutations in the FCT. This finding is consistent with findings of previous studies that indicated the TM domain of F is responsible for targeting the protein to the apical surface (5), and localization to specific lipid microdomains in the plasma membrane appears to depend on an unidentified domain in the ectodomain (17). Therefore, it is likely that the FCT Phe residue we identified is critical for a protein-protein interaction. A simple explanation may be that this residue directly interacts with one of the internal virion proteins, such as M, N, or P, or a complex of these proteins. On the other hand, the F protein is a trimer, and the FCT is located in close proximity to the plasma membrane. It may be that the hydrophobic Phe residue confers a specific conformation to the cytoplasmic portion of the trimer. Finally, the possibility of an interaction with a host

protein or complex of proteins cannot be excluded. Future studies will focus on elucidating the specific protein-protein interactions mediated by the FCT and how these interactions lead to the incorporation of other viral proteins into filaments.

Coordination of RSV assembly by the FCT would be consistent with findings of many other studies citing paramyxovirus glycoprotein cytoplasmic tails as crucial to both assembly and budding (13). For RSV and human metapneumovirus (HMPV), members of the *Pneumovirus* subfamily, the G protein is dispensable for viral replication *in vitro* (18, 19). Although the FCT may be sufficient, optimal incorporation of viral proteins and RNA might require both F and G since residues in the RSV G protein CT are thought to be important for interactions with M (20). However, for the *Paramyxoviridae* subfamily, the requirement of glycoprotein CTs varies with each virus. For measles virus and Sendai virus assembly, the F protein CT is required. Newcastle disease virus F and HN glycoproteins interact with different internal viral proteins, M and N, respectively. In contrast, the F and HN CTs of parainfluenza virus 5 serve somewhat redundant functions (13). The lack of a common theme for the role of CT domains in paramyxoviruses may simply indicate that many questions about the specific mechanisms of viral assembly remain unanswered, and further investigation into the RSV FCT may contribute to general knowledge regarding glycoprotein CT-mediated assembly for other paramyxoviruses.

In addition to viral protein incorporation, the structural formation of RSV particles at the cell surface also requires viral interactions with the host cell lipid membrane. The viral particle membrane first must be deformed outward as an extension of the cell membrane. Then, the particle must be elongated by incorporation of additional membrane to create long filaments. Finally, a scission event must occur to release the viral particle from the cell membrane. All of these processes are energy intensive and require complex coordination of surface proteins and nucleocapsids containing RNA and viral proteins (21). Many viruses usurp endosomal sorting complexes required for transport (ESCRT) machinery to accomplish the task of outward bud formation and membrane scission using late domains found in viral proteins (13). Viral budding using late domains requires the AAA ATPase Vps4. However, inhibition of Vps4 does not affect RSV budding (6), and like other ESCRT-independent viruses, RSV may use viral protein-mediated pushing and pulling forces to initiate membrane bending at lipid microdomains in order to exit the cell (21). RSV has been shown to assemble into filaments at lipid microdomains (22, 23). The RSV F protein has been shown to associate with detergent-resistant membranes (DRMs), as have the RSV M, N, P, M2-1, and L proteins during viral infection (17, 23–25). Furthermore, the M protein associates with lipid microdomains in the presence of the F protein (26). Our data suggest that the Phe residue in the FCT is critical for F-protein interactions with internal virion proteins in order to provide both the pulling and pushing forces needed to bend the membrane in order to form filaments, presumably at lipid microdomains. Our data also provide some insight about how the FCT mediates initial membrane bending and filament elongation. The ability of a shortened CT with only residues Phe-Ser-Asn to form virus-like filaments was reduced by 10-fold. However, once this was initiated, the shortened CT was able to induce filaments that elongated to lengths comparable to those generated by FCT wt. These data suggest that other residues or a minimum length of the CT may be important for initiation of outward bud formation.

Manipulation of the plasma membrane also likely involves a variety of host proteins that function at the cell surface. Many cellular structures extending outward from the cell surface depend on actin polymerization (e.g., microvilli, filapodia, lamellipodia, and membrane ruffles), and lipid microdomains have been linked to the cortical actin network (27). In fact, disruption of actin-associated signaling pathways has been shown to affect filament formation, and β-actin and actin-related proteins have been found in the same sucrose gradient-purified fractions as RSV (15, 28–32). However, actin polymerization has been shown to be dispensable for filament formation, and F-actin is excluded from viral filaments (15). While actin and actin-related proteins likely are involved in aspects of RSV assembly, our data support the hypothesis that the process by which viral proteins extend the cell membrane outward to form filaments is distinct from the process used by actin-based cellular structures. Exclusion of cellular proteins from viral filaments also argues for specific sorting of viral and host proteins into filaments, a process that likely is highly regulated and involves interactions among viral proteins, host proteins, and lipid microdomains.

Despite these studies, the mechanism by which RSV assembles and buds is still incompletely defined. Viral protein-protein and protein-lipid interactions likely play a significant role, and further investigation will yield insight into what motifs mediate these interactions for both viral and cellular glycoproteins. Further study of RSV assembly and budding will contribute to general understanding of how ESCRT pathway-independent viruses can exit the cell and how viral surface and internal proteins contribute to egress. Finally, understanding the mechanisms that drive RSV assembly and budding could lead to targeted development of novel antiviral drugs for prophylactic or therapeutic use against RSV infection.

MATERIALS AND METHODS

Cell culture and wt RSV virus preparations. HEp-2 cells (ATCC CCL-23) were maintained in Opti-MEM I medium (Invitrogen) containing 2% (vol/vol) fetal bovine serum (FBS), 1% (vol/vol) l-glutamine, 2.5 μg/ml amphotericin B, and 1% (vol/vol) penicillin-streptomycin. Suspension 293-F cells were maintained as recommended by the manufacturer (Freestyle 293 expression system; Invitrogen). Transfections were performed using the Effectene transfection reagent (Qiagen) for HEp-2 cells and the Polyfect transfection reagent (Qiagen) for 293-F cells. The RSV wt strain A2 was expanded in HEp-2 cells.

RSV infections. For filament visualization, HEp-2 cell monolayers on 12-mm micro-cover glasses (no. 2; VWR) were inoculated at a multiplicity of infection (MOI) of 1.0 and incubated for 24 h. For flow cytometric analysis, HEp-2 cells in tissue culture flasks were inoculated at an MOI of 3.0 and incubated for 24 h. For the virus-like particle (VLP) assay, 293-F cells were infected at an MOI of 0.05 for 72 h.

Generation of RSV F protein mutant constructs. All DNAs encoding the RSV fusion (F) protein constructs in this study were made from a sequence-optimized cDNA encoding the RSV wt strain A2 F protein in the pcDNA3.1 plasmid vector (Invitrogen) (5). DNAs encoding RSV F proteins with truncations or other alterations of the cytoplasmic tail at the C terminus of the protein were cloned using PCR primers to amplify the desired length of the tail and subcloned into pcDNA3.1. Targeted mutations, insertions, or deletions were introduced using the Lightning site-directed mutagenesis kit (Stratagene) and confirmed by sequencing.

Filament formation. Plasmids encoding the wt or a mutant RSV F protein along with pcDNA3.1 plasmids containing inserts encoding the

RSV A2 strain matrix (M), nucleoprotein (N), and phosphoprotein (P) gene (synthesized by GeneArt, Regensburg, Germany) were transfected into HEp-2 cell culture monolayers using 0.2 μg of each plasmid DNA, and cells were incubated for 72 h. Cells were fixed, immunostained, and imaged as described below. All images for virus-like filament formation were collected in a single experiment using identical microscopy parameters.

Fixation and immunostaining. Cells were fixed with 3.7% (wt/vol) paraformaldehyde in phosphate-buffered saline (PBS) for 10 min. Cells were permeabilized with 0.3% (wt/vol) Triton X-100 and 3.7% paraformaldehyde in PBS for 10 min at room temperature (RT). After fixation, cells were blocked in 3% (wt/vol) bovine serum albumin (BSA) in PBS for 60 min, followed by addition of primary antibody (Ab) in the blocking solution for 60 min. Cells were then washed three times in PBS, and species-specific IgG Alexa Fluor (Invitrogen) was added at a dilution of 1:1,000 in block solution for 60 min to detect primary Abs. Cells were washed three times in PBS and fixed on glass slides using the Prolong Antifade kit (Invitrogen). All steps were performed at RT. Images were obtained on a Zeiss inverted LSM510 confocal microscope using a 63×/1.40 Plan-Apochromat oil lens. Anti-RSV M (clone B135), anti-RSV P protein (clone 3_5), and anti-RSV N protein (clone B130) monoclonal Abs were a kind gift of Earling Norrby and Ewa Bjorling. An anti-RSV F protein humanized mouse monoclonal Ab (palivizumab; MedImmune) was obtained from the Vanderbilt Pharmacy. F-actin was visualized using rhodamine phalloidin, and To-Pro-3 iodide was used to visualize the nucleus (Invitrogen).

Imaging with RSV-specific RNA probe and live cell delivery. Single-copy sensitive RNA probes designed to target the RSV genomic gene start regions were delivered into RSV wt- or mock-infected HEp-2 cells using streptolysin O reversible permeabilization 24 h after inoculation, as previously described (14). After probe delivery, cells were immunostained for RSV proteins as described above. Images were processed in Volocity imaging software (version 5.1; Improvision). Shadow and highlight input sliders were adjusted to the beginning and end of the histogram curve to optimize tonal levels for the entire image; middle tones were not adjusted.

Quantitative analysis of images. To determine filament length, images from 12 high-powered fields were obtained on a Zeiss inverted LSM510 confocal microscope using a 40×/1.30 Plan-Neofluar oil lens. Images were analyzed using laser scanning microscopy (LSM) image acquisition software (Rel 4.2; Zeiss). The length of virus-like filaments was determined using the ruler tool in the LSM software to trace individual filaments in the images. The four longest filaments measured per cell were used in calculation of overall filament length for each construct. For quantitation of the percentage of RSV F-transfected cells showing filaments, images from 20 high-powered fields were collected on a Zeiss inverted LSM510 confocal microscope using a 20×/0.75 Plan-Apochromat lens. The percentage of RSV F-transfected cells with filaments was calculated by counting the total number of RSV F-transfected cells with filaments and dividing that number by the total number of RSV F-transfected cells.

Quantitative analysis of total cell lysate. HEp-2 cells in 6-well plates were transfected with 0.4 μg of plasmid DNA encoding the indicated F-protein cytoplasmic tail (CT) construct using the Qiagen Effectene transfection reagent. Cells were harvested at 48 h after transfection using a single detergent lysis buffer (50 mM Tris-HCl, 150 mM NaCl, 1% Triton X-100, pH 8.0) containing a 1:200 dilution of mammalian protease inhibitor cocktail (Sigma). Lysates were separated on 4 to 12% NuPAGE bis-Tris gels and transferred to polyvinylidene difluoride (PVDF) membranes using an iBlot dry blotting system (Invitrogen). Membranes were blocked for 1 h using Odyssey blocking buffer (Li-Cor) diluted 1:1 in PBS. Primary Abs for β-actin (1:5,000; Abcam) or the RSV F protein (motavizumab expressed from recombinant cDNA; 0.85 μg/ml) were diluted in blocking buffer diluted 1:1 with PBS + 0.1% Tween 20 (PBS-T), applied to membranes, and incubated overnight at 4°C. Membranes then were washed four times in PBS + 0.1% Tween for 5 min each. Secondary Abs were diluted 1:2,500 (goat anti-human IRDye 680CW; Kirkegaard & Perry Labs Inc.) or 1:5,000 (goat anti-mouse IRDye 800CW; Li-Cor) in blocking buffer and added to each membrane for 60 min. Membranes were washed four times in PBS-T. Bands were imaged and quantitated using the Odyssey infrared imaging system. The quantitative signals from RSV F protein bands were normalized against those of β-actin in the same lane and used to generate an expression (exp) ratio that represented a comparison of expression of the mutant F protein to that of the wt F protein.

Flow cytometric assay for quantitative surface expression of RSV F. HEp-2 cells on 6-well plates were transfected with 0.4 μg of each plasmid encoding the wt RSV M, N, and P proteins and either RSV F wt or a mutant F construct using the Effectene transfection reagent (Qiagen). After 48 h, cells were treated with 20 mM EDTA in PBS to form a single-cell suspension. Cells were washed two times in wash buffer (2% FBS in PBS) and then incubated with palivizumab at 1 μg/ml for 30 min at RT. Cell were again washed two times with wash buffer and immunostained with an Alexa Fluor goat anti-mouse 488 secondary Ab at a final concentration of 2 μg/ml. Cells were washed two times in wash buffer and analyzed on a 5-laser custom LSR II flow cytometer (Becton Dickinson) in the Vanderbilt Medical Center Flow Cytometry Shared Resource. Data analysis was performed using the FlowJo software program (version 7.6.1). Weighted mean fluorescent intensity (MFI) was calculated by multiplying the raw mean fluorescent intensity by the frequency of positive cells. All flow cytometry data from Fig. 3, 4, and 5 were collected using the same negative and positive control samples in three independent experiments. Statistical analysis was performed using a Student's *t* test. *P* values less than 0.05 were considered significant.

VLP assay. A recent protocol developed for the generation of human metapneumovirus VLPs (R. G. Cox and J. V. Williams, unpublished results) was modified for the preparation of RSV VLPs. 293-F cells were transfected with plasmids encoding either vector alone or RSV M, N, P, and the indicated RSV F construct in equal amounts. Seventy-two hours after transfection, cell supernatants and pellets were separated and collected by using low-speed centrifugation. Cell pellets were resuspended in cell lysis buffer as described above. Cell supernatant was pelleted through a 20% sucrose cushion using a Sorvall Surespin 630 rotor at 26,000 rpm for 90 min. The resulting pellet was resuspended in equal volumes of cell lysis buffer with protease inhibitors (Sigma). Western blotting was performed as described above. The quantitative signals from RSV F, M, N, or P protein bands were corrected for background using vector alone and then normalized to the signal from wt FCT. Bars represent the means and standard deviations for three independent experiments. Statistical analysis was performed using Student's *t* test. All values less than 0.05 were considered significant.

Transmission electron microscopy. VLP transfections were prepared as described for the VLP assay with FCT wt. For RSV-infected samples, 293-F cells were inoculated at an MOI of 0.05 for 72 h. Cell supernatants were clarified and pelleted though 20% sucrose in sterile MHN buffer (0.1 M $MgSO_4$, 50 mM HEPES, 150 mM NaCl). Pellets were resuspended in 20% sucrose in MHN, applied to formvar-carbon grids with 300 mesh Cu (Ted Pella Inc.), and stained with 1% aqueous sodium phosphotungstate acid (Electron Microscopy Sciences). Grids were imaged on a FEI Morgagni electron microscope operated at an acceleration voltage of 100 kV. Images were collected using a 1,000 × 1,000 active pixel charge-coupled-device (CCD) camera (AMT) at a magnification of ×44,000. Image contrast was enhanced in the Adobe Photoshop (CS5) software program using the levels adjustment. Shadow and highlight input sliders were adjusted to the beginning and end of the histogram curve to optimize tonal levels for the entire image; middle tones were not adjusted.

ACKNOWLEDGMENTS

This work was supported by the Vanderbilt Medical Scientist Training Program National Institute of General Medical Sciences/NIH grant T32 GM007347, Burroughs Wellcome Fund Clinical Scientist Award in Translation Research (to J.E.C.), a grant from the March of Dimes (J.E.C.), and NIH grants R01 GM 094198 (to P.J.S.) and R01 AI85062 (to J.V.W.). Experiments were performed in part through the VUMC Cell

Imaging Shared Resources (supported by NIH grants CA68485, DK20593, DK58404, HD15052, DK59637, and EY08126) and the VMC Flow Cytometry Shared Resource (supported by the Vanderbilt Ingram Cancer Center [P30 CA68485] and the Vanderbilt Digestive Disease Research Center [DK058404]).

We thank Melanie Ohi, Thuy Tran, and Kim Crimin for equipment use and expertise with data collection and analysis. We thank all members of the Crowe Laboratory, especially Natalie Thornburg, for helpful discussion and excellent technical support.

SUPPLEMENTAL MATERIAL

Supplemental material for this article may be found at http://mbio.asm.org/lookup/suppl/doi:10.1128/mBio.00270-11/-/DCSupplemental.

Figure S1, PDF file, 0.3 MB.

REFERENCES

1. **Fuentes S, Tran KC, Luthra P, Teng MN, He B.** 2007. Function of the respiratory syncytial virus small hydrophobic protein. J. Virol. **81**: 8361–8366.
2. **Fields BN, Knipe DM, Howley PM.** 2007. Fields virology, 5th ed. Wolters Kluwer Health/Lippincott Williams & Wilkins, Philadelphia, PA.
3. **Roberts SR, Compans RW, Wertz GW.** 1995. Respiratory syncytial virus matures at the apical surfaces of polarized epithelial cells. J. Virol. **69**: 2667–2673.
4. **Lindquist ME, Lifland AW, Utley TJ, Santangelo PJ, Crowe JE, Jr.** 2010. Respiratory syncytial virus induces host RNA stress granules to facilitate viral replication. J. Virol. **84**:12274–12284.
5. **Brock SC, Heck JM, McGraw PA, Crowe JE, Jr.** 2005. The transmembrane domain of the respiratory syncytial virus F protein is an orientation-independent apical plasma membrane sorting sequence. J. Virol. **79**: 12528–12535.
6. **Utley TJ, et al.** 2008. Respiratory syncytial virus uses a Vps4-independent budding mechanism controlled by Rab11-FIP2. Proc. Natl. Acad. Sci. U. S. A. **105**:10209–10214.
7. **Bächi T.** 1988. Direct observation of the budding and fusion of an enveloped virus by video microscopy of viable cells. J. Cell Biol. **107**:1689–1695.
8. **Santangelo PJ, Bao G.** 2007. Dynamics of filamentous viral RNPs prior to egress. Nucleic Acids Res. **35**:3602–3611.
9. **Brock SC, Goldenring JR, Crowe JE, Jr.** 2003. Apical recycling systems regulate directional budding of respiratory syncytial virus from polarized epithelial cells. Proc. Natl. Acad. Sci. U. S. A. **100**:15143–15148.
10. **Bächi T, Howe C.** 1973. Morphogenesis and ultrastructure of respiratory syncytial virus. J. Virol. **12**:1173–1180.
11. **Branigan PJ, et al.** 2006. The cytoplasmic domain of the F protein of human respiratory syncytial virus is not required for cell fusion. J. Gen. Virol. **87**:395–398.
12. **Oomens AG, Bevis KP, Wertz GW.** 2006. The cytoplasmic tail of the human respiratory syncytial virus F protein plays critical roles in cellular localization of the F protein and infectious progeny production. J. Virol. **80**:10465–10477.
13. **Harrison MS, Sakaguchi T, Schmitt AP.** 2010. Paramyxovirus assembly and budding: building particles that transmit infections. Int. J. Biochem. Cell Biol. **42**:1416–1429.
14. **Santangelo PJ, et al.** 2009. Single molecule-sensitive probes for imaging RNA in live cells. Nat. Methods **6**:347–349.
15. **Jeffree CE, et al.** 2007. Ultrastructural analysis of the interaction between F-actin and respiratory syncytial virus during virus assembly. Virology **369**:309–323.
16. **Teng MN, Collins PL.** 1998. Identification of the respiratory syncytial virus proteins required for formation and passage of helper-dependent infectious particles. J. Virol. **72**:5707–5716.
17. **Fleming EH, Kolokoltsov AA, Davey RA, Nichols JE, Roberts NJ, Jr.** 2006. Respiratory syncytial virus F envelope protein associates with lipid rafts without a requirement for other virus proteins. J. Virol. **80**: 12160–12170.
18. **Biacchesi S, et al.** 2004. Recombinant human metapneumovirus lacking the small hydrophobic SH and/or attachment G glycoprotein: deletion of G yields a promising vaccine candidate. J. Virol. **78**:12877–12887.
19. **Teng MN, Whitehead SS, Collins PL.** 2001. Contribution of the respiratory syncytial virus G glycoprotein and its secreted and membrane-bound forms to virus replication *in vitro* and *in vivo*. Virology **289**: 283–296.
20. **Ghildyal R, et al.** 2005. Interaction between the respiratory syncytial virus G glycoprotein cytoplasmic domain and the matrix protein. J. Gen. Virol. **86**:1879–1884.
21. **Chen BJ, Lamb RA.** 2008. Mechanisms for enveloped virus budding: can some viruses do without an ESCRT? Virology **372**:221–232.
22. **Brown G, et al.** 2004. Analysis of the interaction between respiratory syncytial virus and lipid-rafts in Hep2 cells during infection. Virology **327**:175–185.
23. **McCurdy LH, Graham BS.** 2003. Role of plasma membrane lipid microdomains in respiratory syncytial virus filament formation. J. Virol. **77**:1747–1756.
24. **Marty A, Meanger J, Mills J, Shields B, Ghildyal R.** 2004. Association of matrix protein of respiratory syncytial virus with the host cell membrane of infected cells. Arch. Virol. **149**:199–210.
25. **McDonald TP, Pitt AR, Brown G, Rixon HW, Sugrue RJ.** 2004. Evidence that the respiratory syncytial virus polymerase complex associates with lipid rafts in virus-infected cells: a proteomic analysis. Virology **330**: 147–157.
26. **Henderson G, Murray J, Yeo RP.** 2002. Sorting of the respiratory syncytial virus matrix protein into detergent-resistant structures is dependent on cell-surface expression of the glycoproteins. Virology **300**:244–254.
27. **Lillemeier BF, Pfeiffer JR, Surviladze Z, Wilson BS, Davis MM.** 2006. Plasma membrane-associated proteins are clustered into islands attached to the cytoskeleton. Proc. Natl. Acad. Sci. U. S. A. **103**:18992–18997.
28. **Burke E, Dupuy L, Wall C, Barik S.** 1998. Role of cellular actin in the gene expression and morphogenesis of human respiratory syncytial virus. Virology **252**:137–148.
29. **Fernie BF, Gerin JL.** 1982. Immunochemical identification of viral and nonviral proteins of the respiratory syncytial virus virion. Infect. Immun. **37**:243–249.
30. **Gower TL, et al.** 2005. RhoA signaling is required for respiratory syncytial virus-induced syncytium formation and filamentous virion morphology. J. Virol. **79**:5326–5336.
31. **Radhakrishnan A, et al.** 2010. Protein analysis of purified respiratory syncytial virus particles reveals an important role for heat shock protein 90 in virus particle assembly. Mol. Cell. Proteomics **9**:1829–1848.
32. **Ulloa L, Serra R, Asenjo A, Villanueva N.** 1998. Interactions between cellular actin and human respiratory syncytial virus (HRSV). Virus Res. **53**:13–25.

REFERENCES

1. **Altschul, S. F.**, **T. L. Madden**, **A. A. Schäffer**, **J. Zhang**, **Z. Zhang**, **W. Miller**, **and D. J. Lipman**. 1997. Gapped BLAST and PSI-BLAST: a new generation of protein database search programs. Nucleic Acids Res. **25**:3389–3402.

2. **Batonick, M.**, **A. G. P. Oomens**, **and G. W. Wertz**. 2008. Human respiratory syncytial virus glycoproteins are not required for apical targeting and release from polarized epithelial cells. J. Virol. **82**:8664–8672.

3. **Bächi, T.** 1988. Direct observation of the budding and fusion of an enveloped virus by video microscopy of viable cells. J. Cell Biol. **107**:1689–1695.

4. **Bächi, T.**, **and C. Howe**. 1973. Morphogenesis and ultrastructure of respiratory syncytial virus. J. Virol. **12**:1173–1180.

5. **Behera, A. K.**, **H. Matsuse**, **M. Kumar**, **X. Kong**, **R. F. Lockey**, **and S. S. Mohapatra**. 2001. Blocking intercellular adhesion molecule-1 on human epithelial cells decreases respiratory syncytial virus infection. Biochem. Biophys. Res. Commun. **280**:188–195.

6. **Biacchesi, S.**, **M. H. Skiadopoulos**, **L. Yang**, **E. W. Lamirande**, **K. C. Tran**, **B. R. Murphy**, **P. L. Collins**, **and U. J. Buchholz**. 2004. Recombinant human Metapneumovirus lacking the small hydrophobic SH and/or attachment G glycoprotein: deletion of G yields a promising vaccine candidate. J. Virol. **78**:12877–12887.

7. **Bitko, V.**, **A. Oldenburg**, **N. E. Garmon**, **and S. Barik**. 2003. Profilin is required for viral morphogenesis, syncytium formation, and cell-specific stress fiber induction by respiratory syncytial virus. BMC Microbiol. **3**:9.

8. **Branigan, P. J.**, **N. D. Day**, **C. Liu**, **L. L. Gutshall**, **J. A. Melero**, **R. T. Sarisky**, **and A. M. Del Vecchio**. 2006. The cytoplasmic domain of the F protein of Human respiratory syncytial virus is not required for cell fusion. J. Gen. Virol. **87**:395–398.

9. **Brock, S. C.**, **J. R. Goldenring**, **and J. E. Crowe, Jr**. 2003. Apical recycling systems regulate directional budding of respiratory syncytial virus from polarized epithelial cells. Proc. Natl. Acad. Sci. U.S.A. **100**:15143–15148.

10. **Brock, S. C.**, **J. M. Heck**, **P. A. McGraw**, **and J. E. Crowe, Jr**. 2005. The transmembrane domain of the respiratory syncytial virus F protein is an orientation-independent apical plasma membrane sorting sequence. J. Virol. **79**:12528–12535.

11. **Brown, D. A.**, **and J. K. Rose**. 1992. Sorting of GPI-anchored proteins to glycolipid-enriched membrane subdomains during transport to the apical cell surface. Cell **68**:533–544.

12. **Brown, G.**, **J. Aitken**, **H. W. M. Rixon**, **and R. J. Sugrue**. 2002. Caveolin-1 is incorporated into mature respiratory syncytial virus particles during virus assembly on the surface of virus-infected cells. J. Gen. Virol. **83**:611–621.

13. **Brown, G.**, **C. E. Jeffree**, **T. McDonald**, **H. W. M. Rixon**, **J. D. Aitken**, **and R. J. Sugrue**. 2004. Analysis of the interaction between respiratory syncytial virus and lipid-rafts in Hep2 cells during infection. Virology **327**:175–185.

14. **Burke, E.**, **L. Dupuy**, **C. Wall**, **and S. Barik**. 1998. Role of cellular actin in the gene expression and morphogenesis of human respiratory syncytial virus. Virology **252**:137–148.

15. **Burke, E.**, **N. M. Mahoney**, **S. C. Almo**, **and S. Barik**. 2000. Profilin is required for optimal actin-dependent transcription of respiratory syncytial virus genome RNA. J. Virol. **74**:669–675.

16. **Carter, C. J.** 2010. APP, APOE, complement receptor 1, clusterin and PICALM and their involvement in the herpes simplex life cycle. Neurosci. Lett. **483**:96–100.

17. **Casanova, J. E.**, **X. Wang**, **R. Kumar**, **S. G. Bhartur**, **J. Navarre**, **J. E. Woodrum**, **Y. Altschuler**, **G. S. Ray**, **and J. R. Goldenring**. 1999. Association of Rab25 and Rab11a with the apical recycling system of polarized Madin-Darby canine kidney cells. Mol. Biol. Cell **10**:47–61.

18. **Chen, B. J.**, **and R. A. Lamb**. 2008. Mechanisms for enveloped virus budding: can some viruses do without an ESCRT? Virology **372**:221–232.

19. **Chibalina, M. V.**, **R. C. Roberts**, **S. D. Arden**, **J. Kendrick-Jones**, **and F. Buss**. 2008. Rab8-optineurin-myosin VI: analysis of interactions and functions in the secretory pathway. Meth. Enzymol. **438**:11–24.

20. **Chin, J.**, **R. L. Magoffin**, **L. A. Shearer**, **J. H. Schieble**, **and E. H. Lennette**. 1969. Field evaluation of a respiratory syncytial virus vaccine and a trivalent parainfluenza virus vaccine in a pediatric population. Am. J. Epidemiol. **89**:449–463.

21. **Collins, P. L.**, **and J. A. Melero**. 2011. Progress in understanding and controlling respiratory syncytial virus: still crazy after all these years. Virus Res **162**:80–99.

22. **Cordo, S. M.**, **N. A. Candurra**, **and E. B. Damonte**. 1999. Myristic acid analogs are inhibitors of Junin virus replication. Microbes Infect. **1**:609–614.

23. **Empey, K. M.**, **R. S. Peebles**, **and J. K. Kolls**. 2010. Pharmacologic advances in the treatment and prevention of respiratory syncytial virus. Clin. Infect. Dis. **50**:1258–1267.

24. **Falsey, A. R.** 2007. Respiratory syncytial virus infection in adults. Semin Respir Crit Care Med **28**:171–181.

25. **Falsey, A. R.**, **P. A. Hennessey**, **M. A. Formica**, **C. Cox**, **and E. E. Walsh**. 2005. Respiratory syncytial virus infection in elderly and high-risk adults. N. Engl. J. Med. **352**:1749–1759.

26. **Feldman, S. A.**, **S. Audet**, **and J. A. Beeler**. 2000. The fusion glycoprotein of human respiratory syncytial virus facilitates virus attachment and infectivity via an interaction with cellular heparan sulfate. J. Virol. **74**:6442–6447.

27. **Fernie, B. F.**, **and J. L. Gerin**. 1982. Immunochemical identification of viral and nonviral proteins of the respiratory syncytial virus virion. Infect. Immun. **37**:243–249.

28. **Fleming, E. H.**, **A. A. Kolokoltsov**, **R. A. Davey**, **J. E. Nichols**, **and N. J. Roberts**. 2006. Respiratory syncytial virus F envelope protein associates with lipid rafts without a requirement for other virus proteins. J. Virol. **80**:12160–12170.

29. **Formstecher, E.**, **S. Aresta**, **V. Collura**, **A. Hamburger**, **A. Meil**, **A. Trehin**, **C. Reverdy**, **V. Betin**, **S. Maire**, **C. Brun**, **B. Jacq**, **M. Arpin**, **Y. Bellaiche**, **S. Bellusci**, **P. Benaroch**, **M. Bornens**, **R. Chanet**, **P. Chavrier**, **O. Delattre**, **V. Doye**, **R. Fehon**, **G. Faye**, **T. Galli**, **J.-A. Girault**, **B. Goud**, **J. de Gunzburg**, **L. Johannes**, **M.-P. Junier**, **V. Mirouse**, **A. Mukherjee**, **D. Papadopoulo**, **F. Perez**, **A. Plessis**, **C. Rossé**, **S. Saule**, **D. Stoppa-Lyonnet**, **A. Vincent**, **M. White**, **P. Legrain**, **J. Wojcik**, **J. Camonis**, **and L. Daviet**. 2005. Protein interaction mapping: a Drosophila case study. Genome Res. **15**:376–384.

30. **Fromont-Racine, M.**, **J. C. Rain**, **and P. Legrain**. 1997. Toward a functional analysis of the yeast genome through exhaustive two-hybrid screens. Nat. Genet. **16**:277–282.

31. **Fuentes, S.**, **K. C. Tran**, **P. Luthra**, **M. N. Teng**, **and B. He**. 2007. Function of the respiratory syncytial virus small hydrophobic protein. J. Virol. **81**:8361–8366.

32. **Gaudin, Y.**, **A. Barge**, **C. Ebel**, **and R. W. Ruigrok**. 1995. Aggregation of VSV M protein is reversible and mediated by nucleation sites: implications for viral assembly. Virology **206**:28–37.

33. **Ghildyal, R.**, **J. Mills**, **M. Murray**, **N. Vardaxis**, **and J. Meanger**. 2002. Respiratory syncytial virus matrix protein associates with nucleocapsids in infected cells. J. Gen. Virol. **83**:753–757.

34. **Ghildyal, R.**, **A. Ho**, **and D. A. Jans**. 2006. Central role of the respiratory syncytial virus matrix protein in infection. FEMS Microbiol. Rev. **30**:692–705.

35. **Ghildyal, R.**, **D. Li**, **I. Peroulis**, **B. Shields**, **P. G. Bardin**, **M. N. Teng**, **P. L. Collins**, **J. Meanger**, **and J. Mills**. 2005. Interaction between the respiratory syncytial virus G glycoprotein cytoplasmic domain and the matrix protein. J. Gen. Virol. **86**:1879–1884.

36. **Goldenring, J. R.**, **J. Smith**, **H. D. Vaughan**, **P. Cameron**, **W. Hawkins**, **and J. Navarre**. 1996. Rab11 is an apically located small GTP-binding protein in epithelial tissues. Am. J. Physiol. **270**:G515–25.

37. **Gonzalez, I. M.**, **R. A. Karron**, **M. Eichelberger**, **E. E. Walsh**, **V. W. Delagarza**, **R. Bennett**, **R. M. Chanock**, **B. R. Murphy**, **M. L. Clements-Mann**, **and A. R. Falsey**. 2000. Evaluation of the live attenuated cpts 248/404 RSV vaccine in combination with a subunit RSV vaccine (PFP-2) in healthy young and older adults. Vaccine **18**:1763–1772.

38. **Gower, T. L.**, **M. E. Peeples**, **P. L. Collins**, **and B. S. Graham**. 2001. RhoA is activated during respiratory syncytial virus infection. Virology **283**:188–196.

39. **Gower, T. L.**, **M. K. Pastey**, **M. E. Peeples**, **P. L. Collins**, **L. H. McCurdy**, **T. K. Hart**, **A. Guth**, **T. R. Johnson**, **and B. S. Graham**. 2005. RhoA signaling is required for respiratory syncytial virus-induced syncytium formation and filamentous virion morphology. J. Virol. **79**:5326–5336.

40. **Graham, B. S.** 2011. Biological challenges and technological opportunities for respiratory syncytial virus vaccine development. Immunol. Rev. **239**:149–166.

41. **Hall, C. B.**, **G. A. Weinberg**, **M. K. Iwane**, **A. K. Blumkin**, **K. M. Edwards**, **M. A. Staat**, **P. Auinger**, **M. R. Griffin**, **K. A. Poehling**, **D. Erdman**, **C. G. Grijalva**, **Y. Zhu**, **and P. Szilagyi**. 2009. The burden of respiratory syncytial virus infection in young children. N. Engl. J. Med. **360**:588–598.

42. **Harpen, M.**, **T. Barik**, **A. Musiyenko**, **and S. Barik**. 2009. Mutational analysis reveals a noncontractile but interactive role of actin and profilin in viral RNA-dependent RNA synthesis. J. Virol. **83**:10869–10876.

43. **Harrison, M. S.**, **T. Sakaguchi**, **and A. P. Schmitt**. 2010. Paramyxovirus assembly and budding: building particles that transmit infections. Int. J. Biochem. Cell Biol. **42**:1416–1429.

44. **Henderson, G.**, **J. Murray**, **and R. P. Yeo**. 2002. Sorting of the respiratory syncytial virus matrix protein into detergent-resistant structures is dependent on cell-surface expression of the glycoproteins. Virology **300**:244–254.

45. **Huang, Y. T.**, **R. R. Romito**, **B. P. De**, **and A. K. Banerjee**. 1993. Characterization of the in vitro system for the synthesis of mRNA from human respiratory syncytial virus. Virology **193**:862–867.

46. **Hurley, J. H.**, **E. Boura**, **L.-A. Carlson**, **and B. Różycki**. 2010. Membrane budding. Cell **143**:875–887.

47. **Jeffree, C. E.**, **G. Brown**, **J. Aitken**, **D. Y. Su-Yin**, **B.-H. Tan**, **and R. J. Sugrue**. 2007. Ultrastructural analysis of the interaction between F-actin and respiratory syncytial virus during virus assembly. Virology **369**:309–323.

48. **Jeffree, C. E.**, **H. W. M. Rixon**, **G. Brown**, **J. Aitken**, **and R. J. Sugrue**. 2003. Distribution of the attachment (G) glycoprotein and GM1 within the envelope of mature respiratory syncytial virus filaments revealed using field emission scanning electron microscopy. Virology **306**:254–267.

49. **Jin, H.**, **D. Clarke**, **H. Z. Zhou**, **X. Cheng**, **K. Coelingh**, **M. Bryant**, **and S. Li**. 1998. Recombinant human respiratory syncytial virus (RSV) from cDNA and construction of subgroup A and B chimeric RSV. Virology **251**:206–214.

50. **Kallewaard, N. L.**, **A. L. Bowen**, **and J. E. Crowe**. 2005. Cooperativity of actin and microtubule elements during replication of respiratory syncytial virus. Virology **331**:73–81.

51. **Kapikian, A. Z.**, **R. H. Mitchell**, **R. M. Chanock**, **R. A. Shvedoff**, **and C. E. Stewart**. 1969. An epidemiologic study of altered clinical reactivity to respiratory syncytial (RS) virus infection in children previously vaccinated with an inactivated RS virus vaccine. Am. J. Epidemiol. **89**:405–421.

52. **Kenworthy, A. K.**, **B. J. Nichols**, **C. L. Remmert**, **G. M. Hendrix**, **M. Kumar**, **J. Zimmerberg**, **and J. Lippincott-Schwartz**. 2004. Dynamics of putative raft-associated proteins at the cell surface. J. Cell Biol. **165**:735–746.

53. **Krilov, L.** 2006. Respiratory syncytial virus (RSV) infection. Emedicine.medscape.com/article/971488

54. **Levine, S.**, **R. Klaiber-Franco**, **and P. R. Paradiso**. 1987. Demonstration that glycoprotein G is the attachment protein of respiratory syncytial virus. J. Gen.

Virol. **68 (Pt 9)**:2521–2524.

55. **Li, D.**, **D. A. Jans**, **P. G. Bardin**, **J. Meanger**, **J. Mills**, **and R. Ghildyal**. 2008. Association of respiratory syncytial virus M protein with viral nucleocapsids is mediated by the M2-1 protein. J. Virol. **82**:8863–8870.

56. **Lillemeier, B. F.**, **J. R. Pfeiffer**, **Z. Surviladze**, **B. S. Wilson**, **and M. M. Davis**. 2006. Plasma membrane-associated proteins are clustered into islands attached to the cytoskeleton. Proc. Natl. Acad. Sci. U.S.A. **103**:18992–18997.

57. **Lindquist, M. E.**, **A. W. Lifland**, **T. J. Utley**, **P. J. Santangelo**, **and J. E. Crowe**. 2010. Respiratory syncytial virus induces host RNA stress granules to facilitate viral replication. J. Virol. **84**:12274–12284.

58. **Lindquist, M. E.**, **B. A. Mainou**, **T. S. Dermody**, **and J. E. Crowe, Jr**. 2011. Activation of protein kinase R is required for induction of stress granules by respiratory syncytial virus but dispensable for viral replication. Virology **413**:103–110.

59. **Low, K.-W.**, **T. Tan**, **K. Ng**, **B.-H. Tan**, **and R. J. Sugrue**. 2008. The RSV F and G glycoproteins interact to form a complex on the surface of infected cells. Biochem. Biophys. Res. Commun. **366**:308–313.

60. **Malhotra, R.**, **M. Ward**, **H. Bright**, **R. Priest**, **M. R. Foster**, **M. Hurle**, **E. Blair**, **and M. Bird**. 2003. Isolation and characterisation of potential respiratory syncytial virus receptor(s) on epithelial cells. Microbes Infect. **5**:123–133.

61. **Marty, A.**, **J. Meanger**, **J. Mills**, **B. Shields**, **and R. Ghildyal**. 2004. Association of matrix protein of respiratory syncytial virus with the host cell membrane of infected cells. Arch. Virol. **149**:199–210.

62. **McCurdy, L. H.**, **and B. S. Graham**. 2003. Role of plasma membrane lipid microdomains in respiratory syncytial virus filament formation. J. Virol. **77**:1747–1756.

63. **McDonald, T. P.**, **A. R. Pitt**, **G. Brown**, **H. W. M. Rixon**, **and R. J. Sugrue**. 2004. Evidence that the respiratory syncytial virus polymerase complex associates with lipid rafts in virus-infected cells: a proteomic analysis. Virology **330**:147–157.

64. **Mitra, R.**, **P. Baviskar**, **R. R. Duncan-Decocq**, **D. Patel**, **and A. G. P. Oomens**. 2012. The Human Respiratory Syncytial Virus Matrix Protein is Required for Maturation of Viral Filaments. J. Virol.

65. **Mok, H.**, **S. Lee**, **D. W. Wright**, **and J. E. Crowe**. 2008. Enhancement of the CD8+ T cell response to a subdominant epitope of respiratory syncytial virus by deletion of an immunodominant epitope. Vaccine **26**:4775–4782.

66. **Money, V. A.**, **H. K. McPhee**, **J. A. Mosely**, **J. M. Sanderson**, **and R. P. Yeo**. 2009. Surface features of a Mononegavirales matrix protein indicate sites of membrane interaction. Proc. Natl. Acad. Sci. U.S.A. **106**:4441–4446.

67. **Mostov, K. E.** 1994. Transepithelial transport of immunoglobulins. Annu. Rev. Immunol. **12**:63–84.

68. **Mostov, K. E.**, **M. Verges**, **and Y. Altschuler**. 2000. Membrane traffic in polarized epithelial cells. Curr. Opin. Cell Biol. **12**:483–490.

69. **Oomens, A. G. P.**, **K. P. Bevis**, **and G. W. Wertz**. 2006. The cytoplasmic tail of the human respiratory syncytial virus F protein plays critical roles in cellular localization of the F protein and infectious progeny production. J. Virol. **80**:10465–10477.

70. **Pasteur, I.** February 1998. Fast and exhaustive method for selecting a prey polypeptide interacting with ... U.S. Patent 6187535. US Patent Office.

71. **Pasteur, I.** October 2002. Fast and exhaustive method for selecting a prey polypeptide interacting with ... U.S. Patent 6913886. US Patent Office.

72. **Pasteur, I.** August 2000. Fast and exhaustive method for selecting a prey polypeptide interacting with ... U.S. Patent 6531284. US Patent Office.

73. **Pereira-Leal, J. B.**, **and M. C. Seabra**. 2001. Evolution of the Rab family of small GTP-binding proteins. J. Mol. Biol. **313**:889–901.

74. **Petrenko, A. A.**, **L. S. Pavlova**, **A. I. Karseladze**, **F. L. Kisseljov**, **and N. P. Kisseljova**. 2006. Downregulation of genes encoding for subunits of adaptor complex-3 in cervical carcinomas. Biochemistry Mosc. **71**:1153–1160.

75. **Radhakrishnan, A.**, **D. Yeo**, **G. Brown**, **M. Z. Myaing**, **L. R. Iyer**, **R. Fleck**, **B.-H. Tan**, **J. Aitken**, **D. Sanmun**, **K. Tang**, **A. Yarwood**, **J. Brink**, **and R. J. Sugrue**. 2010. Protein analysis of purified respiratory syncytial virus particles reveals an important role for heat shock protein 90 in virus particle assembly. Mol. Cell Proteomics **9**:1829–1848.

76. **Rain, J. C.**, **L. Selig**, **H. De Reuse**, **V. Battaglia**, **C. Reverdy**, **S. Simon**, **G. Lenzen**, **F. Petel**, **J. Wojcik**, **V. Schächter**, **Y. Chemama**, **A. Labigne**, **and P. Legrain**. 2001. The protein-protein interaction map of Helicobacter pylori. Nature **409**:211–215.

77. **Roberts, S. R.**, **R. W. Compans**, **and G. W. Wertz**. 1995. Respiratory syncytial virus matures at the apical surfaces of polarized epithelial cells. J. Virol. **69**:2667–2673.

78. **Rossman, J. S.**, **X. Jing**, **G. P. Leser**, **and R. A. Lamb**. 2010. Influenza virus M2 protein mediates ESCRT-independent membrane scission. Cell **142**:902–913.

79. **Rossman, J. S.**, **and R. A. Lamb**. 2011. Influenza virus assembly and budding. Virology **411**:229–236.

80. **Santangelo, P. J.**, **and G. Bao**. 2007. Dynamics of filamentous viral RNPs prior to egress. Nucleic Acids Res. **35**:3602–3611.

81. **Santangelo, P. J.**, **A. W. Lifland**, **P. Curt**, **Y. Sasaki**, **G. J. Bassell**, **M. E. Lindquist**, **and J. E. Crowe, Jr**. 2009. Single molecule-sensitive probes for imaging RNA in live cells. Nat. Methods **6**:347–349.

82. **Schwedler, von, U. K.**, **M. Stuchell**, **B. Müller**, **D. M. Ward**, **H.-Y. Chung**, **E. Morita**, **H. E. Wang**, **T. Davis**, **G.-P. He**, **D. M. Cimbora**, **A. Scott**, **H.-G. Kräusslich**, **J. Kaplan**, **S. G. Morham**, **and W. I. Sundquist**. 2003. The protein network of HIV budding. Cell **114**:701–713.

83. **Shaikh, F. Y.**, **R. G. Cox**, **A. W. Lifland**, **A. L. Hotard**, **J. V. Williams**, **M. L. Moore**, **P. J. Santangelo**, **and J. E. Crowe, Jr**. 2012. A critical phenylalanine residue in the respiratory syncytial virus fusion protein cytoplasmic tail mediates assembly of internal viral proteins into viral filaments and particles. MBio **3**.

84. **Smith, E. C.**, **A. Popa**, **A. Chang**, **C. Masante**, **and R. E. Dutch**. 2009. Viral entry mechanisms: the increasing diversity of paramyxovirus entry. FEBS J. **276**:7217–7227.

85. **Studier, F. W.**, **and B. A. Moffatt**. 1986. Use of bacteriophage T7 RNA polymerase to direct selective high-level expression of cloned genes. J. Mol. Biol. **189**:113–130.

86. **Swanson, K. A.**, **E. C. Settembre**, **C. A. Shaw**, **A. K. Dey**, **R. Rappuoli**, **C. W. Mandl**, **P. R. Dormitzer**, **and A. Carfi**. 2011. Structural basis for immunization with postfusion respiratory syncytial virus fusion F glycoprotein (RSV F) to elicit high neutralizing antibody titers. Proc. Natl. Acad. Sci. U.S.A. **108**:9619–9624.

87. **Tani, M.**, **and Y. A. Hannun**. 2007. Neutral sphingomyelinase 2 is palmitoylated on multiple cysteine residues. Role of palmitoylation in subcellular localization. J. Biol. Chem. **282**:10047–10056.

88. **Taylor, M. P.**, **O. O. Koyuncu**, **and L. W. Enquist**. 2011. Subversion of the actin cytoskeleton during viral infection. Nat. Rev. Microbiol. **9**:427–439.

89. **Tayyari, F.**, **D. Marchant**, **T. J. Moraes**, **W. Duan**, **P. Mastrangelo**, **and R. G. Hegele**. 2011. Identification of nucleolin as a cellular receptor for human respiratory syncytial virus. Nat. Med. **17**:1132–1135.

90. **Teng, F. Y.**, **Y. Wang**, **and B. L. Tang**. 2001. The syntaxins. Genome Biol. **2**:REVIEWS3012.

91. **Teng, M. N.**, **and P. L. Collins**. 1998. Identification of the respiratory syncytial virus proteins required for formation and passage of helper-dependent infectious particles. J. Virol. **72**:5707–5716.

92. **Teng, M. N.**, **S. S. Whitehead**, **and P. L. Collins**. 2001. Contribution of the respiratory syncytial virus G glycoprotein and its secreted and membrane-bound forms to virus replication in vitro and in vivo. Virology **289**:283–296.

93. **Trajkovic, K.**, **C. Hsu**, **S. Chiantia**, **L. Rajendran**, **D. Wenzel**, **F. Wieland**, **P. Schwille**, **B. Brügger**, **and M. Simons**. 2008. Ceramide triggers budding of exosome vesicles into multivesicular endosomes. Science **319**:1244–1247.

94. **Tripp, R. A.**, **L. P. Jones**, **L. M. Haynes**, **H. Zheng**, **P. M. Murphy**, **and L. J. Anderson**. 2001. CX3C chemokine mimicry by respiratory syncytial virus G glycoprotein. Nat. Immunol. **2**:732–738.

95. **Ulloa, L.**, **R. Serra**, **A. Asenjo**, **and N. Villanueva**. 1998. Interactions between cellular actin and human respiratory syncytial virus (HRSV). Virus Res **53**:13–25.

96. **Ullrich, O.**, **S. Reinsch**, **S. Urbé**, **M. Zerial**, **and R. G. Parton**. 1996. Rab11 regulates recycling through the pericentriolar recycling endosome. J. Cell Biol. **135**:913–924.

97. **Utley, T. J.**, **N. A. Ducharme**, **V. Varthakavi**, **B. E. Shepherd**, **P. J. Santangelo**, **M. E. Lindquist**, **J. R. Goldenring**, **and J. E. Crowe, Jr**. 2008. Respiratory syncytial virus uses a Vps4-independent budding mechanism controlled by Rab11-FIP2. Proc. Natl. Acad. Sci. U.S.A. **105**:10209–10214.

98. **Wadhawan, S.**, **B. Dickins**, **and A. Nekrutenko**. 2008. Wheels within wheels: clues to the evolution of the Gnas and Gnal loci. Mol. Biol. Evol. **25**:2745–2757.

99. **Welsch, S.**, **B. Müller**, **and H.-G. Kräusslich**. 2007. More than one door - Budding of enveloped viruses through cellular membranes. FEBS Lett. **581**:2089–2097.

100. **Wojcik, J.**, **I. G. Boneca**, **and P. Legrain**. 2002. Prediction, assessment and validation of protein interaction maps in bacteria. J. Mol. Biol. **323**:763–770.

101. **Yeo, D. S.-Y.**, **R. Chan**, **G. Brown**, **L. Ying**, **R. Sutejo**, **J. Aitken**, **B.-H. Tan**, **M. R. Wenk**, **and R. J. Sugrue**. 2009. Evidence that selective changes in the lipid composition of raft-membranes occur during respiratory syncytial virus infection. Virology **386**:168–182.

102. **Yondola, M.**, **and C. Carter**. 2011. Un-"ESCRT-"ed Budding. Viruses **3**:26–31.

103. 2006. Fields Virology Fifth. Lippincott Williams & Wilkins.